Coherent Disturbances on the Dynamic Tropopause

Kevin A. Biernat

Department of Atmospheric and Environmental Sciences

University at Albany, SUNY

ATM 619: Cyclone Workshop Seminar

What are Coherent Disturbances on the Dynamic Tropopause (DT)?

- Coherent disturbances on the DT are material features
- Can be identified by closed contours of DT potential temperature or DT pressure, indicative of parcel trapping (Hakim 2000; Pyle et al. 2004; Cavallo and Hakim 2009)

0600 UTC 17 November 2013

Potential temperature (K, shaded), wind speed (black, every 10 m s^{-1} starting at 50 m s^{-1}), and wind (m s^{-1}, barbs) on 2-PVU surface. Plotted using 0.5° NCEP CFSR dataset.

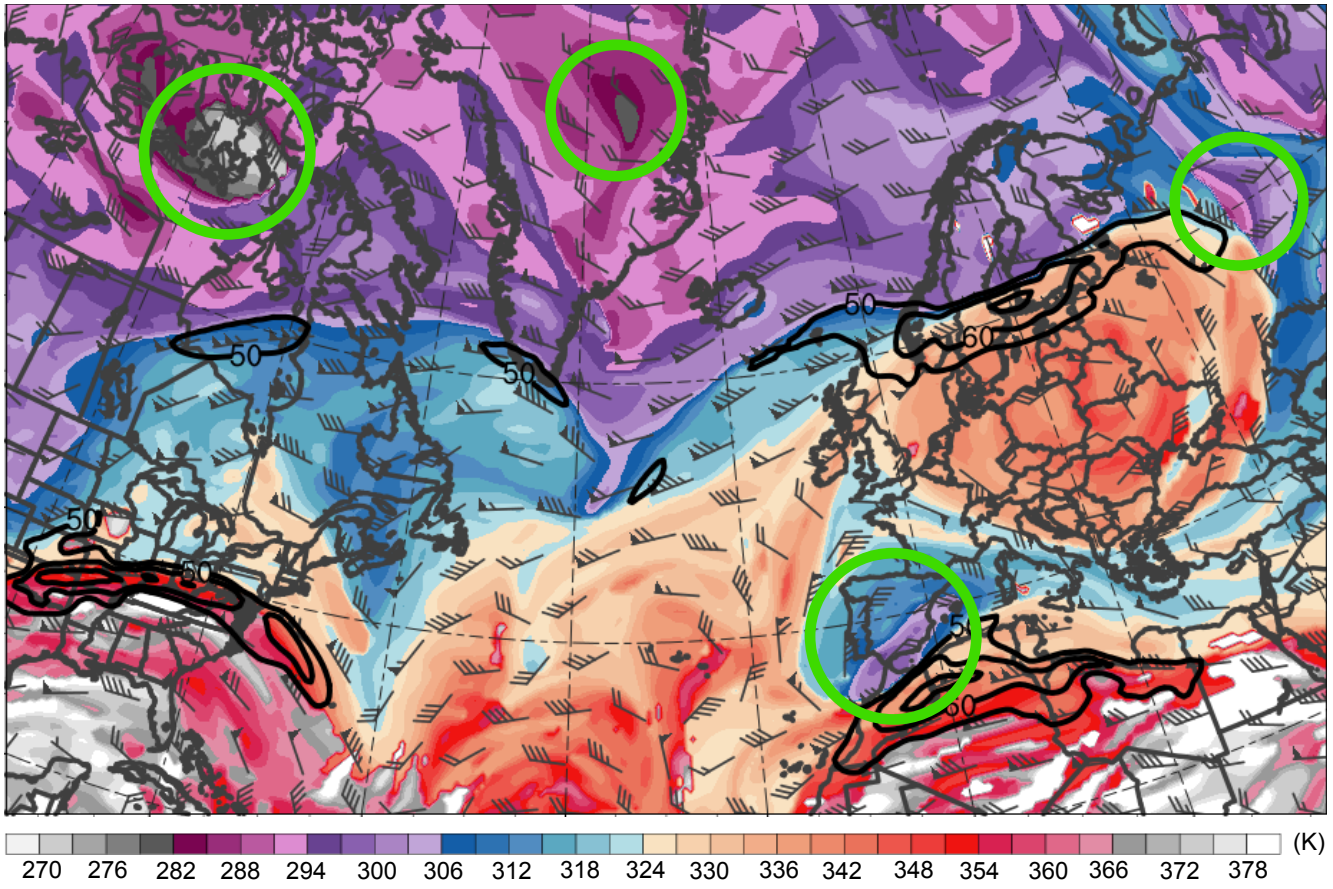

What are Coherent Disturbances on the DT?

- A coherent tropopause disturbance (CTD; Pyle et al. 2004) is defined as a tropopause-based material feature that is not necessarily of high-latitude origin

- A tropopause polar vortex (TPV; Cavallo and Hakim 2009, 2010) is a particular type of CTD, defined as a tropopause-based vortex of high-latitude origin

0600 UTC 17 November 2013

Potential temperature (K, shaded), wind speed (black, every 10 m s^{-1} starting at 50 m s^{-1}), and wind (m s^{-1}, barbs) on 2-PVU surface. Plotted using 0.5° NCEP CFSR dataset.

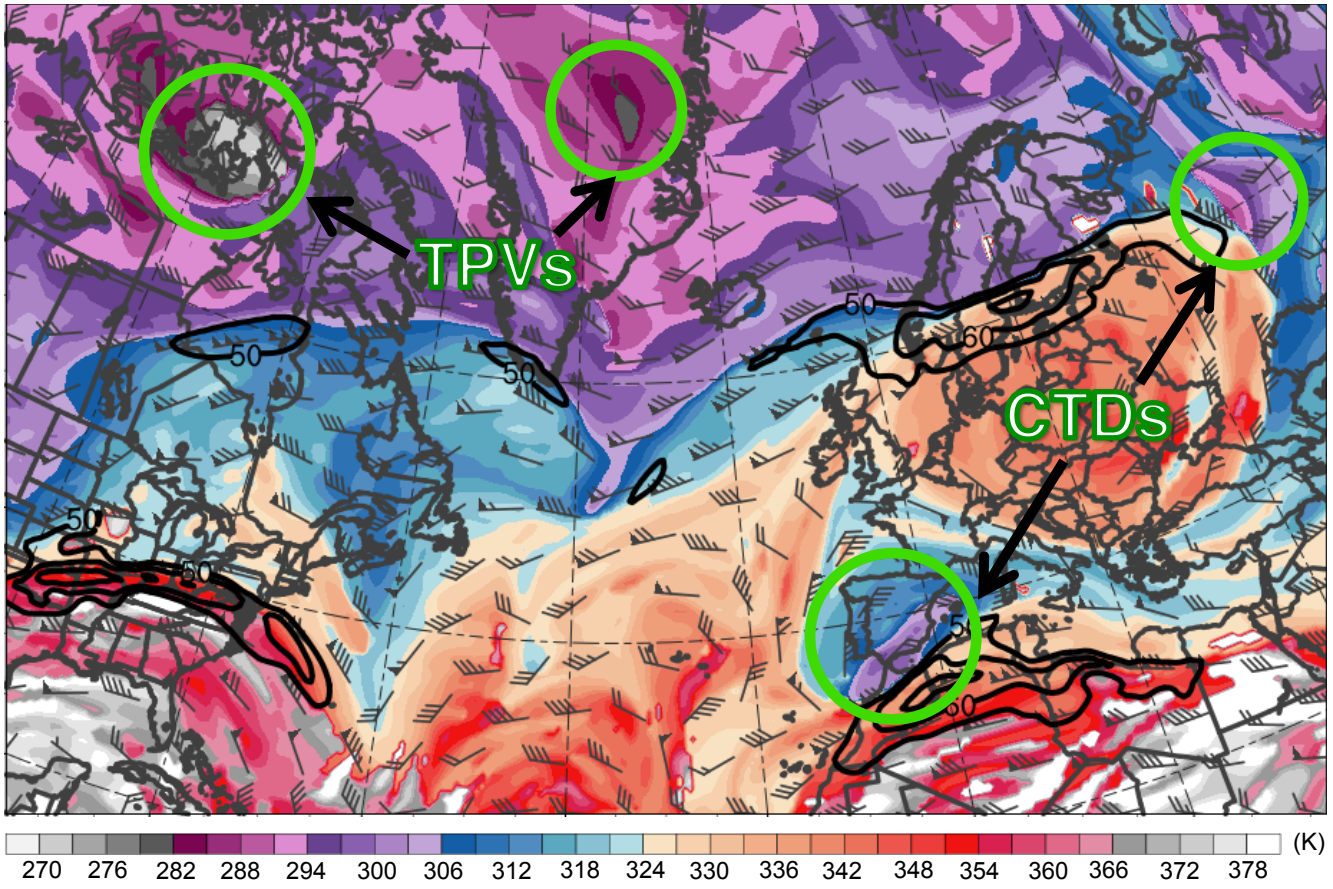

Balanced Vortex Structure using Potential Vorticity (PV)

Thorpe (1985)

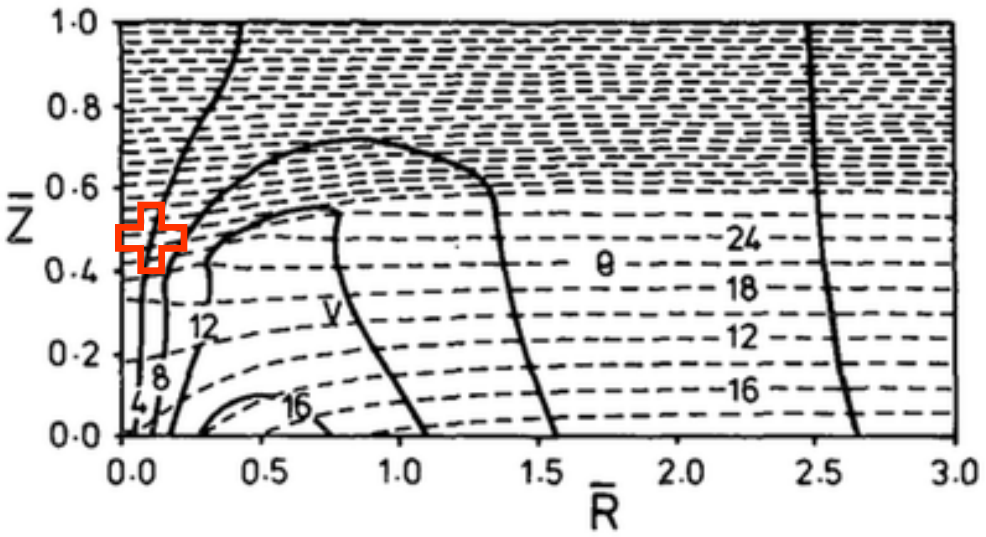

Potential temperature (dashed contours, K) and azimuthal wind (solid contours, m s^{-1}). Adapted from Fig. 3 in Thorpe (1985).

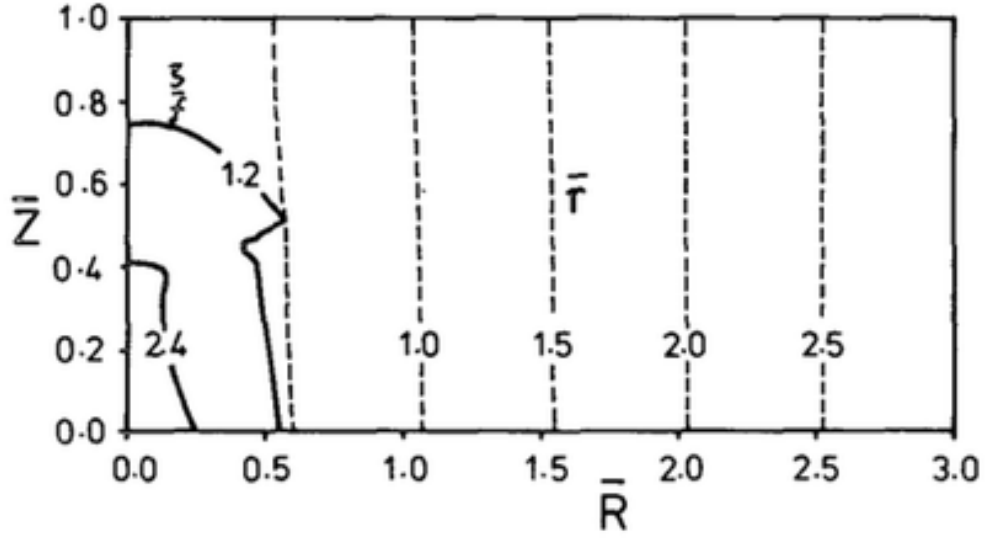

Ratio of relative vorticity to planetary vorticity (solid contours) and radius (dashed contours). Adapted from Fig. 3 in Thorpe (1985).

- Derived equation set analogous to two-dimensional semigeostrophic set for axisymmetric flow in gradient wind balance
- Equation set consists of prognostic equation for PV and two elliptic (diagnostic) equations for the potential function giving the balanced vortex structure
- Vortex structure completely determined at any time by solution of potential function equation and interior variations of PV
- Found that increased surface temperature, a lower tropopause, or larger tropospheric PV within core of vortex are each consistent with cyclonic circulation

Structure of Tropopause-based PV Anomalies

Hoskins et al. (1985)

positive (cyclonic) PV anomaly

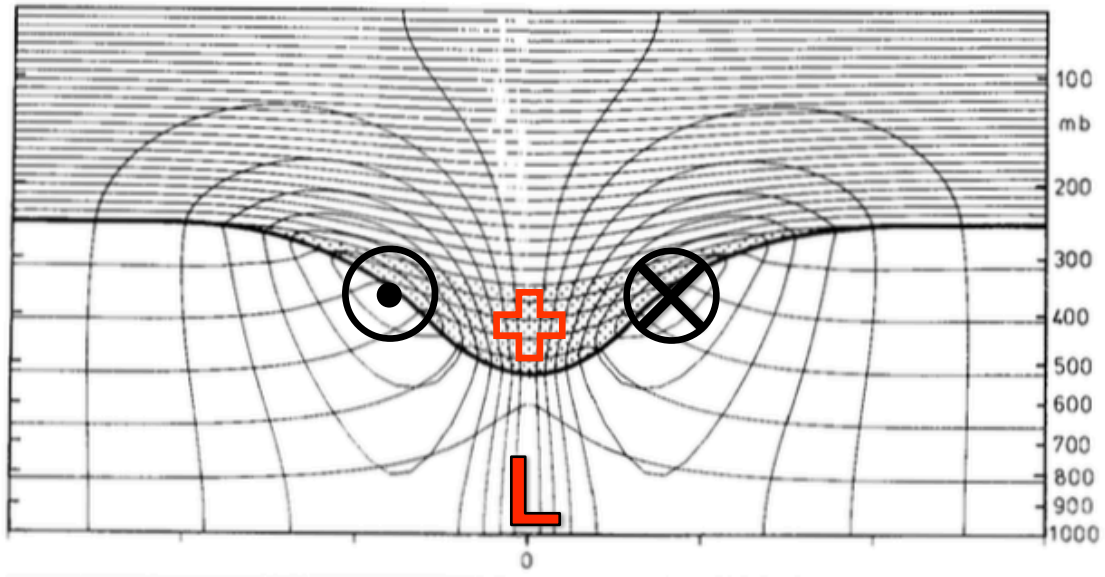

a

negative (anticyclonic) PV anomaly

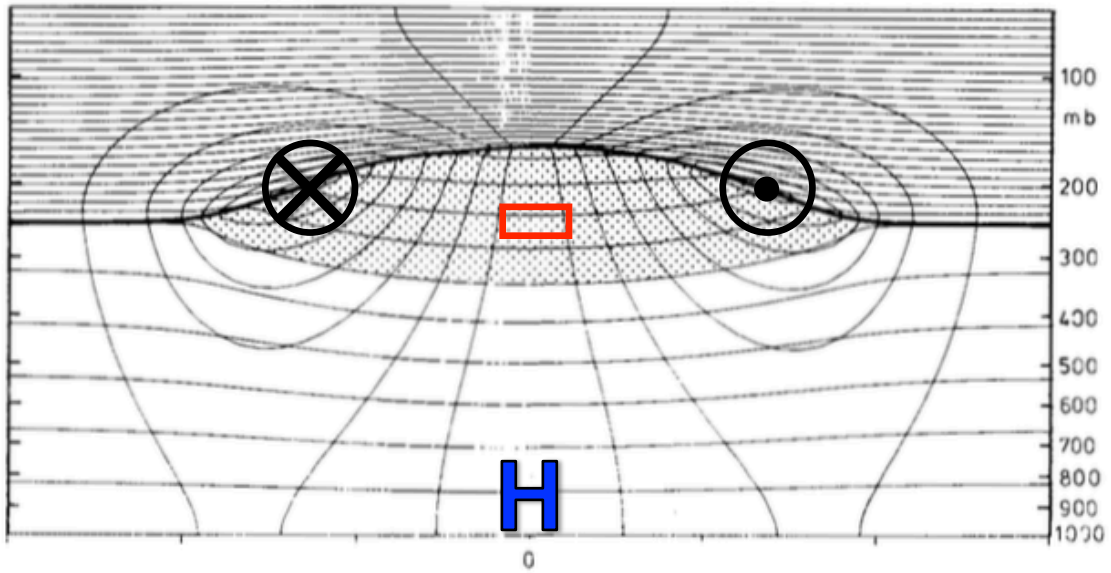

b

Potential temperature (solid contours, every 5 K) and azimuthal wind (thin contours, every 3 m s^{-1}). Thick line is tropopause. Stippled regions represent the PV anomalies. Surface pressure anomaly is (top) −41 hPa and (bottom) +13 hPa and relative vorticity extrema (located at tropopause) are (top) 1.7 × f and (bottom) −0.6 × f where f = 10^{-4} s^{-1} . Calculations done following method of Thorpe (1985). Adapted from Fig. 15 in Hoskins et al. 1985).

Cyclonic PV Anomalies and Cyclogenesis

Hoskins et al. (1985)

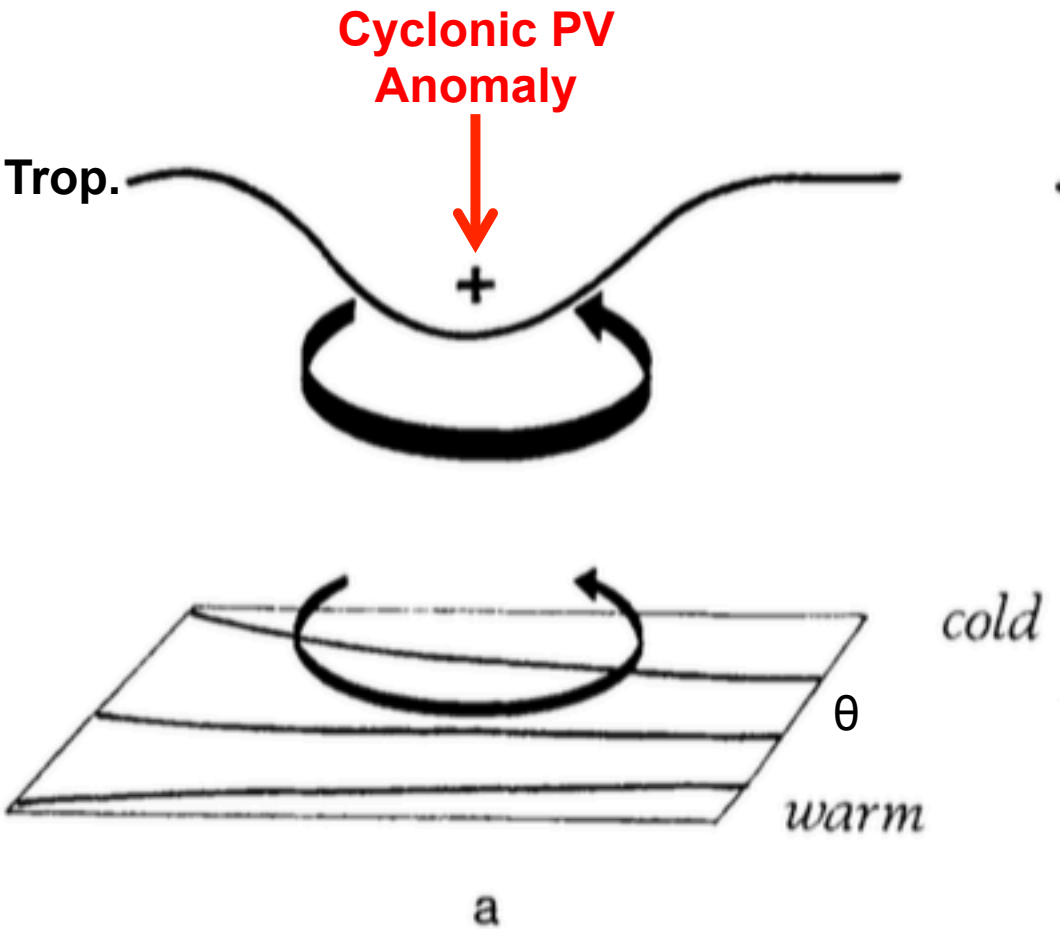

$t = t_0$

Cyclonic PV Anomalies and Cyclogenesis

Hoskins et al. (1985)

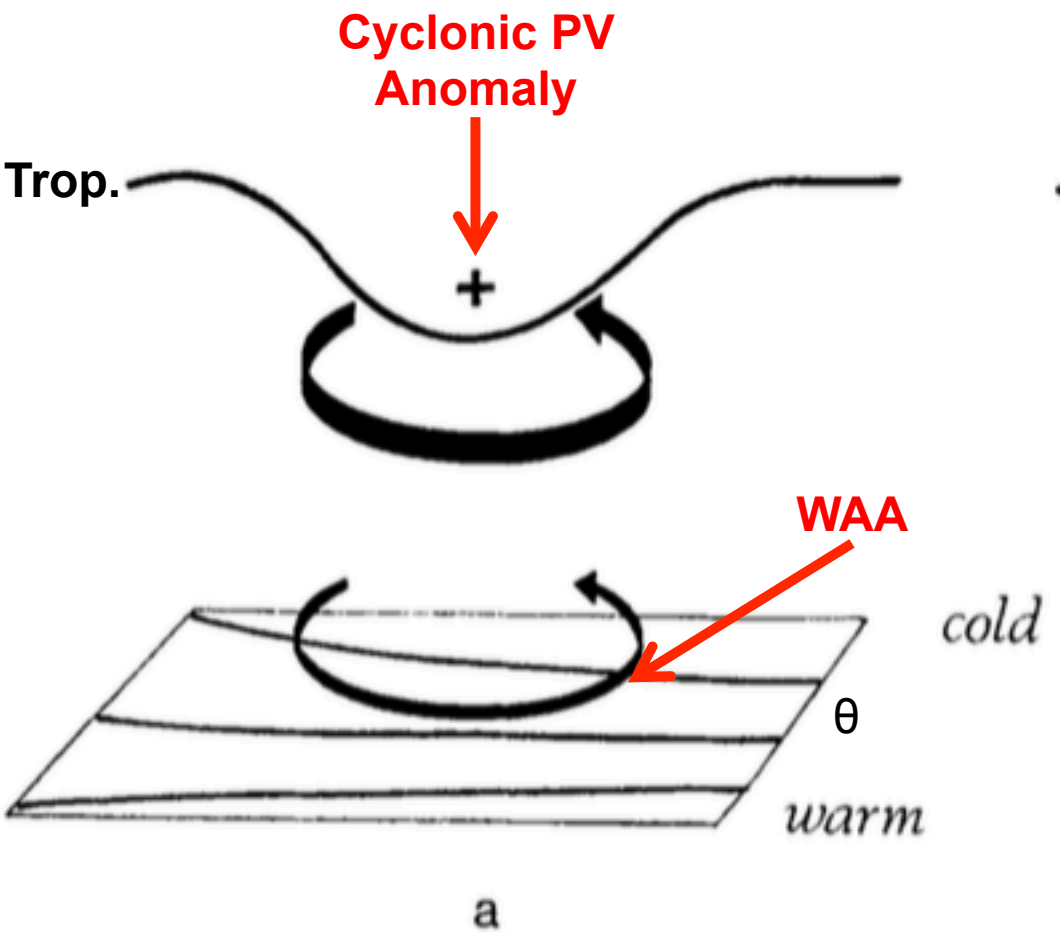

$t = t_0$

Cyclonic PV Anomalies and Cyclogenesis

Hoskins et al. (1985)

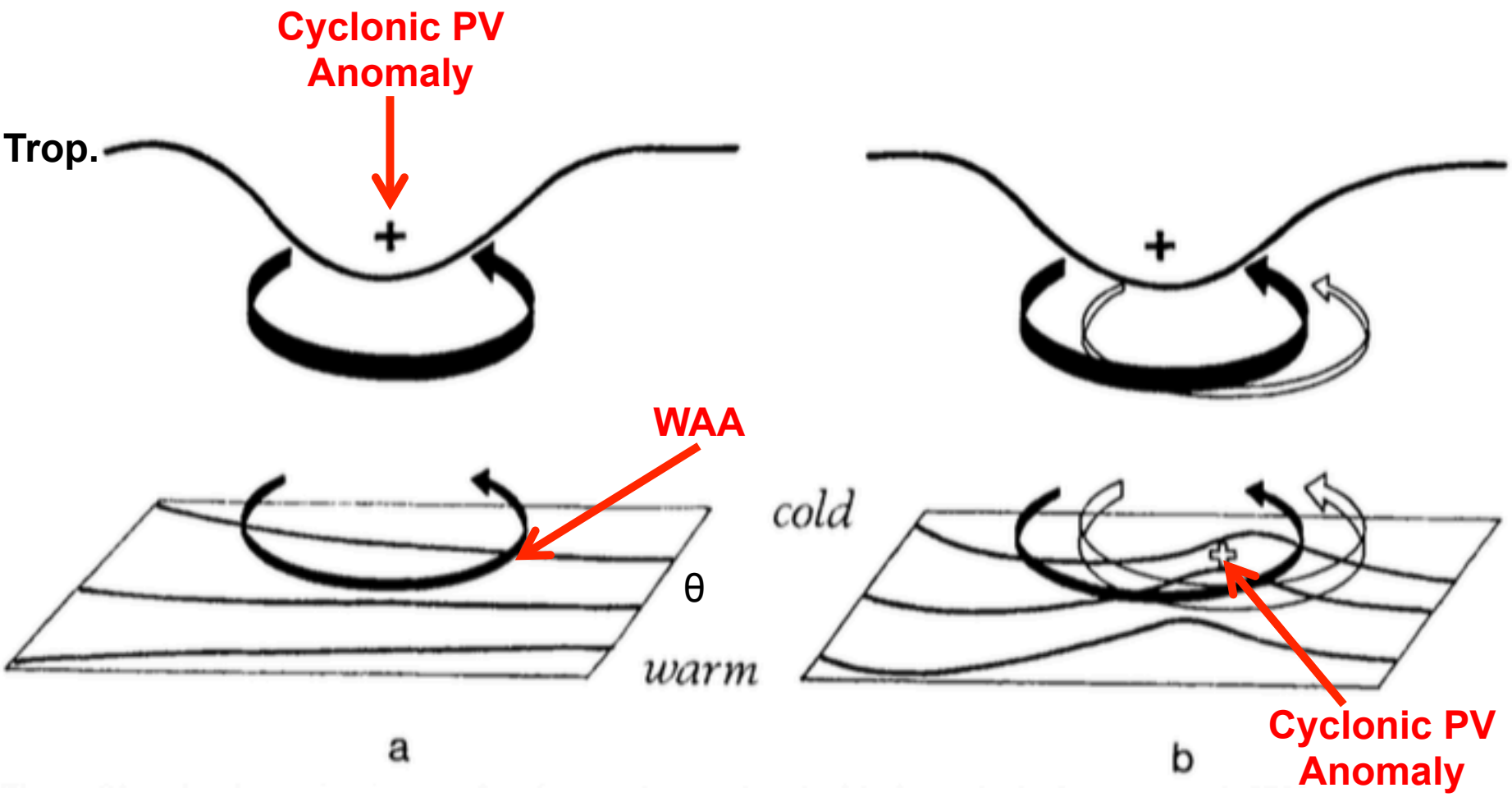

Cyclonic PV Anomalies and Cyclogenesis

Hoskins et al. (1985)

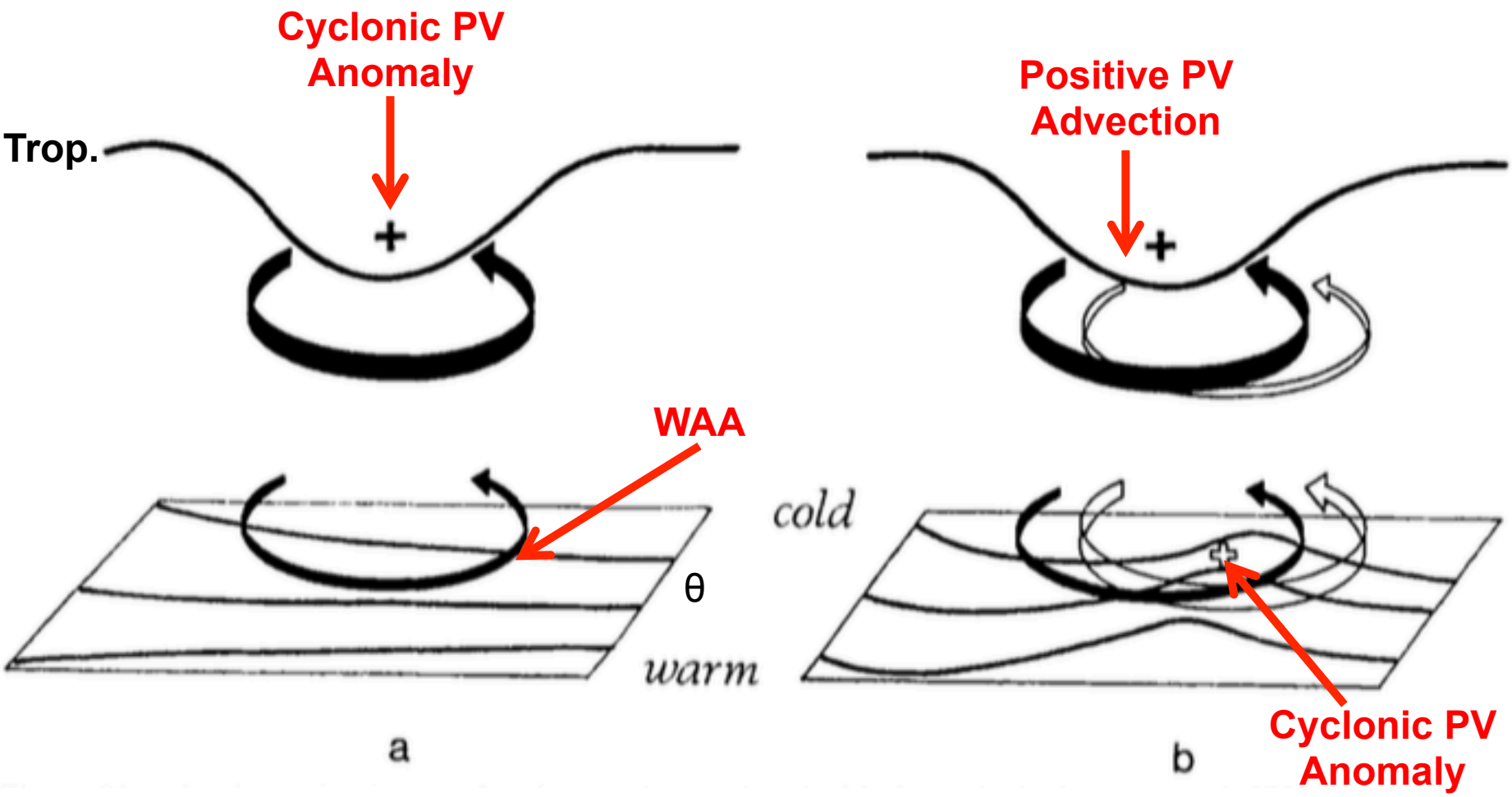

Cyclonic PV Anomalies and Cyclogenesis

Hoskins et al. (1985)

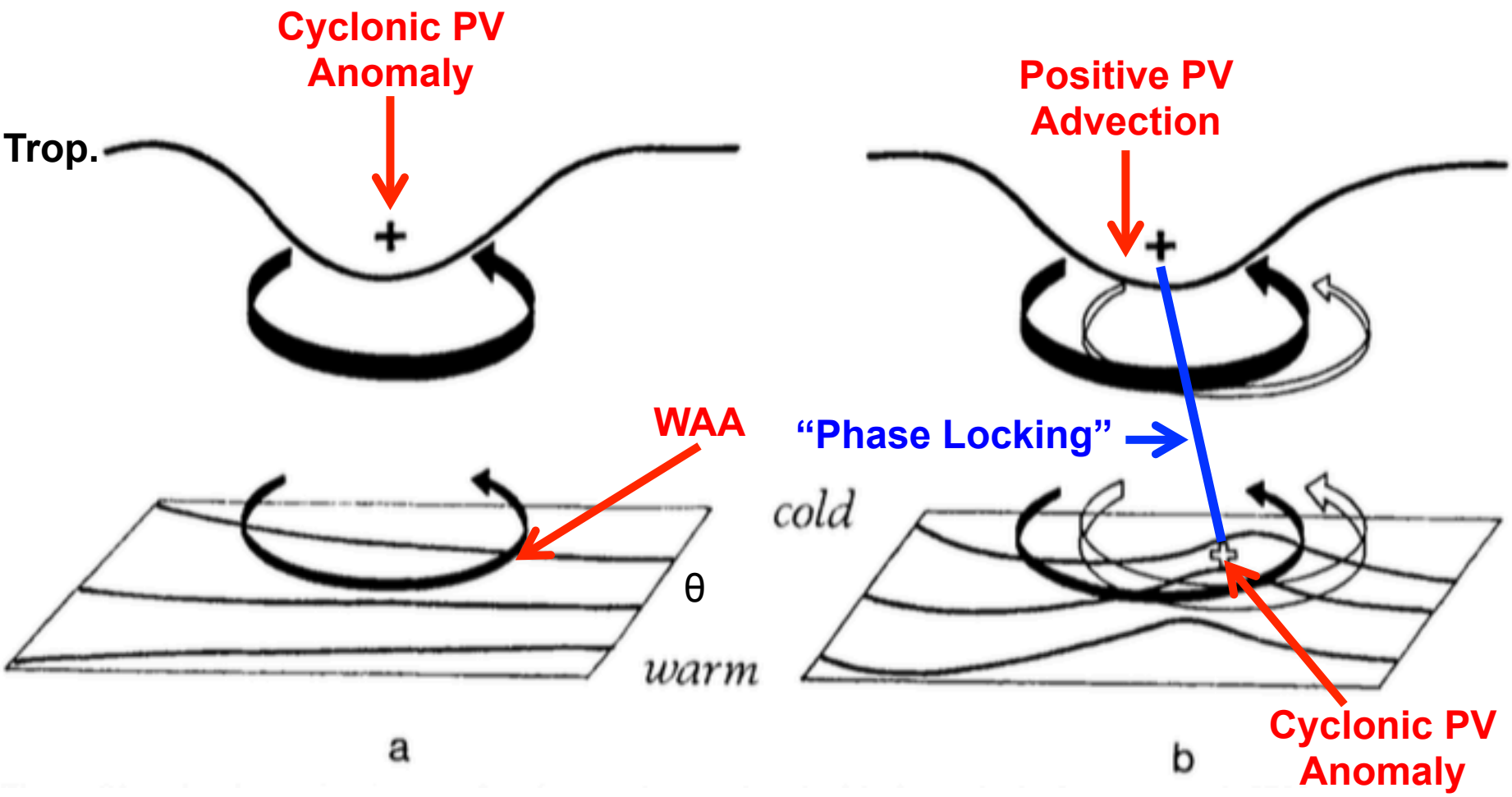

Hoskins et al. (1985)

Including Moist Processes

$$H \sim \frac{fL}{N}$$

H: Rossby penetration depth
f: Coriolis parameter
L: horizontal scale of flow
N: static stability

$$N^2 = \frac{g}{\theta}\frac{\partial \theta}{\partial z}$$

- Moist processes may modify amplification process
- Ascent in region of reduced N beneath approaching upper-level PV anomaly
- If enough moisture, condensation will lead to further reduction in N
- This results in larger H
- Positive feedback between PV anomalies will be enhanced

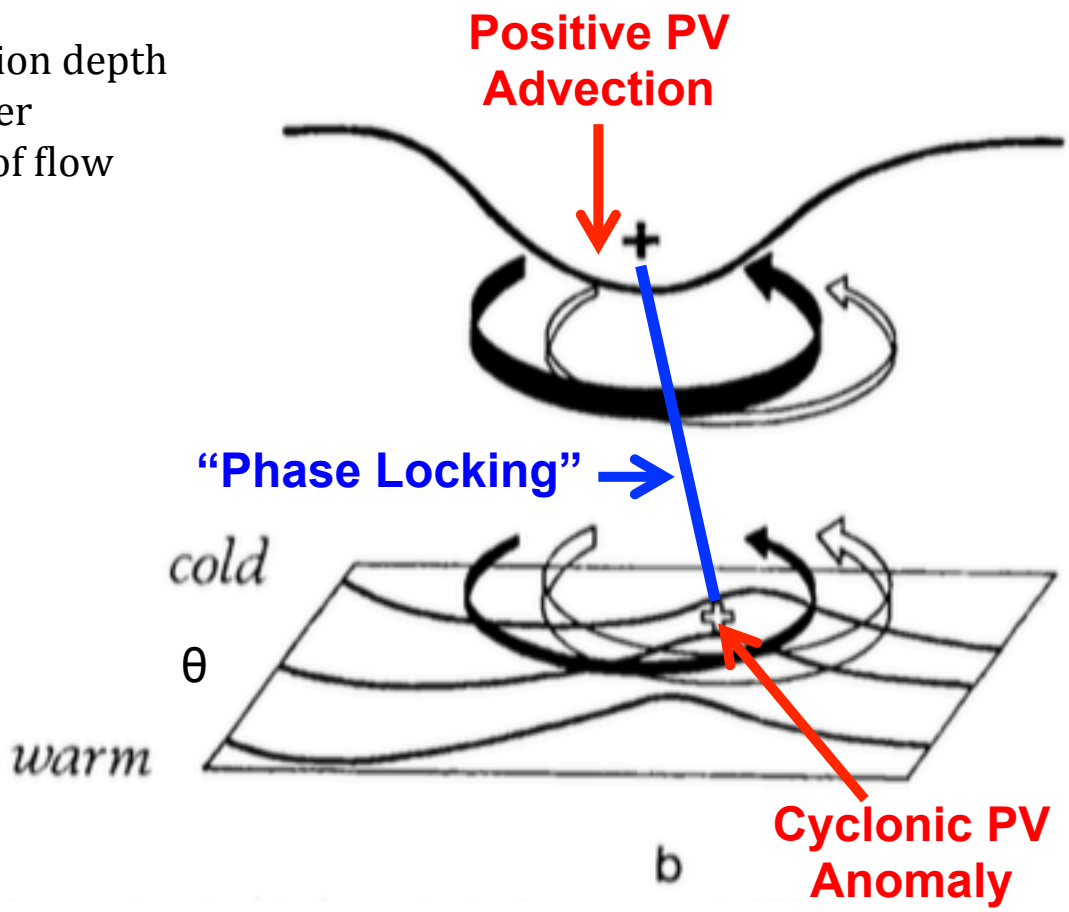

$t = t_0 + \Delta t$

"Coupling Development"

Takayabu (1991)

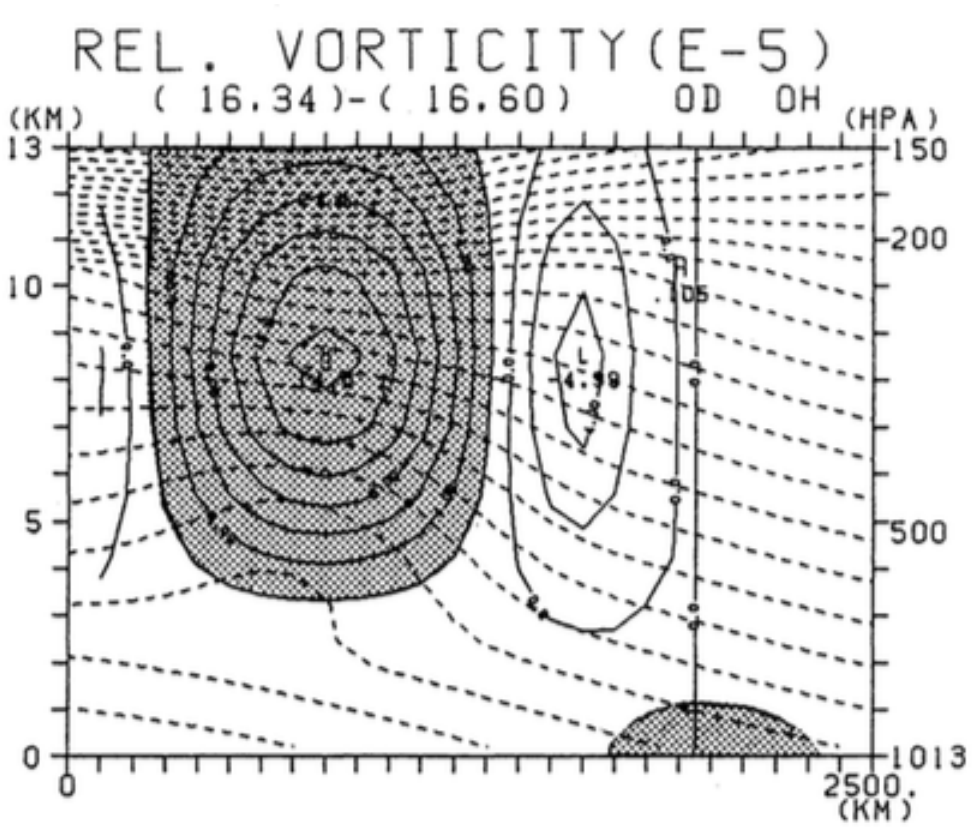

Meridional–height cross section of initial disturbances with potential temperature (dashed contours, every 5 K) and relative vorticity (solid contours, every 2×10^{-5} s^{-1}). Relative vorticity values greater than 2×10^{-5} s^{-1} are shaded for the upper vortex and relative vorticity values greater than 1×10^{-5} s^{-1} are shaded for lower vortex (located 1500 km east of cross section). Adapted from Fig. 3 of Takayabu (1991).

- Used simplified three-dimensional, β-plane channel, dry primitive equation model to simulate rapid cyclogenesis resulting from coupling of upper and lower tropospheric vortices
- Used a simple baroclinic westerly jet as basic flow and superimposed finite amplitude upper vortex and lower vortex
- Initial upper vortex associated with temperature anomaly of −9 K in upper-troposphere, while lower vortex associated with temperature anomaly of +4 K at surface
- Initial upper vortex placed 1200 km north of basic state jet axis, while initial lower vortex is placed on jet axis, 1500 km east of upper vortex

"Coupling Development"

Takayabu (1991)

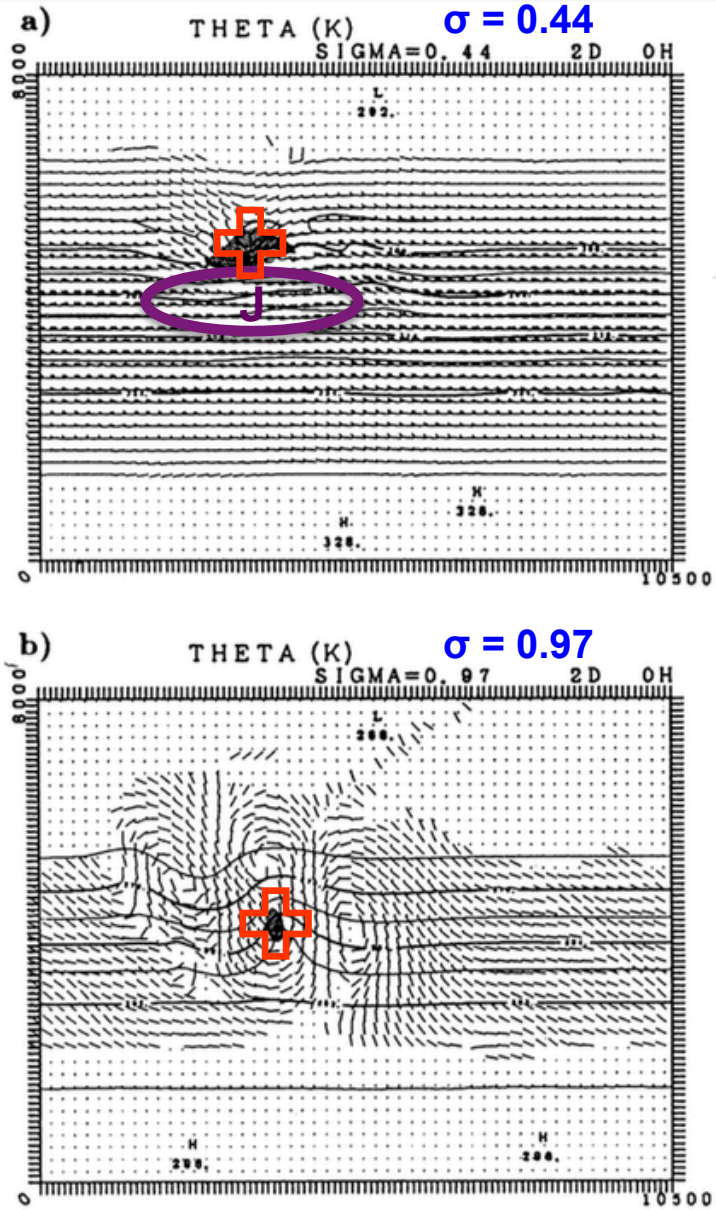

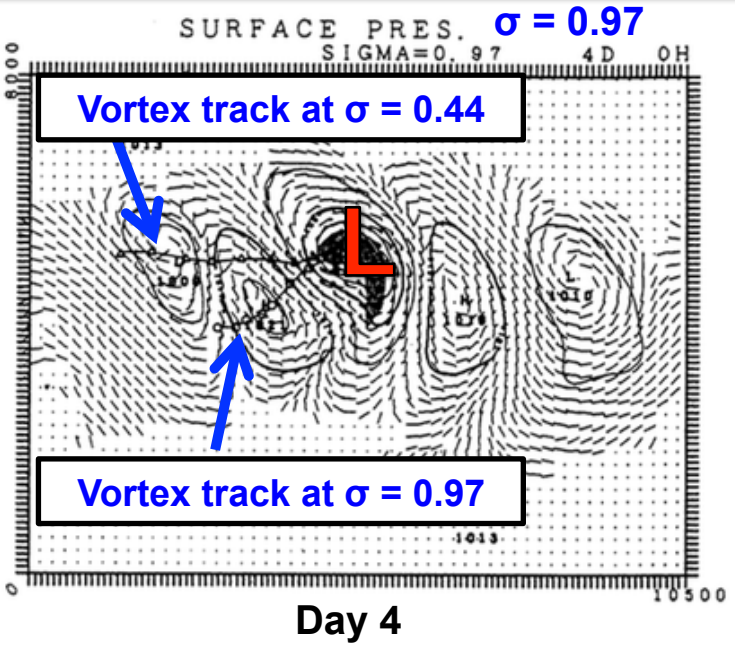

(left) Potential temperature (solid, contoured every 4 K), wind (flags and barbs), and relative vorticity greater than 4×10^{-5} s^{-1} (shading) at (top) σ = 0.44 and (bottom) σ = 0.97. Adapted from Fig. 5 in Takayabu (1991).

(right) Surface pressure (solid, contoured every 4 hPa), winds (flags and barbs), and relative vorticity greater than 4×10^{-5} s^{-1} (shading) at σ = 0.97. Adapted from Fig. 6 in Takayabu (1991).

“Coupling Development”

Takayabu (1991)

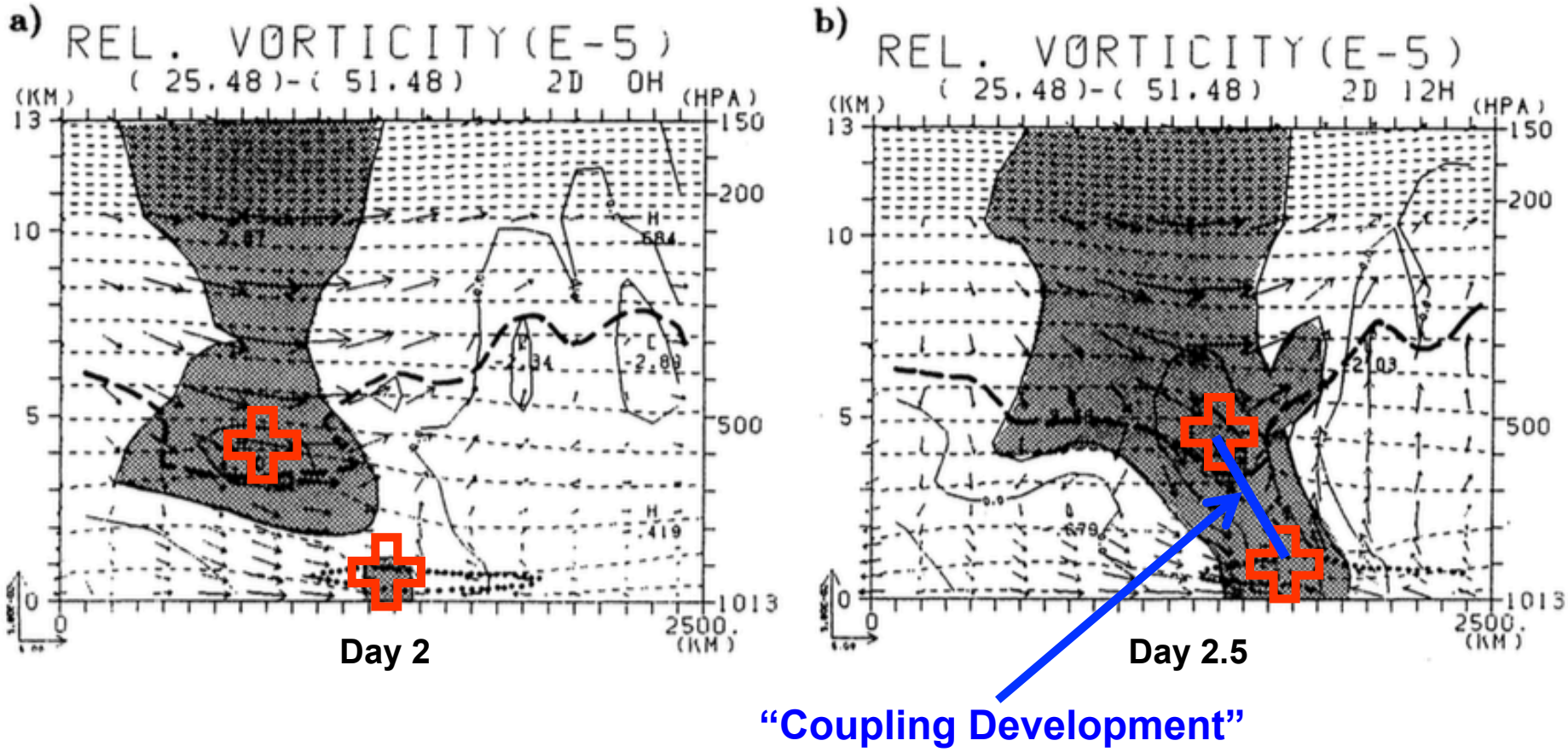

Zonal–height cross section at a latitude between upper and lower-level vortices (denoted by plus symbols). Potential temperature (thin dashed contours, every 5 K), relative vorticity (every 4×10^{-5} s^{-1}), motion along section (vectors). Thick solid line corresponding to tropopause represents 1.0 PVU surface and thick dotted line corresponding to low-level cyclonic PV anomaly represents 0.6 PVU surface.

The Arctic Tropopause Fold and Arctic Jet

Shapiro et al. (1987)

0000 UTC 20 January 1985

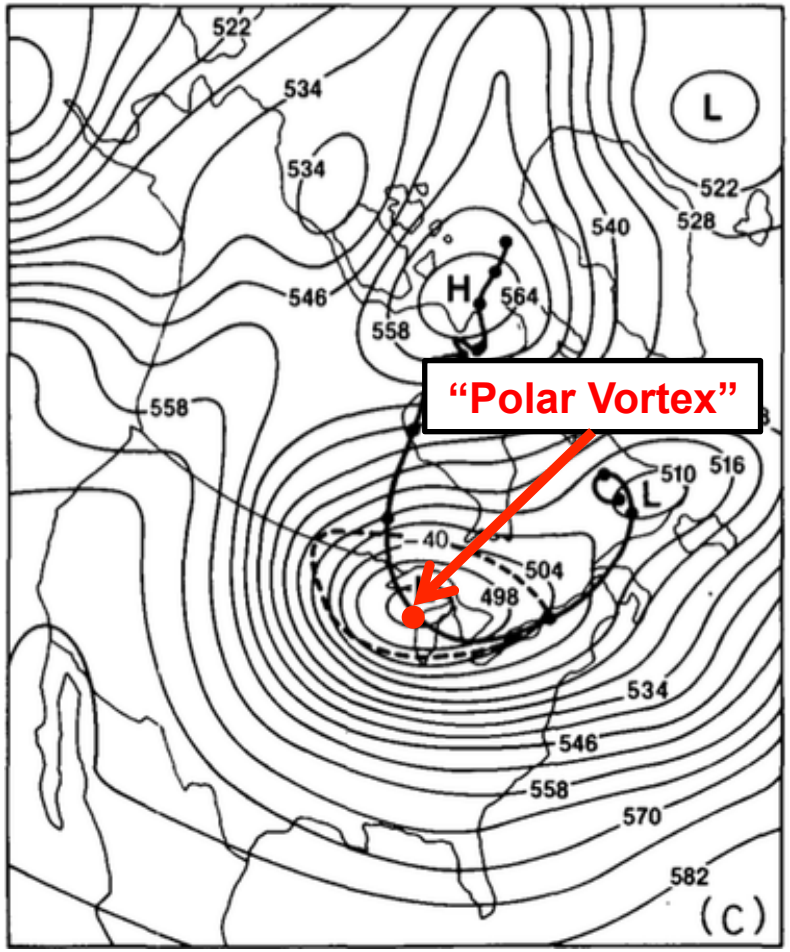

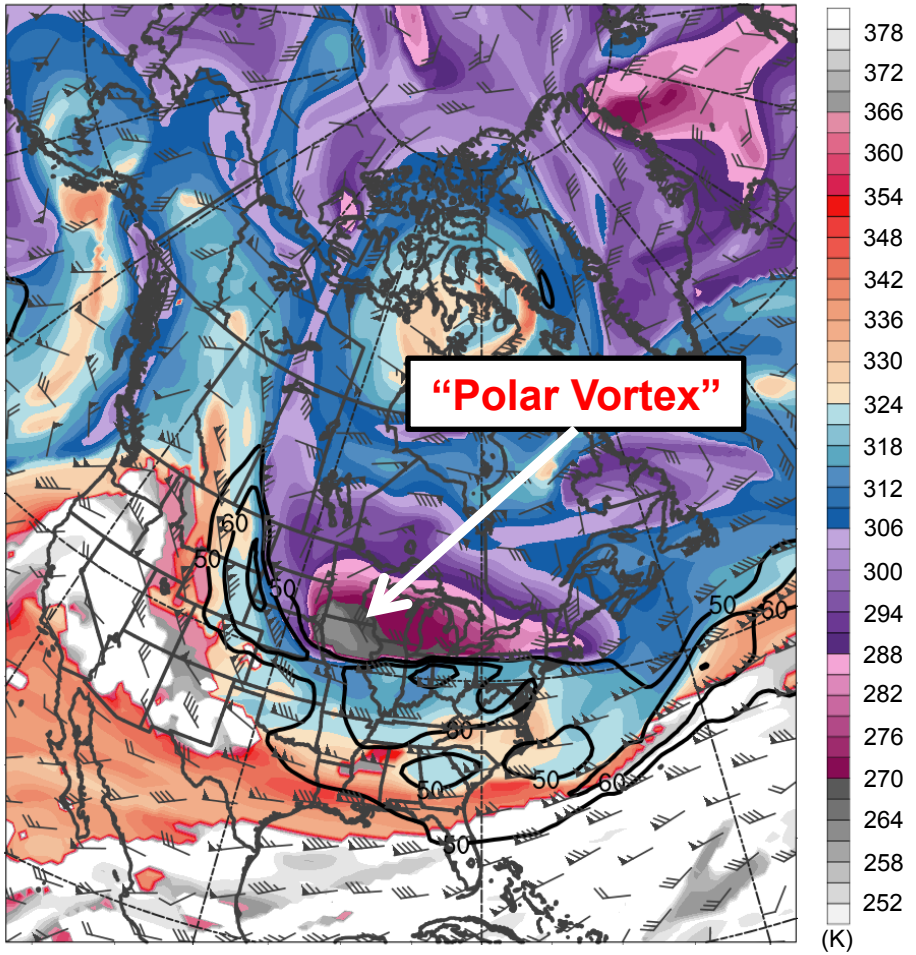

500-hPa geopotential height (black, every 6 dam) and −40°C isotherm (dashed contour); track of polar vortex from 0000 UTC 12 January to 0000 UTC 24 January 1985 (heavy black). Adapted from Fig. 5 in Shapiro et al. (1987).

Potential temperature (K, shaded), wind speed (black, every 10 m s^{-1} starting at 50 m s^{-1}), and wind (m s^{-1}, barbs) on 2-PVU surface. Plotted using 0.5° NCEP CFSR dataset.

The Arctic Tropopause Fold and Arctic Jet

Shapiro et al. (1987)

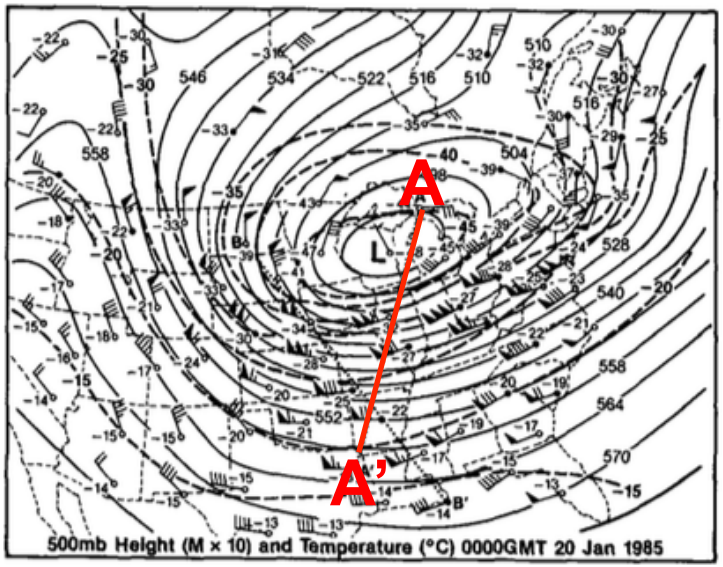

Adapted from Fig. 7 in Shapiro et al. (1987)

0000 UTC 20 January 1985

(upper left) 500-hPa geopotential height (dam, solid contours), temperature (°C, dashed contours), and wind (barbs and flags, m s^{-1}). (lower-left) Cross-section of potential temperature (K, thin solid), wind speed (m s^{-1}, heavy dashed contours), and wind (m s^{-1}, barbs and flags) between Sault Sainte Marie, MI and Longview, TX. Heavy solid line is tropopause (10^{-7} K s^{-1} hPa^{-1} isopleth of PV) and light dashed lines indicate tropospheric frontal and stable layer boundaries. (lower-right) "threefold" structure of tropopause where heavy line is PV discontinuity tropopause, shading is stratospheric air, and light dashed contours represent 40 m s^{-1} isotach.

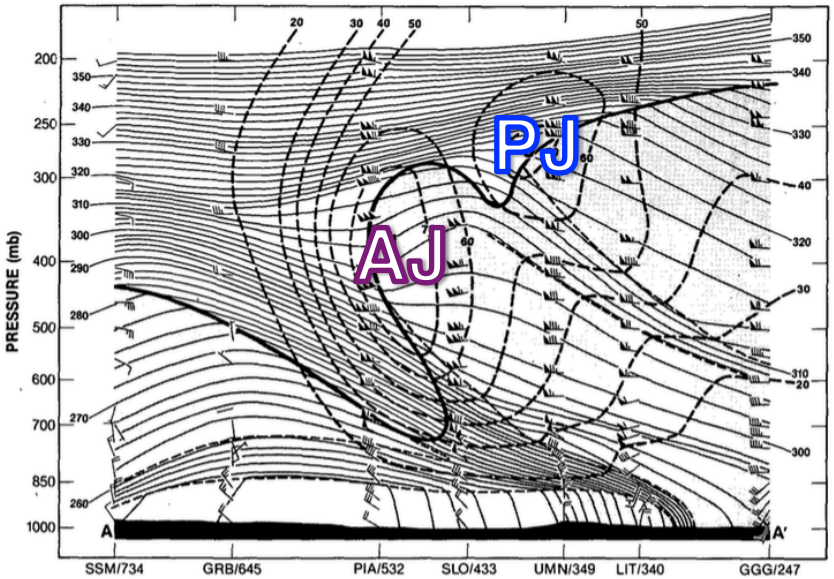

A Adapted from Fig. 9 in Shapiro et al. (1987) A'

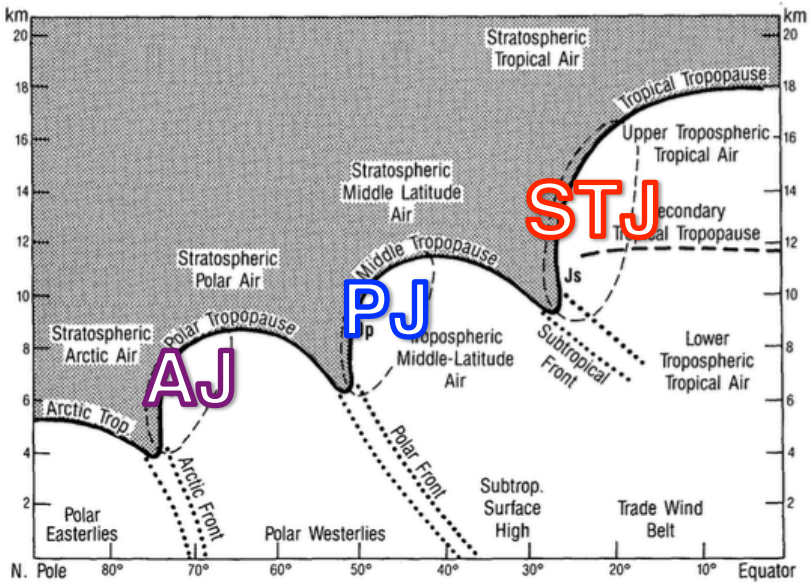

Adapted from Fig. 17 in Shapiro et al. (1987)

1978 Cleveland Superbomb

Hakim et al. (1995, 1996)

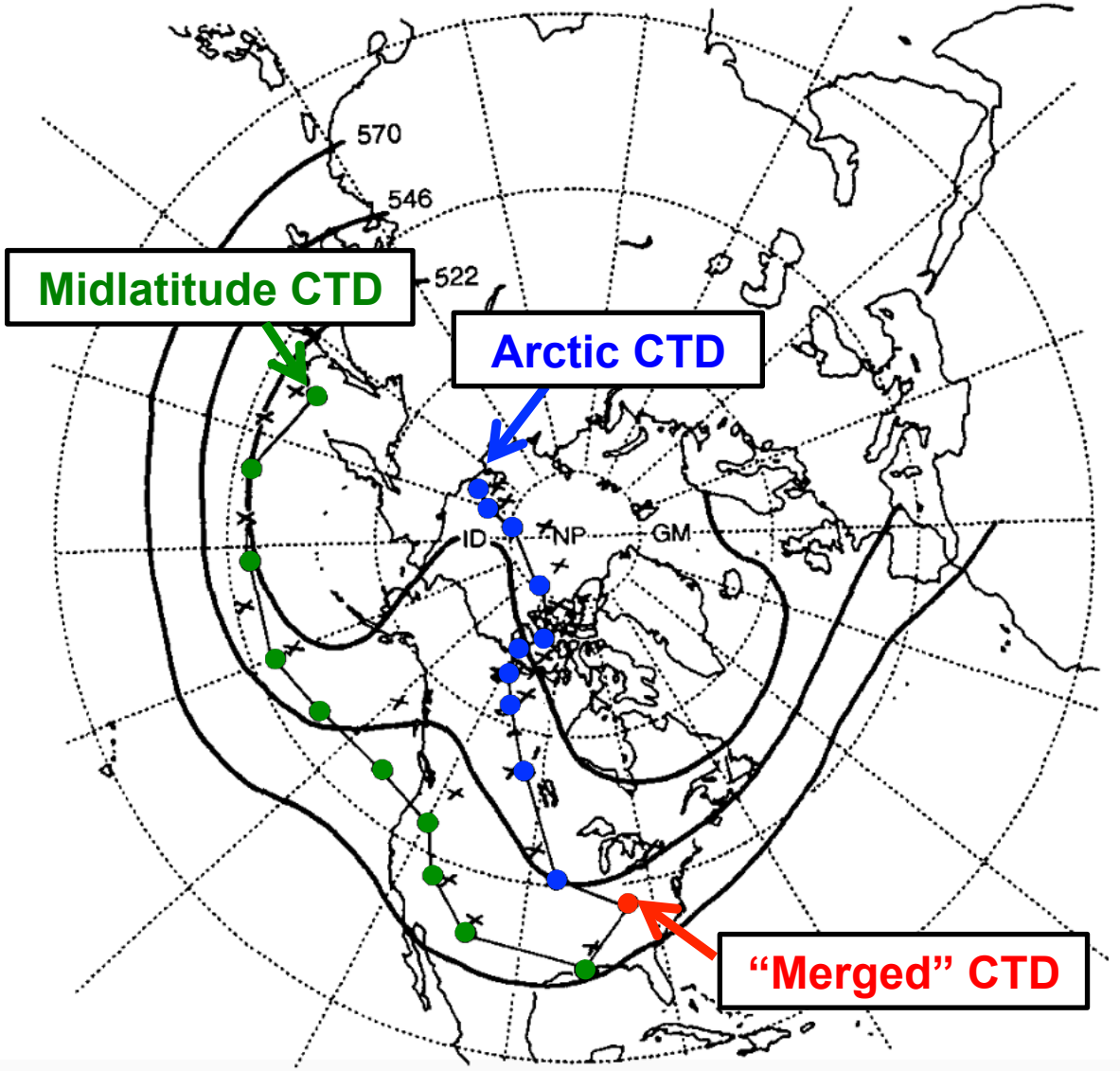

Position of QGPV maxima (colored dots) and 1000–500-hPa thickness minima (black crosses) every 24 h starting at 0000 UTC 17 January and ending 0000 UTC 27 January 1978; time-mean 500-hPa geopotential height field (black, contoured every 120 m) for 17–27 January 1978. Adapted from Fig. 3 in Hakim et al. (1995).

0000 UTC 25 January 1978

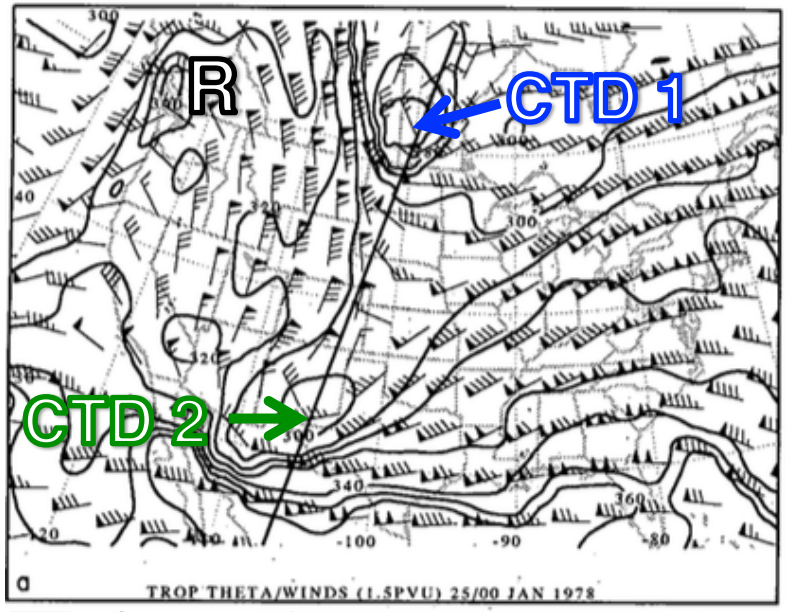

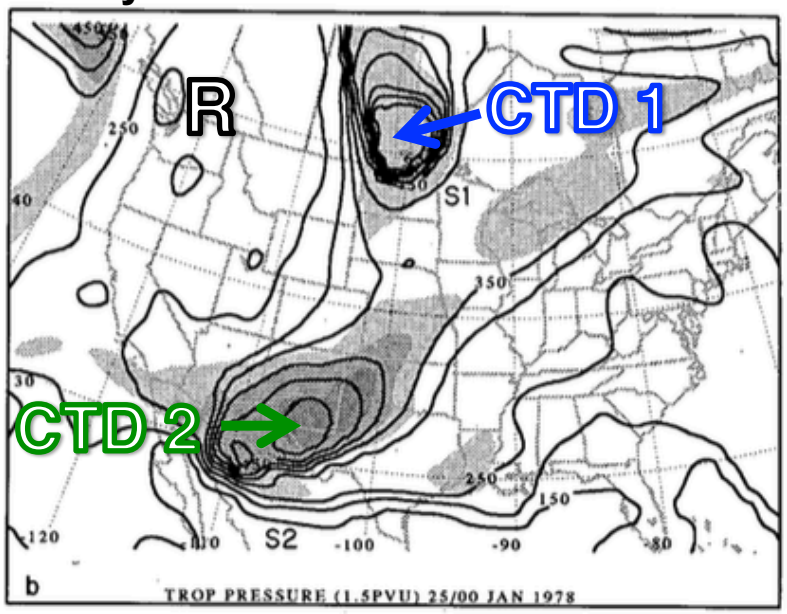

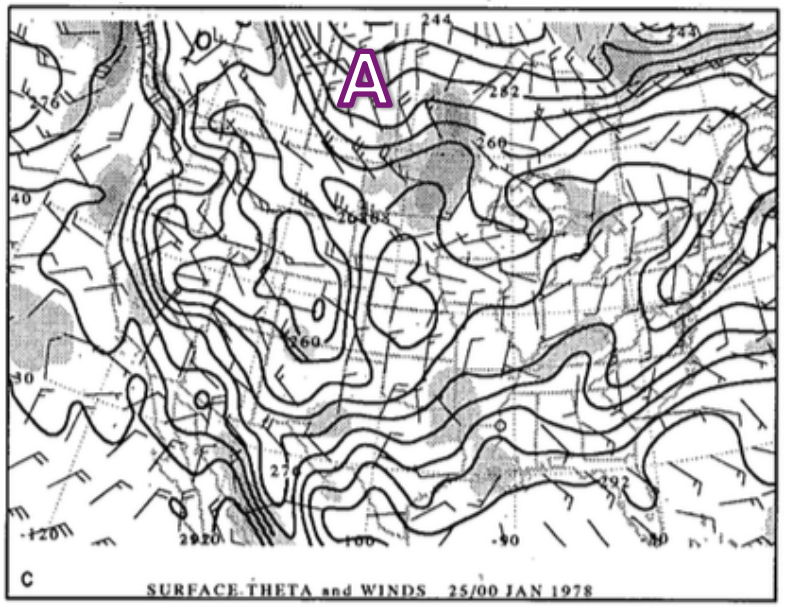

(a) Dynamic tropopause (DT; 1.5 PVU) potential temperature (black contours, every 10 K) and wind (flags and barbs, m s^{-1}); (b) DT pressure (black contours, every 50 hPa) and relative vorticity (shaded every 2×10^{-5} s^{-1} for values greater than 4×10^{-5} s^{-1}); (c) surface potential temperature (black contours, every 4 K) and relative vorticity (shaded every 2×10^{-5} s^{-1} for values greater than 2×10^{-5} s^{-1}). Adapted from Fig. 4 in Hakim et al. (1995).

1978 Cleveland Superbomb

Hakim et al. (1995, 1996)

1200 UTC 25 January 1978

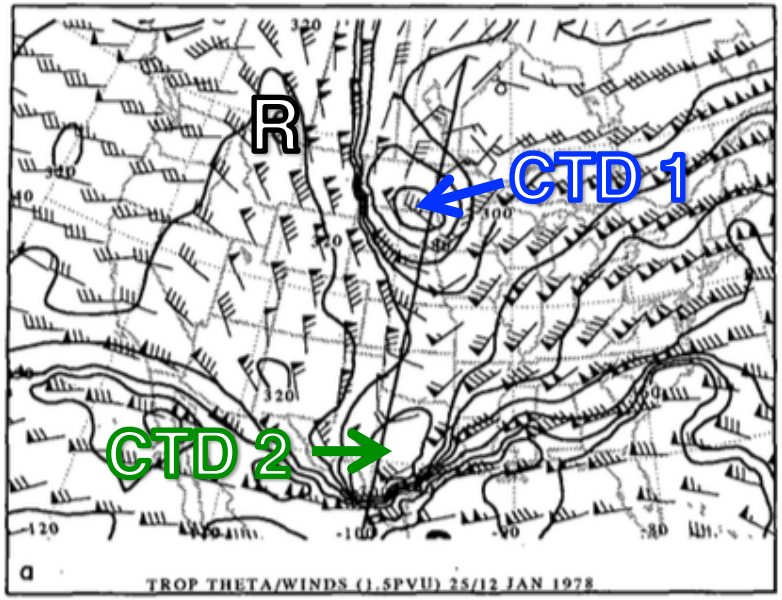

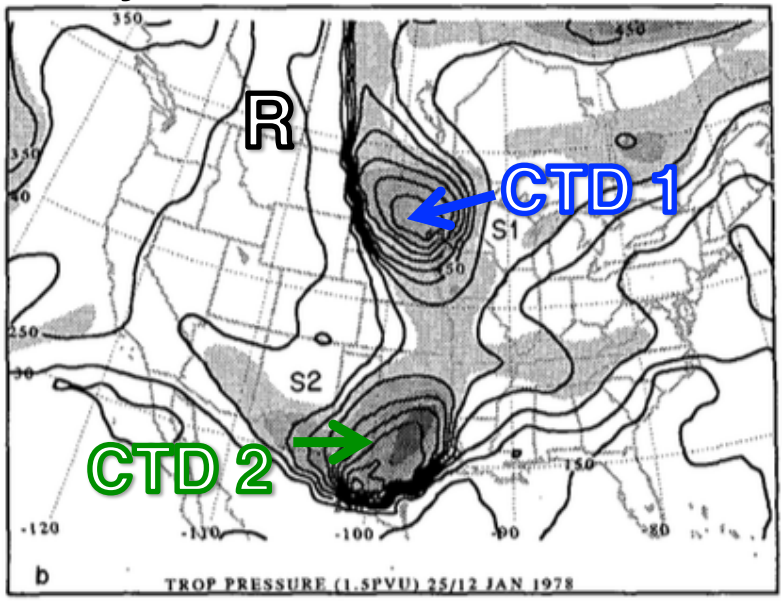

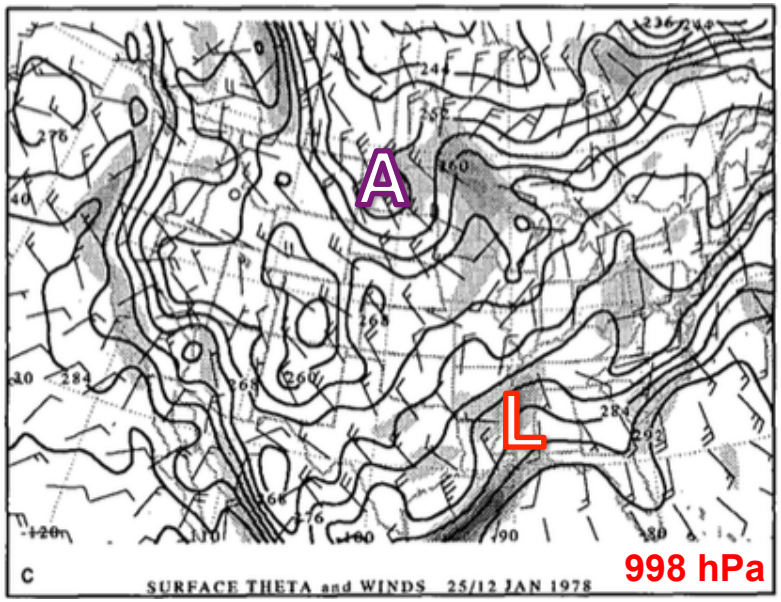

(a) Dynamic tropopause (DT; 1.5 PVU) potential temperature (black contours, every 10 K) and wind (flags and barbs, m s^{-1}); (b) DT pressure (black contours, every 50 hPa) and relative vorticity (shaded every 2×10^{-5} s^{-1} for values greater than 4×10^{-5} s^{-1}); (c) surface potential temperature (black contours, every 4 K) and relative vorticity (shaded every 2×10^{-5} s^{-1} for values greater than 2×10^{-5} s^{-1}). Adapted from Fig. 6 in Hakim et al. (1995).

1978 Cleveland Superbomb

Hakim et al. (1995, 1996)

0000 UTC 26 January 1978

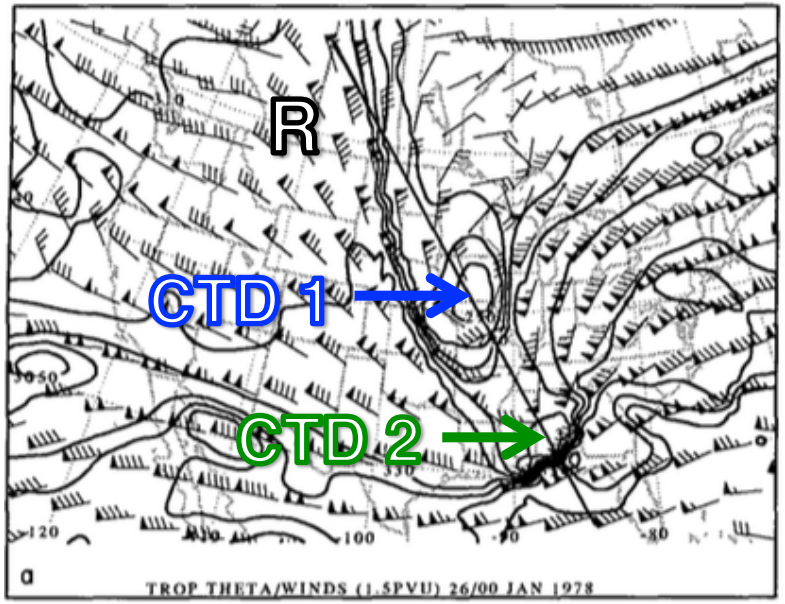

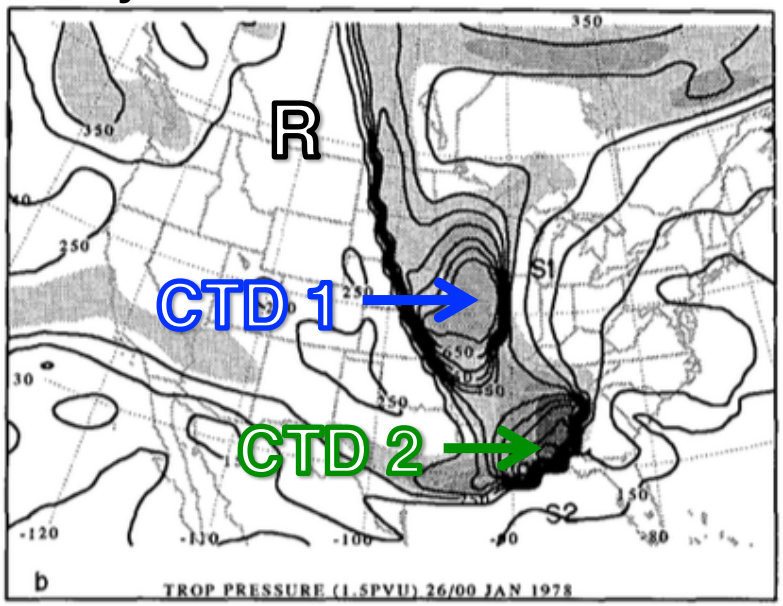

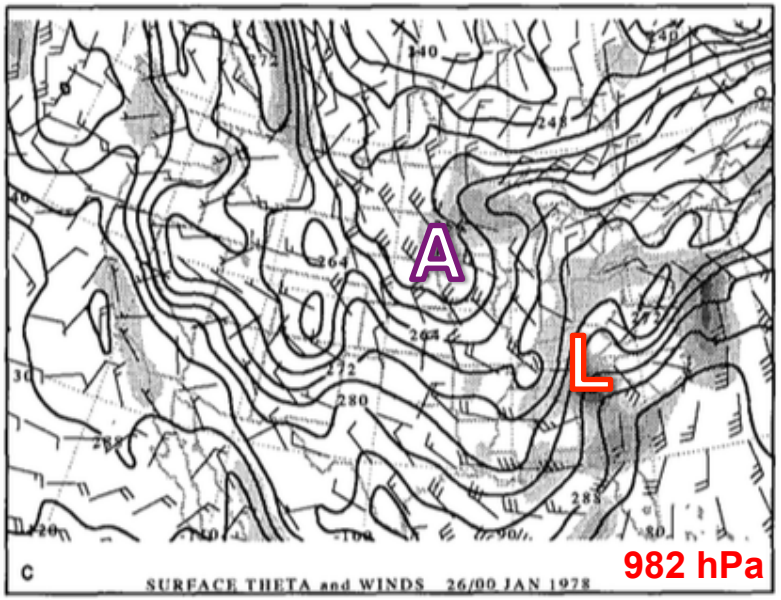

(a) Dynamic tropopause (DT; 1.5 PVU) potential temperature (black contours, every 10 K) and wind (flags and barbs, m s^{-1}); (b) DT pressure (black contours, every 50 hPa) and relative vorticity (shaded every 2×10^{-5} s^{-1} for values greater than 4×10^{-5} s^{-1}); (c) surface potential temperature (black contours, every 4 K) and relative vorticity (shaded every 2×10^{-5} s^{-1} for values greater than 2×10^{-5} s^{-1}). Adapted from Fig. 8 in Hakim et al. (1995).

1978 Cleveland Superbomb

Hakim et al. (1995, 1996)

1200 UTC 26 January 1978

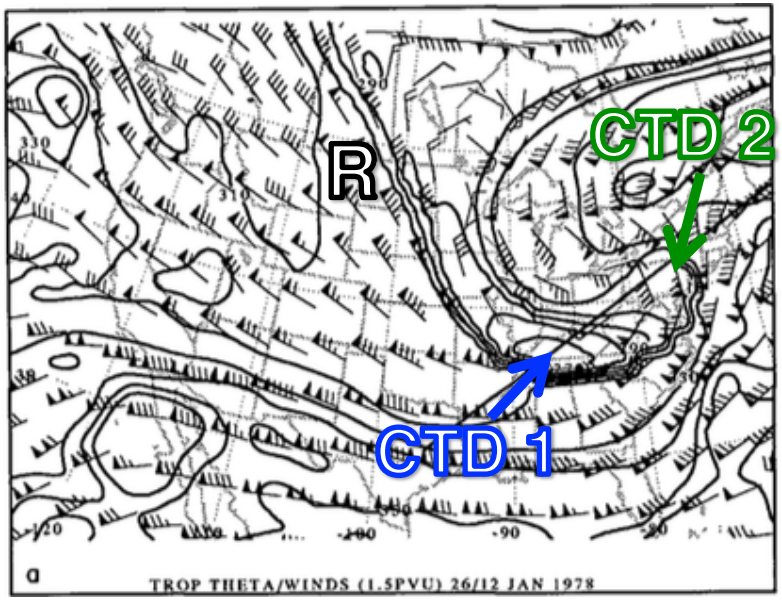

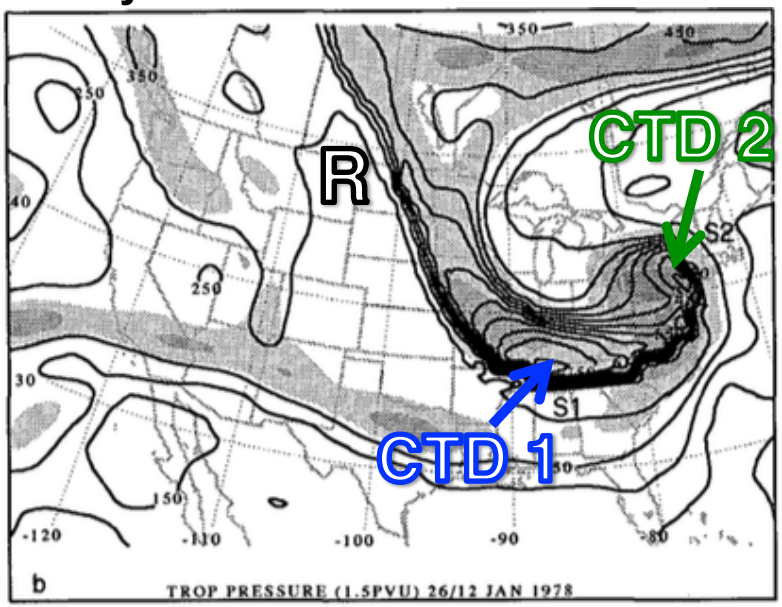

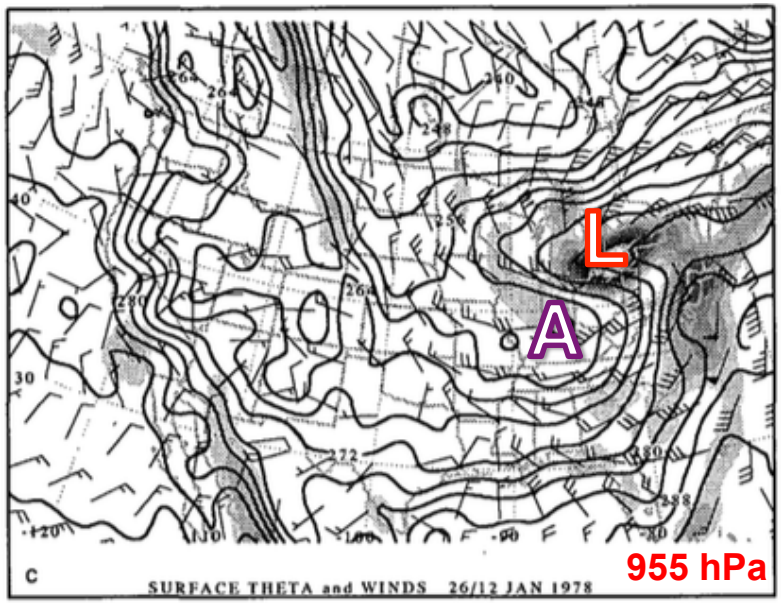

(a) Dynamic tropopause (DT; 1.5 PVU) potential temperature (black contours, every 10 K) and wind (flags and barbs, m s^{-1}); (b) DT pressure (black contours, every 50 hPa) and relative vorticity (shaded every 2×10^{-5} s^{-1} for values greater than 4×10^{-5} s^{-1}); (c) surface potential temperature (black contours, every 4 K) and relative vorticity (shaded every 2×10^{-5} s^{-1} for values greater than 2×10^{-5} s^{-1}). Adapted from Fig. 9 in Hakim et al. (1995).

Climatology of Coherent Disturbances on Tropopause

Hakim (2000)

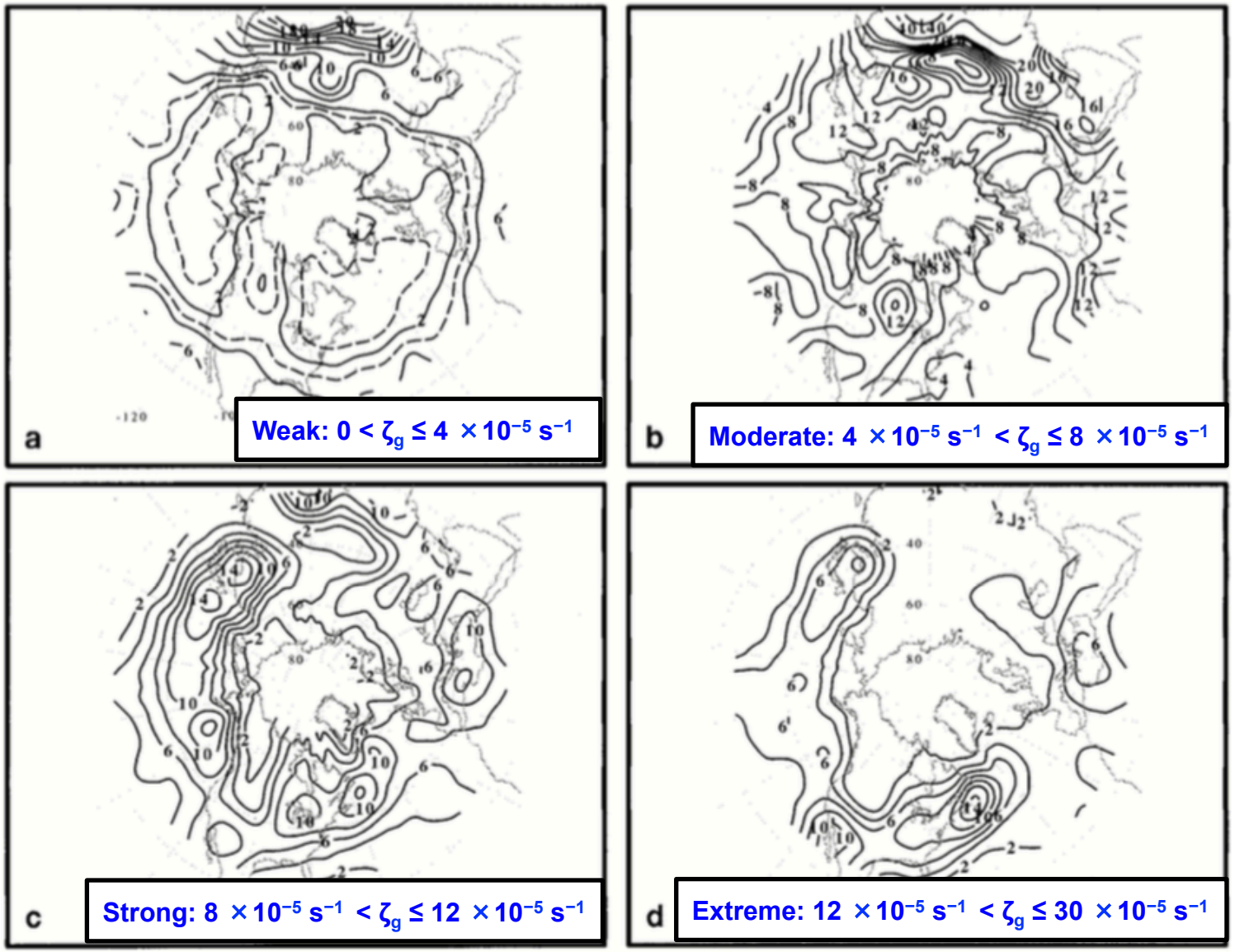

Percentage of date times with occurrences of 500-hPa geostrophic relative vorticity for DJF during 1957–87. Defined as ratio of total number of events occurring within a 10° × 10° box centered at each grid point to total number of data times. Data used is twice-daily NCEP gridded 500-hPa height. Adapted from Fig. 3 in Hakim (2000).

Climatology of Coherent Disturbances on Tropopause

Hakim (2000)

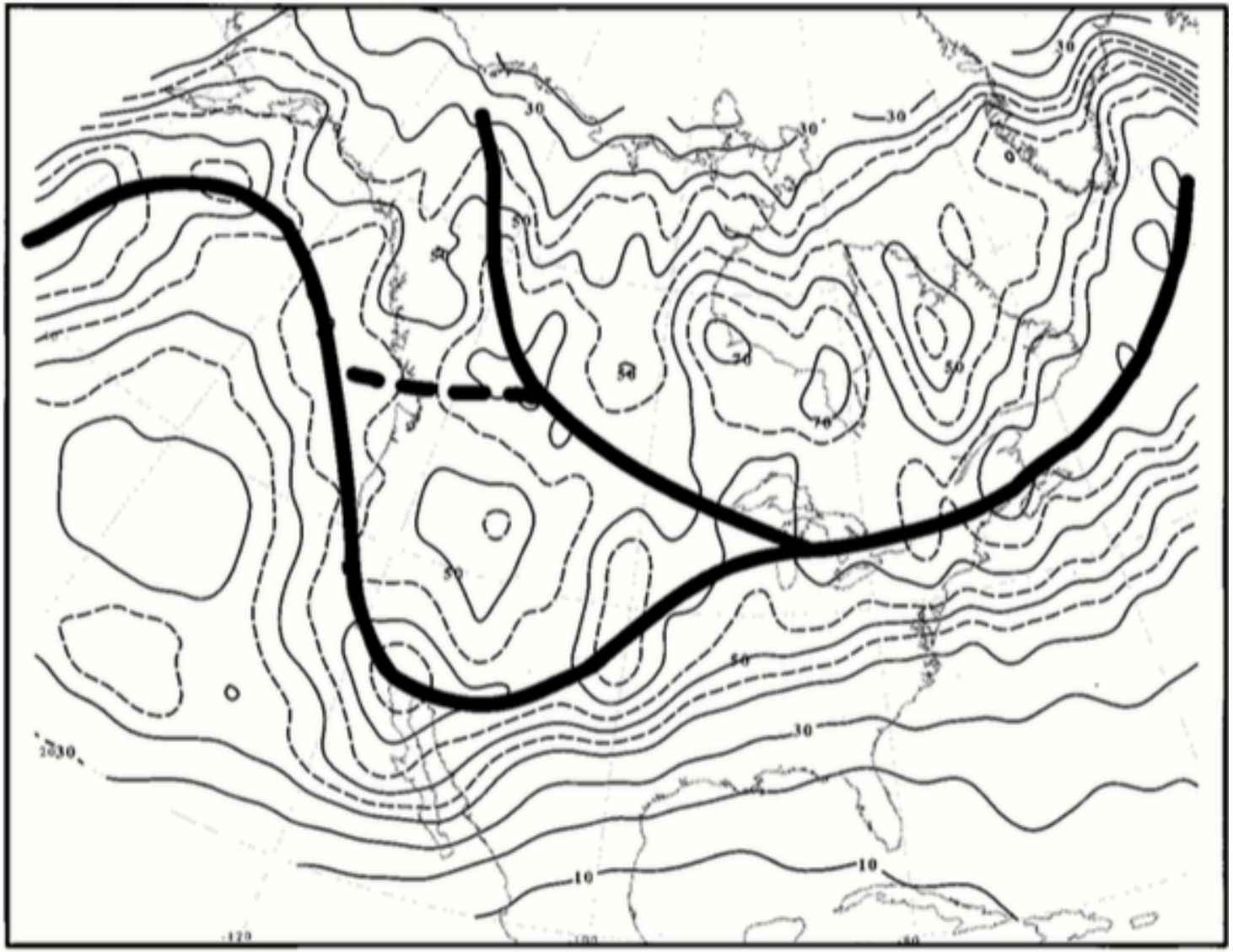

Percentage of 500-hPa vorticity maxima ($4–30 \times 10^{-5}$ s^{-1}) during ERICA period of Dec 1988–Feb 1989. Adapted from Fig. 7 in Hakim (2000).

Climatology of Coherent Disturbances on Tropopause

Hakim (2000)

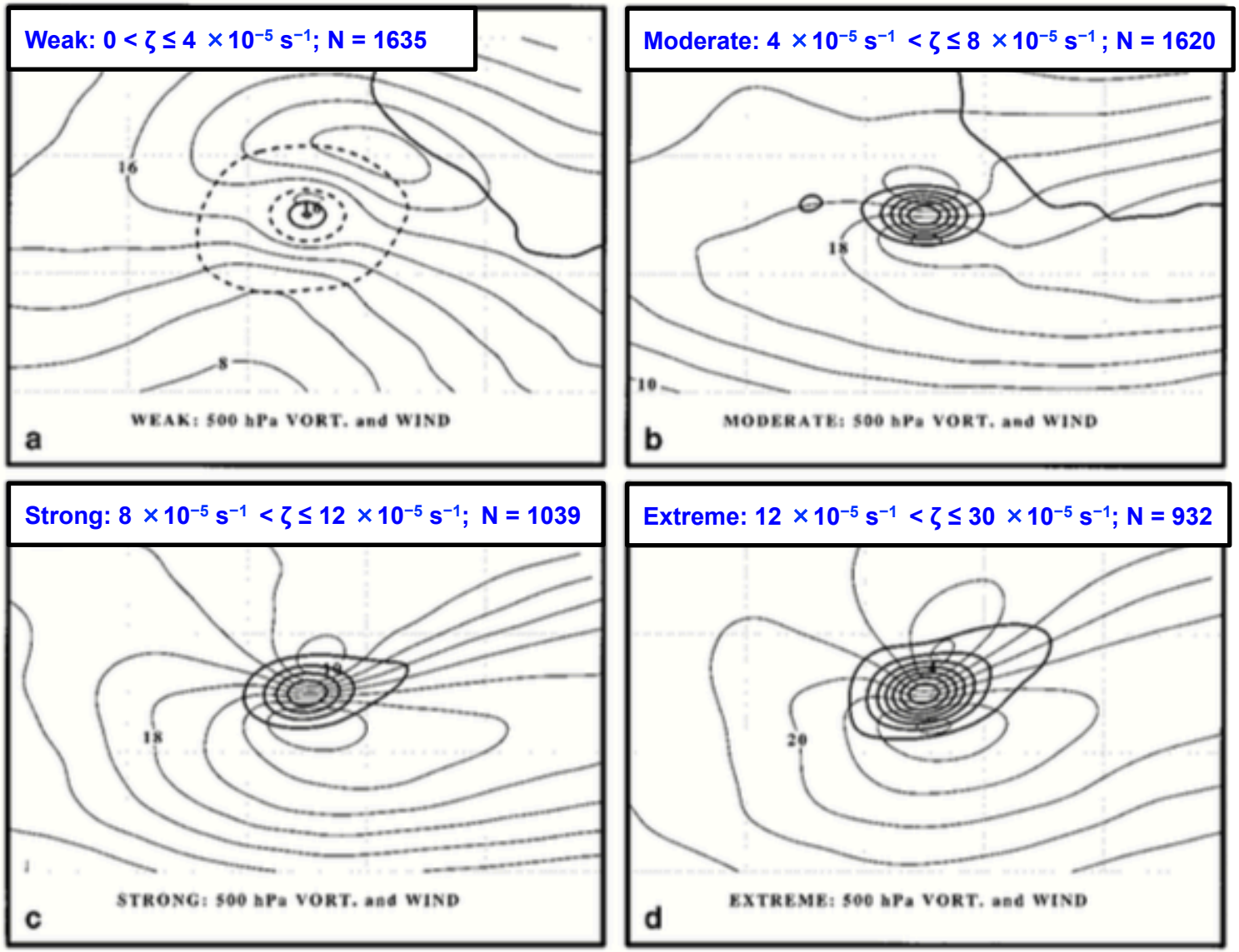

Mean 500-hPa total-wind relative vorticity (thick contours every 1×10^{-5} s^{-1} in top and every 2×10^{-5} s^{-1} in bottom) and total-wind speed (thing contours, every 4 m s^{-1}) for ERICA period of Dec 1988–Feb 1989. Data taken from ECMWF data assimilation system (1.125° × 1.125° interpolated to 1° × 1°). Adapted from Fig. 8 of Hakim (2000).

Climatology of Coherent Disturbances on Tropopause

Hakim (2000)

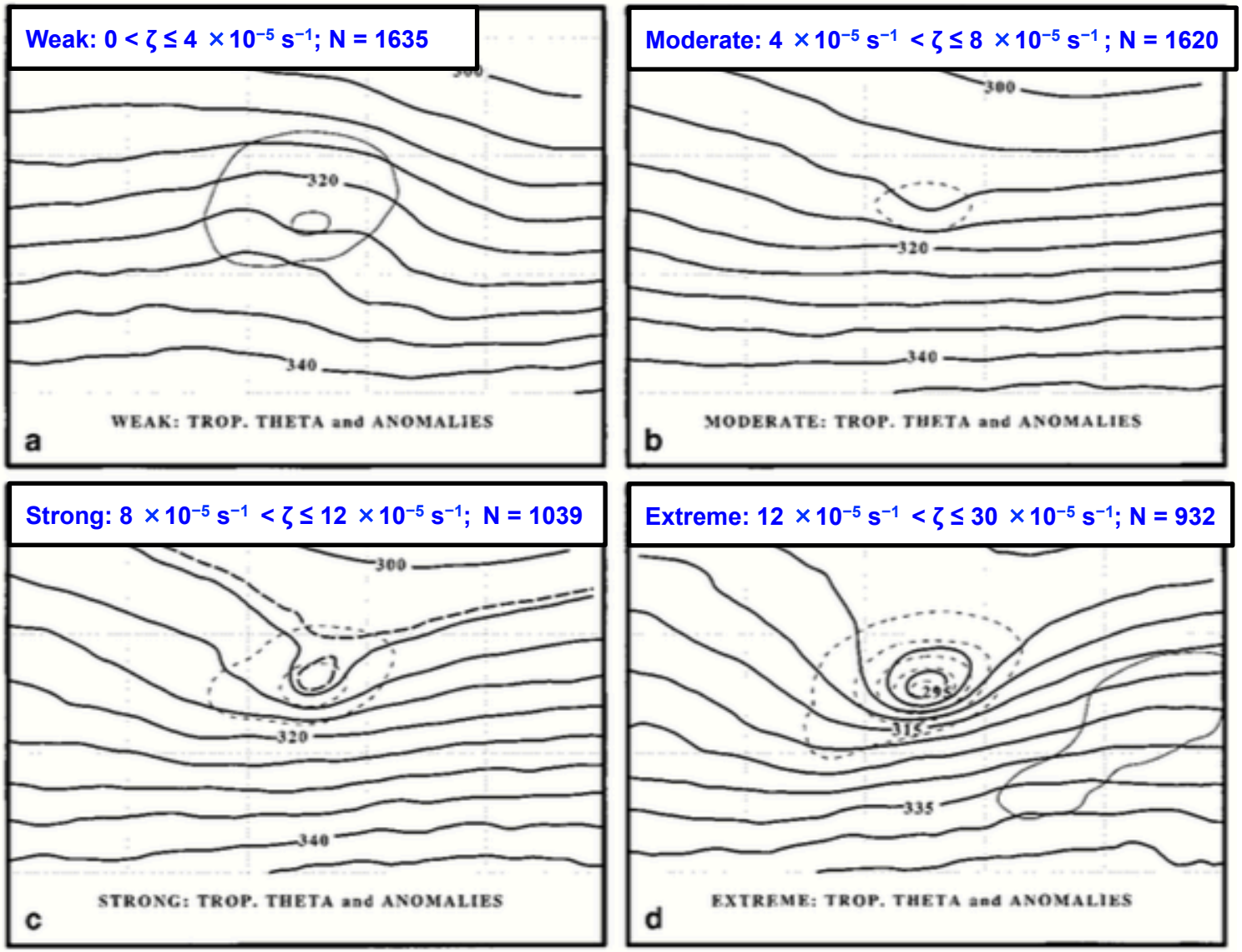

DT potential temperature (solid contours, every 5 K) and anomaly (thin lines every 4 K) for ERICA period of Dec 1988–Feb 1989. Data taken from ECMWF data assimilation system (1.125° × 1.125° interpolated to 1° × 1°). Adapted from Fig. 8 of Hakim (2000).

Climatology of Coherent Disturbances on Tropopause

Hakim (2000)

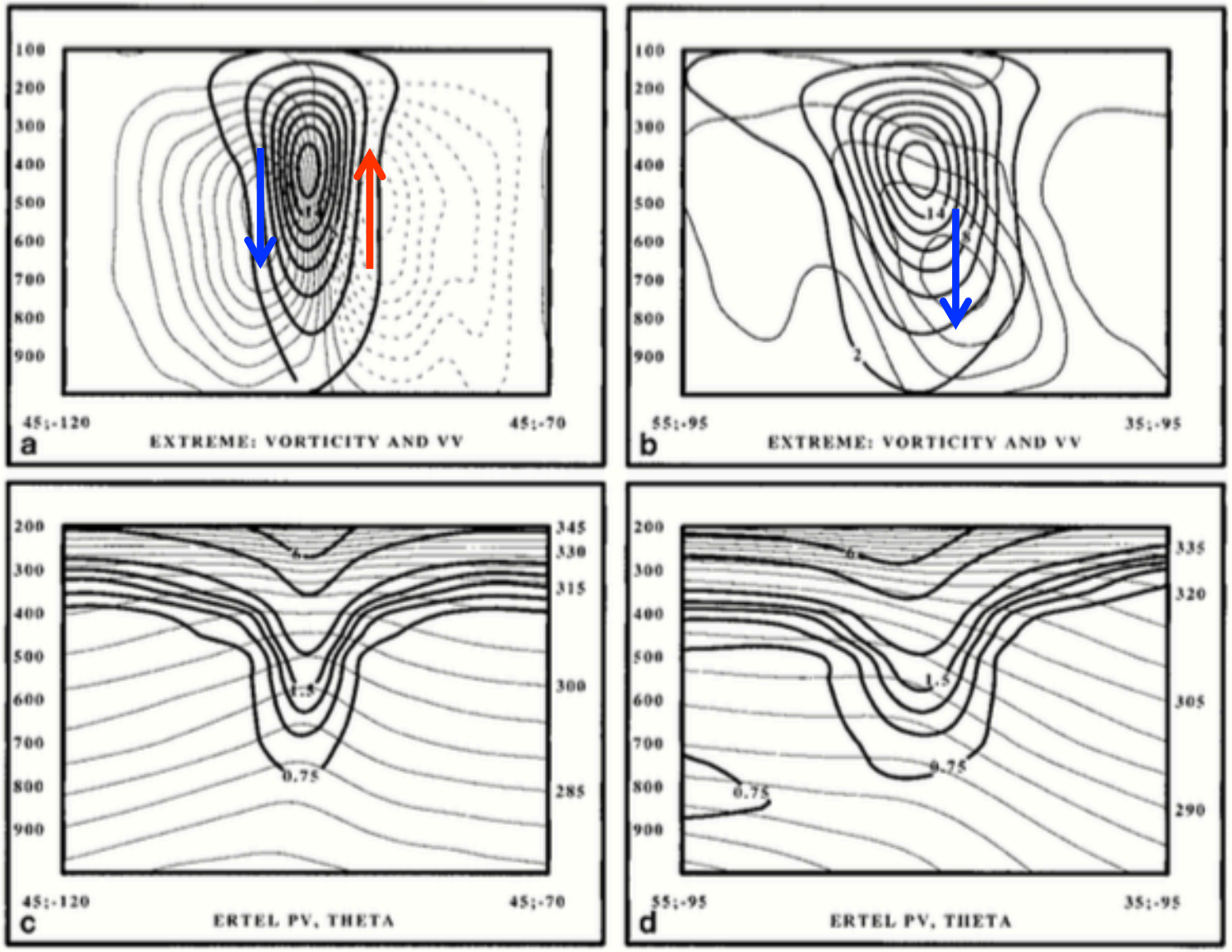

Cross sections of extreme vorticity maximum of (top) Relative vorticity (thick lines, every 2×10^{-5} s^{-1}) and vertical motion (thin lines, every 0.2×10^{-1} Pa s^{-1} and (bottom) EPV (thick lines, PVU) and potential temperature (thin lines, every 5 K). Cross sections are (left) zonal and (right) meridional. Adapted from Fig. 10 in Hakim (2000).

CTD–Jet Interaction

Pyle et al. (2004)

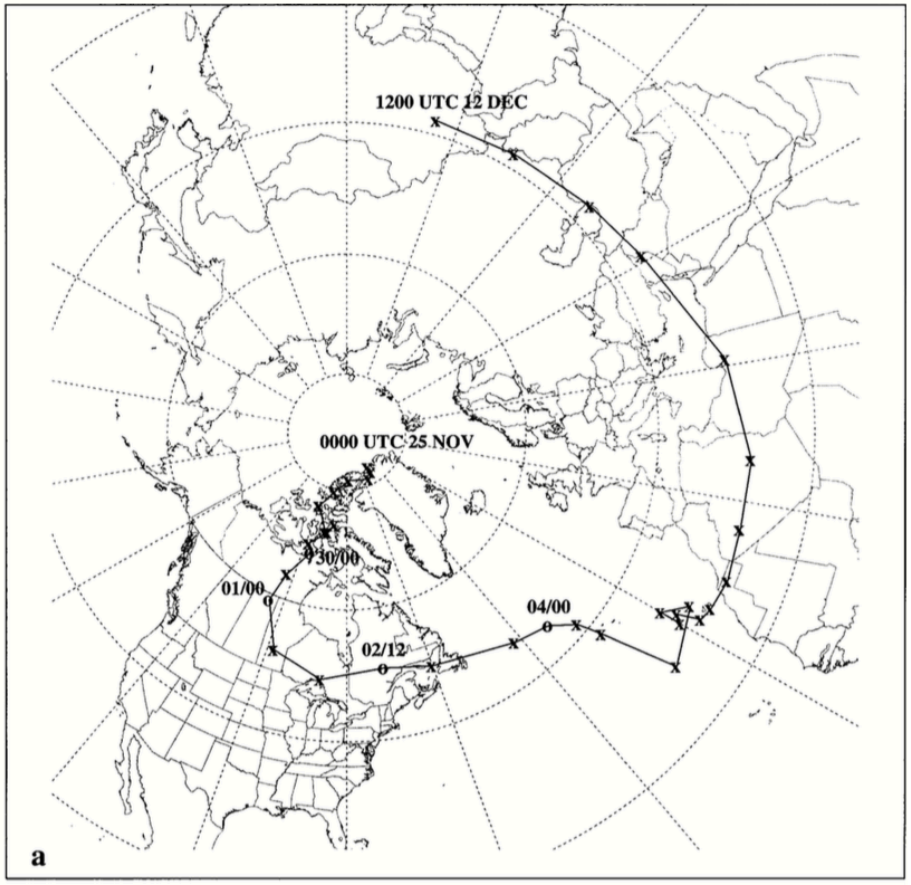

CTD track from 0000 UTC 25 Nov to 1200 UTC 26 Nov 1991. Adapted from Fig. 9 in Pyle et al. 2004.

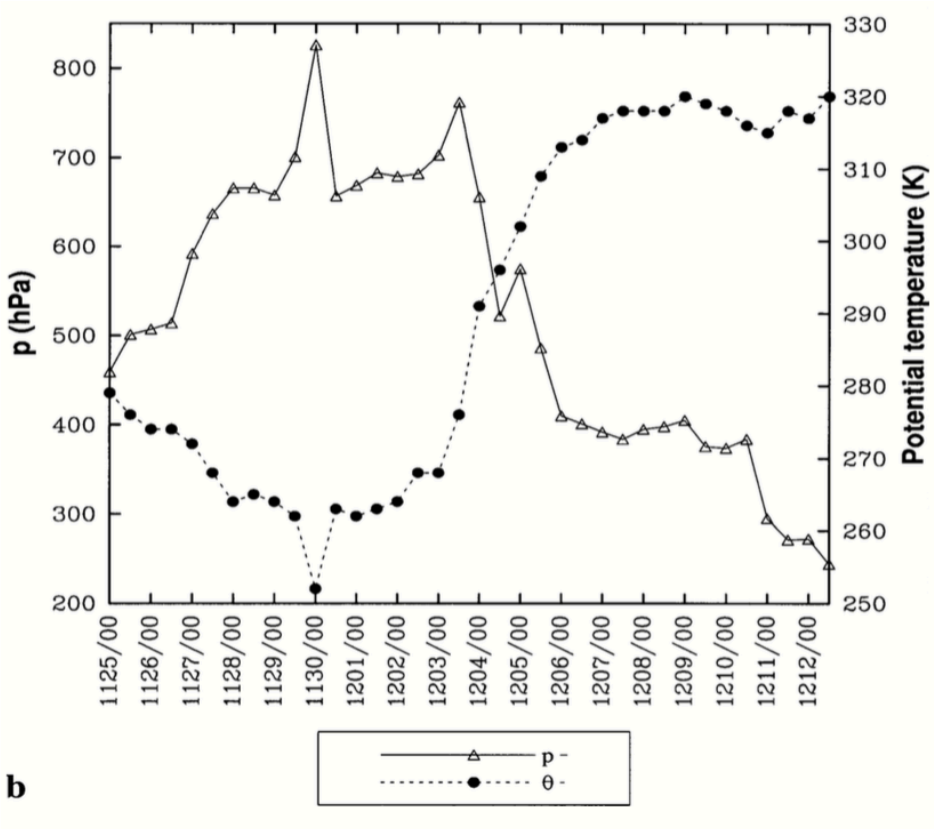

Time series of DT pressure maximum (hPa, triangles) and potential temperature minimum (K, circles) associated with CTD. Adapted from Fig. 9 in Pyle et al. 2004.

CTD–Jet Interaction

Pyle et al. (2004)

- TPV/CTD–jet interactions may lead to formation or intensification of a jet streak
- Gradient of DT potential temperature and pressure becomes locally enhanced as TPV/CTD closely approaches the waveguide/jet stream
- In the figure below, a TPV over northern Canada is separate from a jet streak (J1) upstream

0000 UTC 30 November 1991

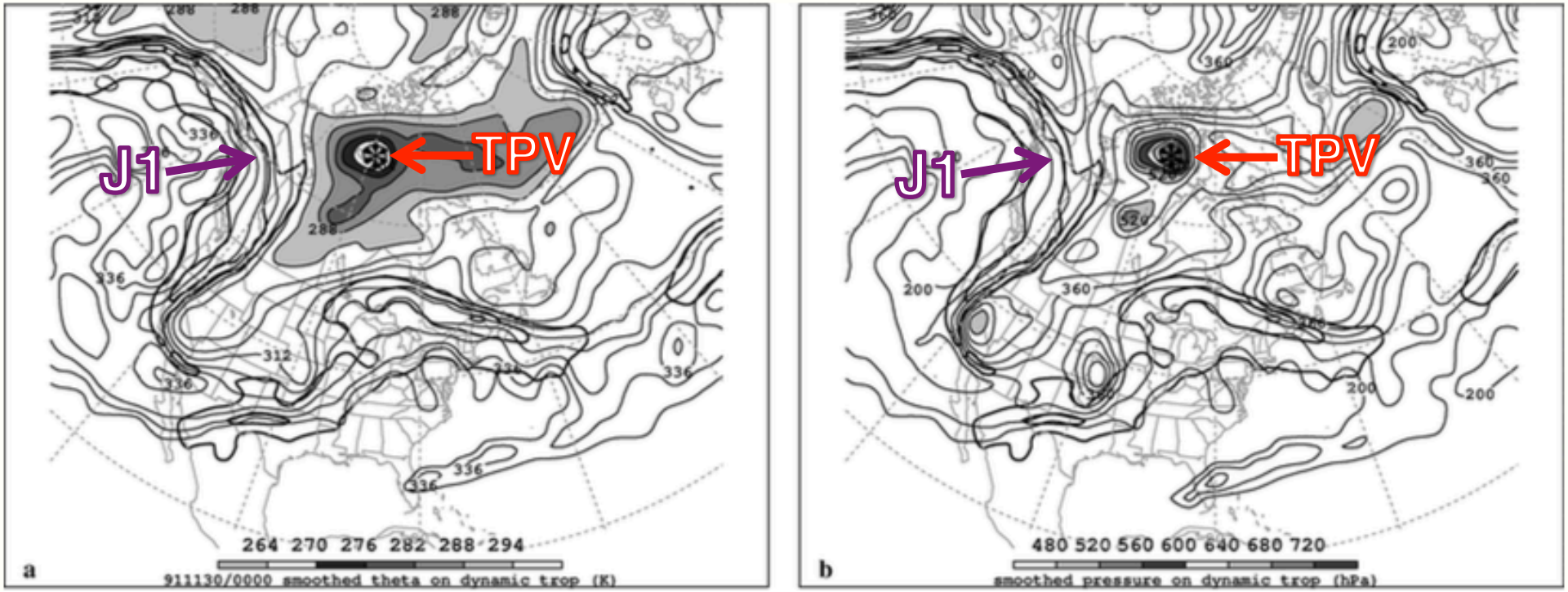

(left) DT (1.5-PVU surface) wind speed (every 15 m s^{-1} starting at 50 m s^{-1}, thick contours) and potential temperature (K, thin contours and shading); (right) same as left except DT pressure (hPa, thin contours and shading).
Adapted from Fig. 10 in Pyle et al. (2004).

CTD–Jet Interaction

Pyle et al. (2004)

- As TPV closely approaches J1, gradient in DT potential temperature and pressure strengthen in between these features, and J1 thus strengthens
- Jet Streak 2 (J2) forms over the central U.S.

0000 UTC 1 December 1991

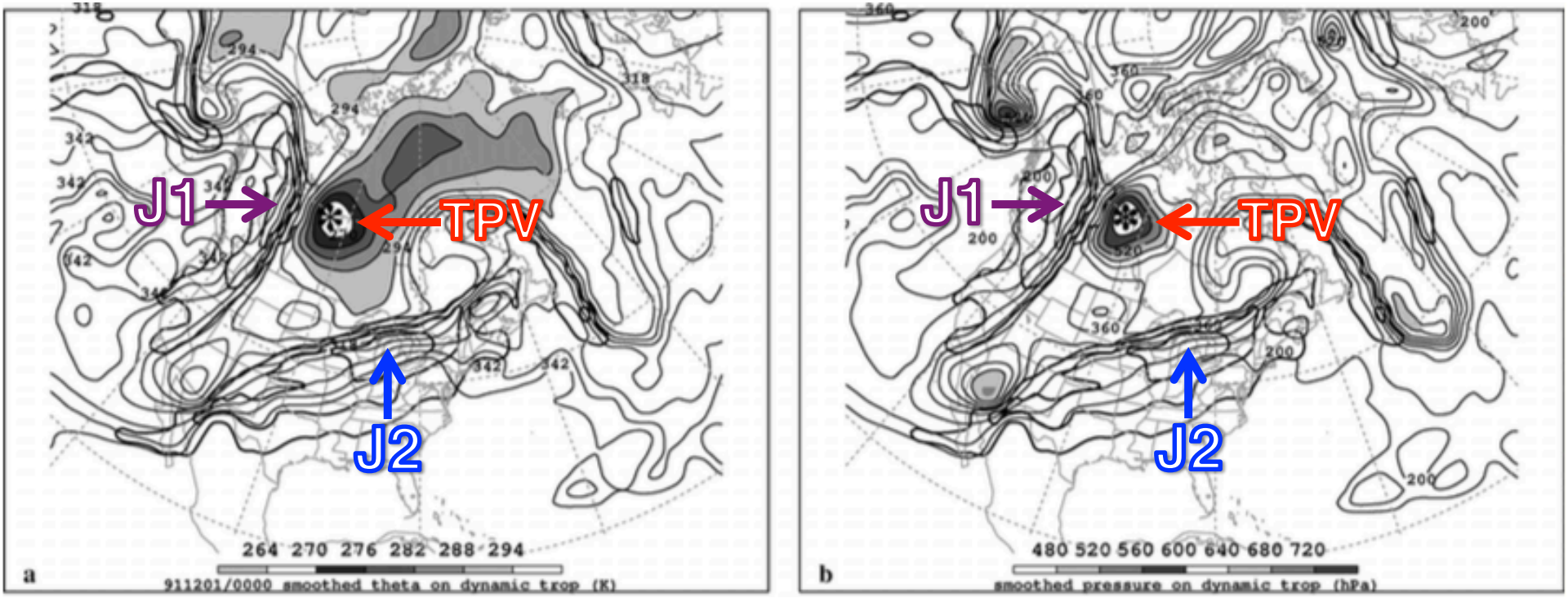

(left) DT (1.5-PVU surface) wind speed (every 15 m s^{-1} starting at 50 m s^{-1}, thick contours) and potential temperature (K, thin contours and shading); (right) same as left except DT pressure (hPa, thin contours and shading).
Adapted from Fig. 11 in Pyle et al. (2004).

CTD–Jet Interaction

Pyle et al. (2004)

- J1 weakens as the TPV shifts away from J1
- TPV has come into close proximity with J2
- J2 has strengthened from 91 to 104 m s^{-1} over past 36 hours (not shown)
- High, localized DT pressure maxima associated with TPV suggest tropopause folding beneath J2 (not shown)

1200 UTC 2 December 1991

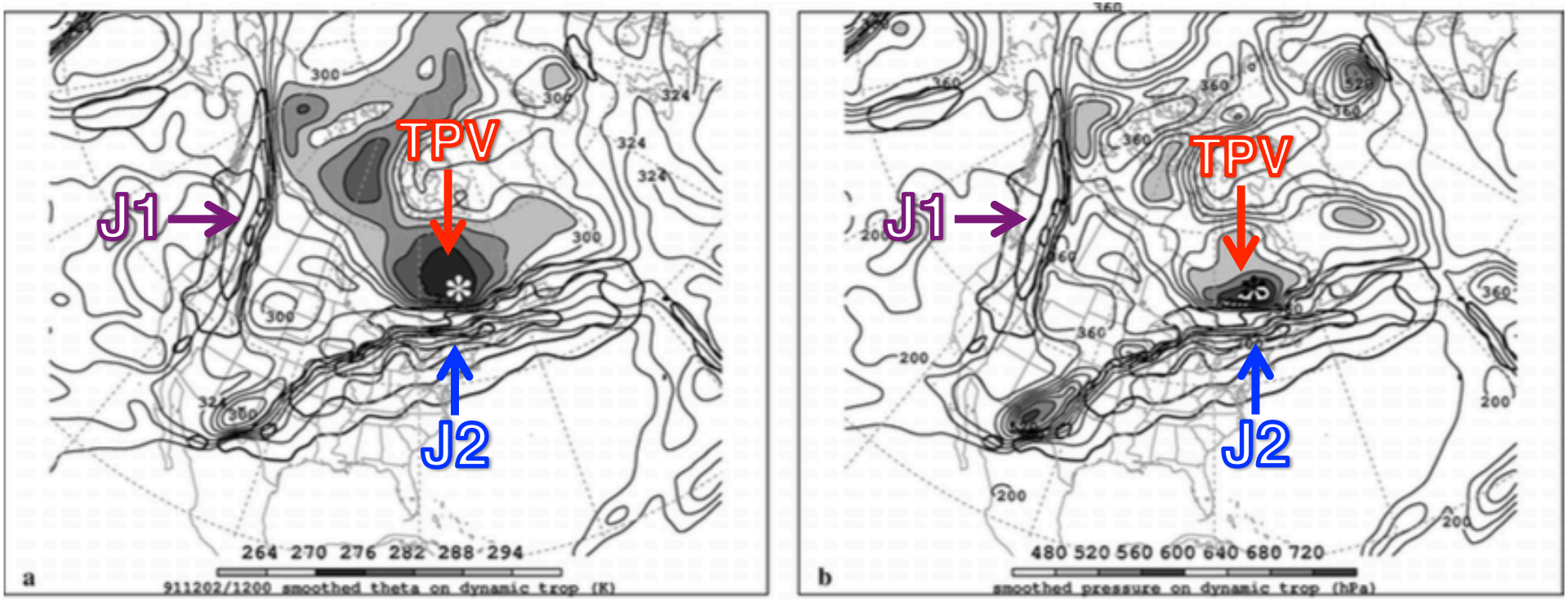

(left) DT (1.5-PVU surface) wind speed (every 15 m s^{-1} starting at 50 m s^{-1}, thick contours) and potential temperature (K, thin contours and shading); (right) same as left except DT pressure (hPa, thin contours and shading).
Adapted from Fig. 12 in Pyle et al. (2004).

CTD–Jet Interaction

Pyle et al. (2004)

- Strong horizontal shear associated with midlatitude jets may lead to deformation and/or destruction of TPVs
- There is a double structure in DT pressure field, indicating fracture of the TPV

0000 UTC 4 December 1991

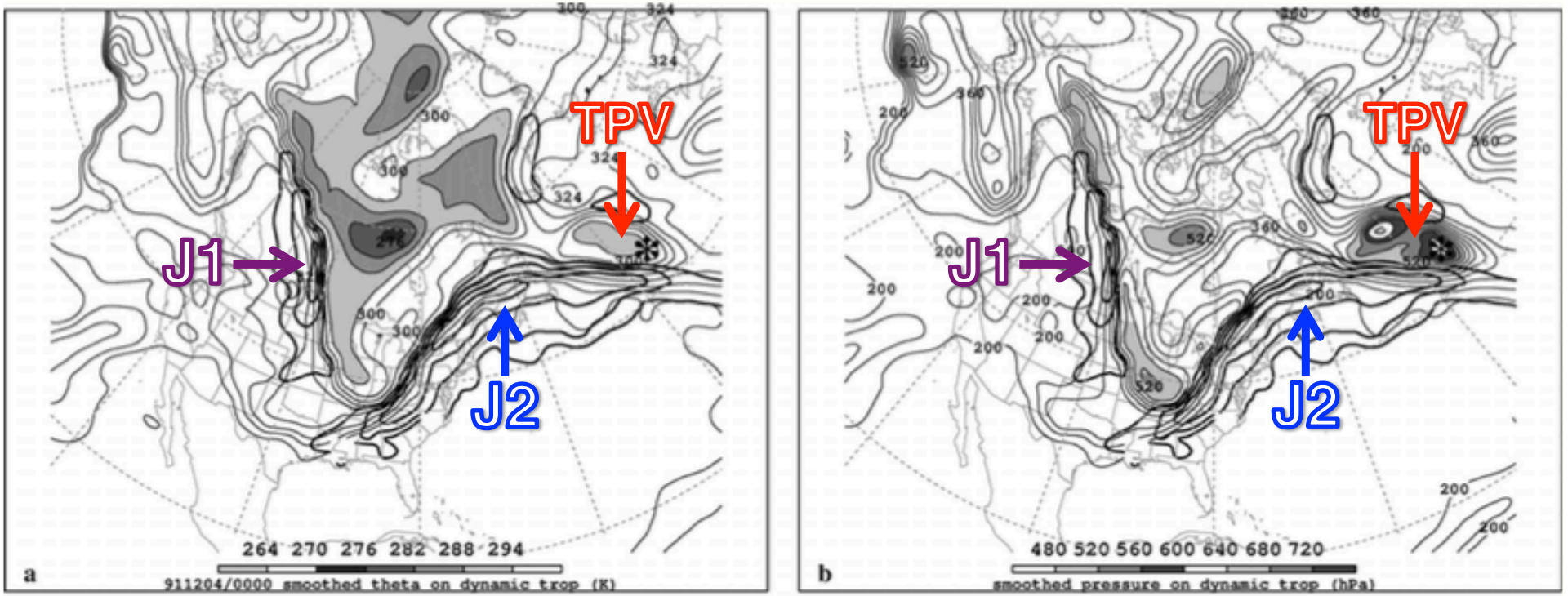

(left) DT (1.5-PVU surface) wind speed (every 15 m s^{-1} starting at 50 m s^{-1}, thick contours) and potential temperature (K, thin contours and shading); (right) same as left except DT pressure (hPa, thin contours and shading).
Adapted from Fig. 13 in Pyle et al. (2004).

CTD/TPV Tracking and Climatology

Hakim and Canavan (2005)

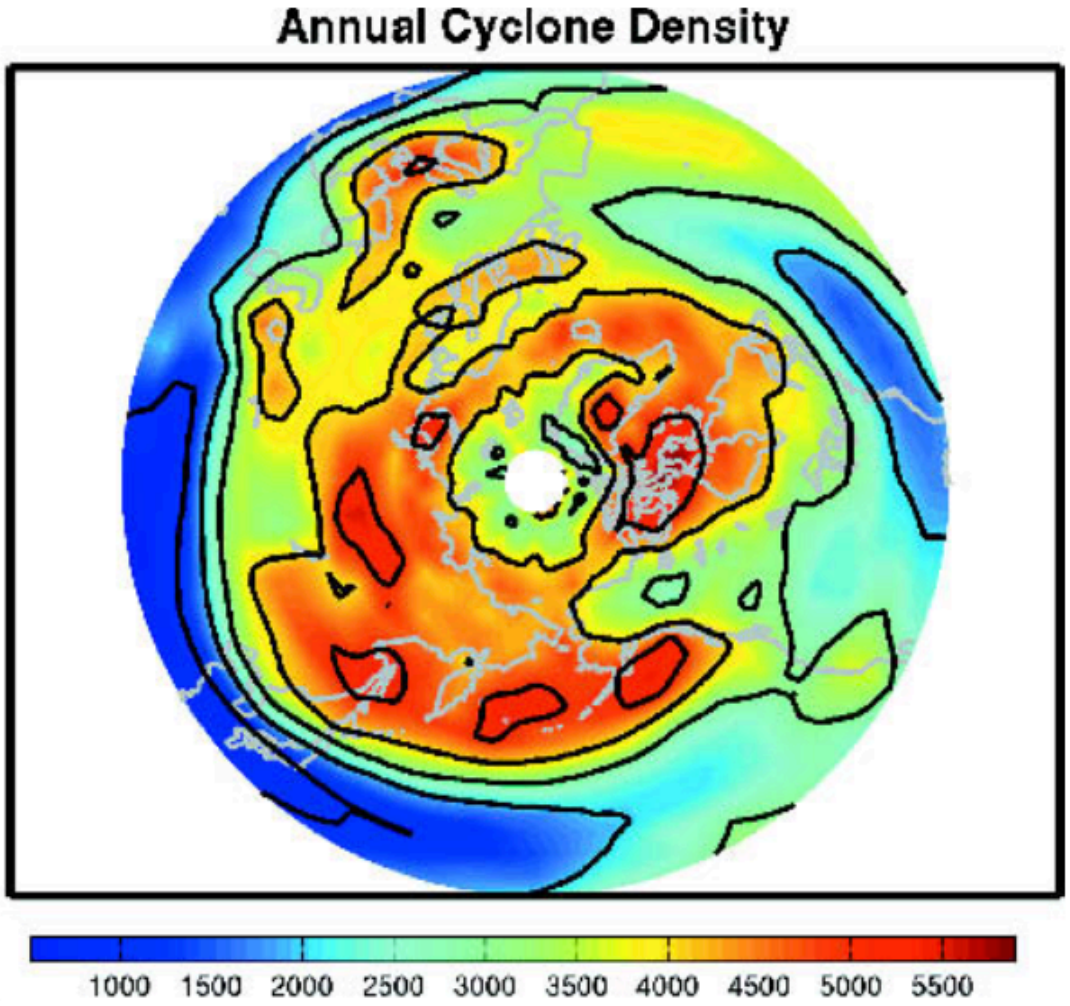

Total number of tropopause cyclonic vortex events. Adapted from Fig. 2 of Hakim and Canavan (2005).

- Utilized 2.5° NCEP–NCAR reanalysis dataset from 1948 through 1999 to track CTDs (including TPVs)
- Tracking algorithm finds local minimum of potential temperature along DT (1.5 PVU surface in this study)
- Grid point is local minimum in DT θ if DT θ value is smaller than any other point within 650 km of grid point
- Last closed contour identified by scanning outward from vortex core along eight equally spaced radials until gradient in DT θ changes and choosing the minimum of these eight DT θ values

CTD/TPV Tracking and Climatology

Hakim and Canavan (2005)

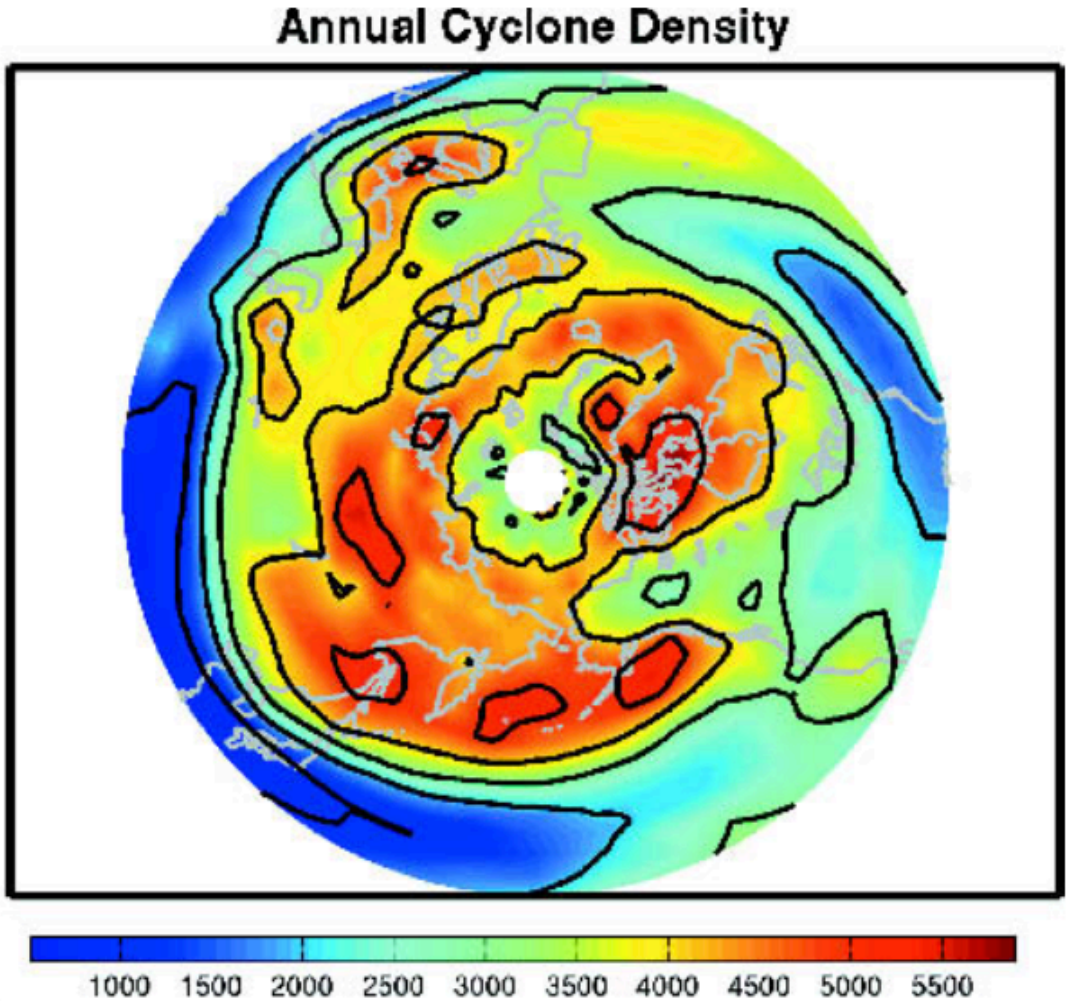

Total number of tropopause cyclonic vortex events. Adapted from Fig. 2 of Hakim and Canavan (2005).

- Vortex track extended from time t_0 to time t_0 + 6 h if another vortex located within 600 km of vortex at time t_0
- If not, retested at t_0 + 12 h; failure to extend track defines a lysis event
- Vortex at time t_0 + 6 h that is unmatched with vortex at time t_0 is marked as a genesis event

CTD/TPV Tracking and Climatology

Hakim and Canavan (2005)

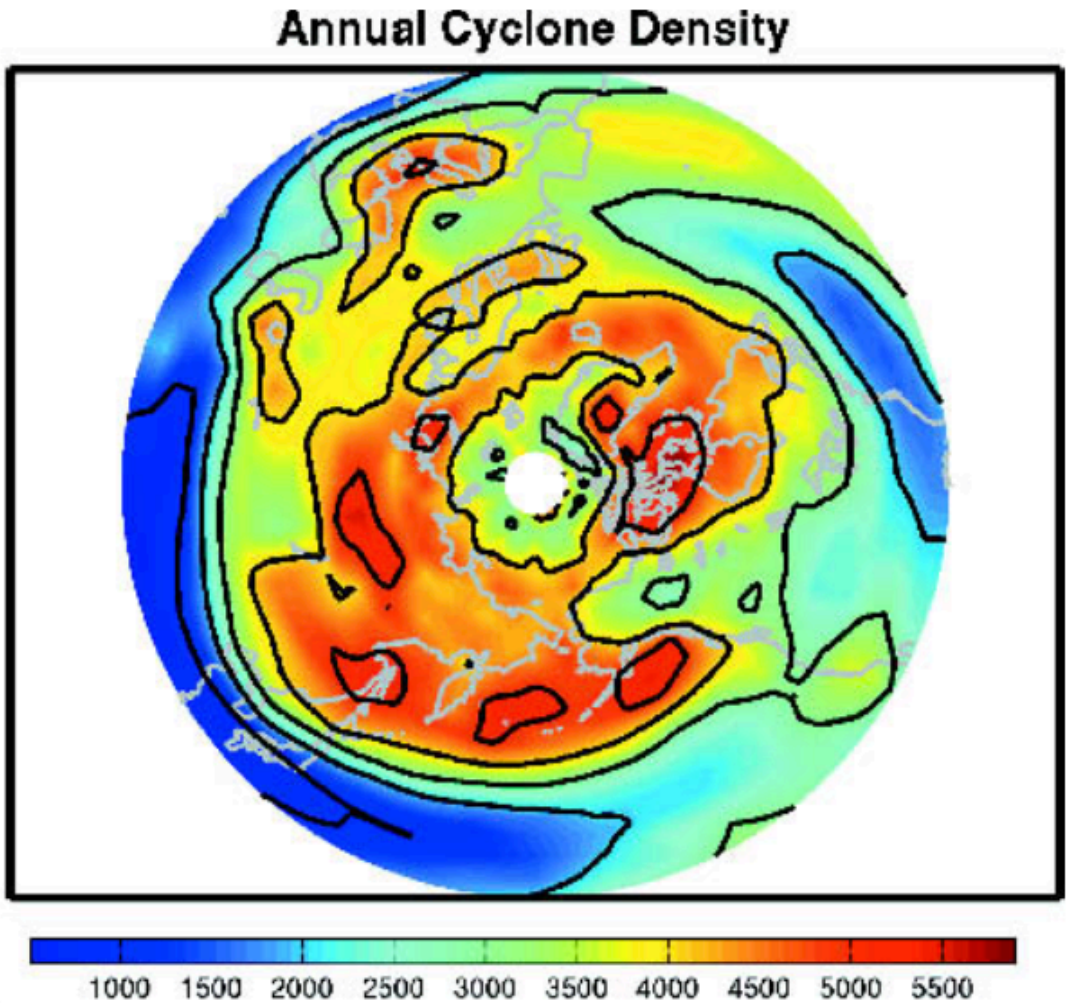

Total number of tropopause cyclonic vortex events. Adapted from Fig. 2 of Hakim and Canavan (2005).

- Total of 1,576,732 cyclones identified
- Identified cyclones correspond to 310,605 cyclone tracks
- Preferred cyclone locations:
  - Cyclonic shear side of jets
  - Canadian Arctic
  - Russia
  - Mediterranean Sea through the Middle East
- 126,522 arctic cyclones (i.e. TPVs) identified
- 9032 TPV tracks (average of 15 cyclones per month

TPV Composite Structure

Cavallo and Hakim (2010)

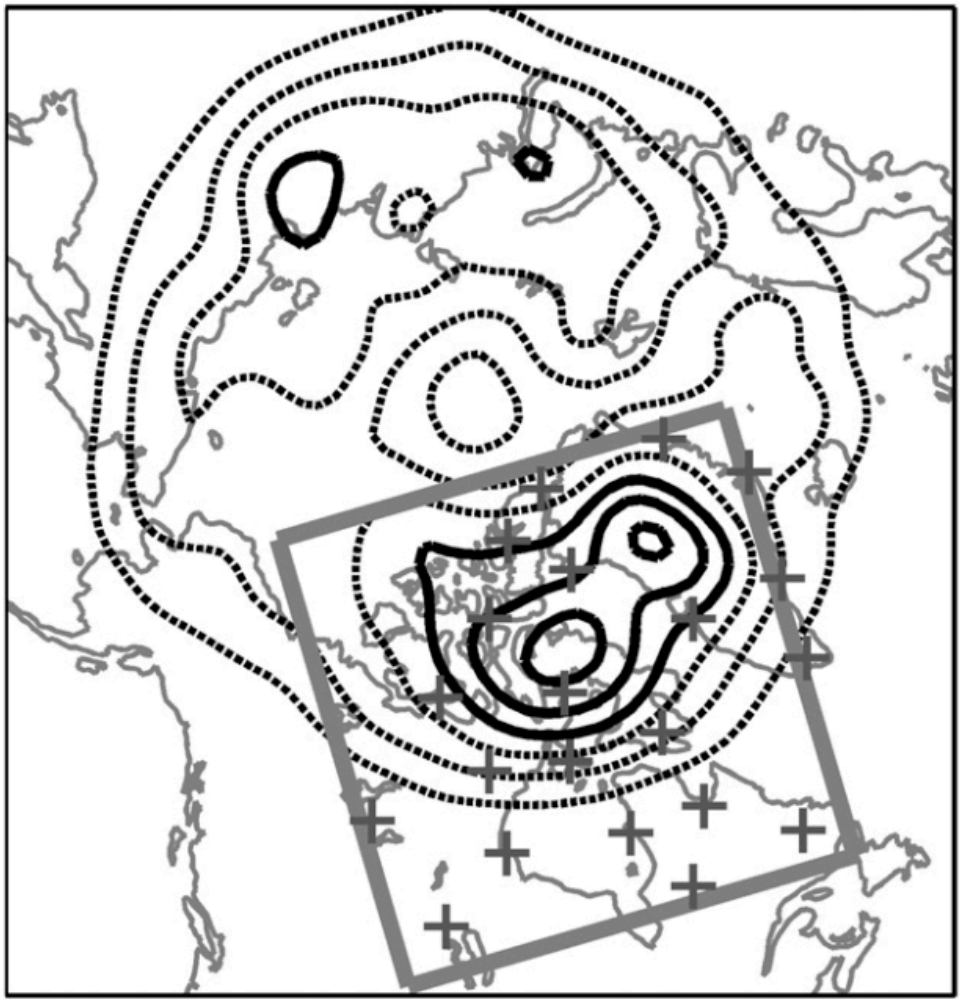

Area-weighted occurrence of intensifying TPVs (referring to location of greatest increase in TPV amplitude during a 24-h period along a unique vortex track) during 1948–99 (contours; contour interval every 50). Values equal to number of unique TPVs within a 5° latitude × 15° longitude box divided by cosine of latitude. Radiosonde stations denoted by "+" symbol. Adapted from Fig. 1 in Cavallo and Hakim (2010).

- Evaluated composite structure of TPVs from 2 August 2007 to 31 July 2009 for domain show in figure
- Used Advanced Research Weather (ARW) version of Weather Research and Forecasting Model (WRF)
- Horizontal grid spacing of 30 km × 30 km, 31 vertical levels, and time step of 120 s
- Forecasts initialized with GFS analyses at 0000 UTC daily
- Boundary conditions derived from GFS forecasts every 3 h
- Only considered TPVs with minimum DT θ at least 2 standard deviations below domain mean

TPV Composite Structure

Cavallo and Hakim (2010)

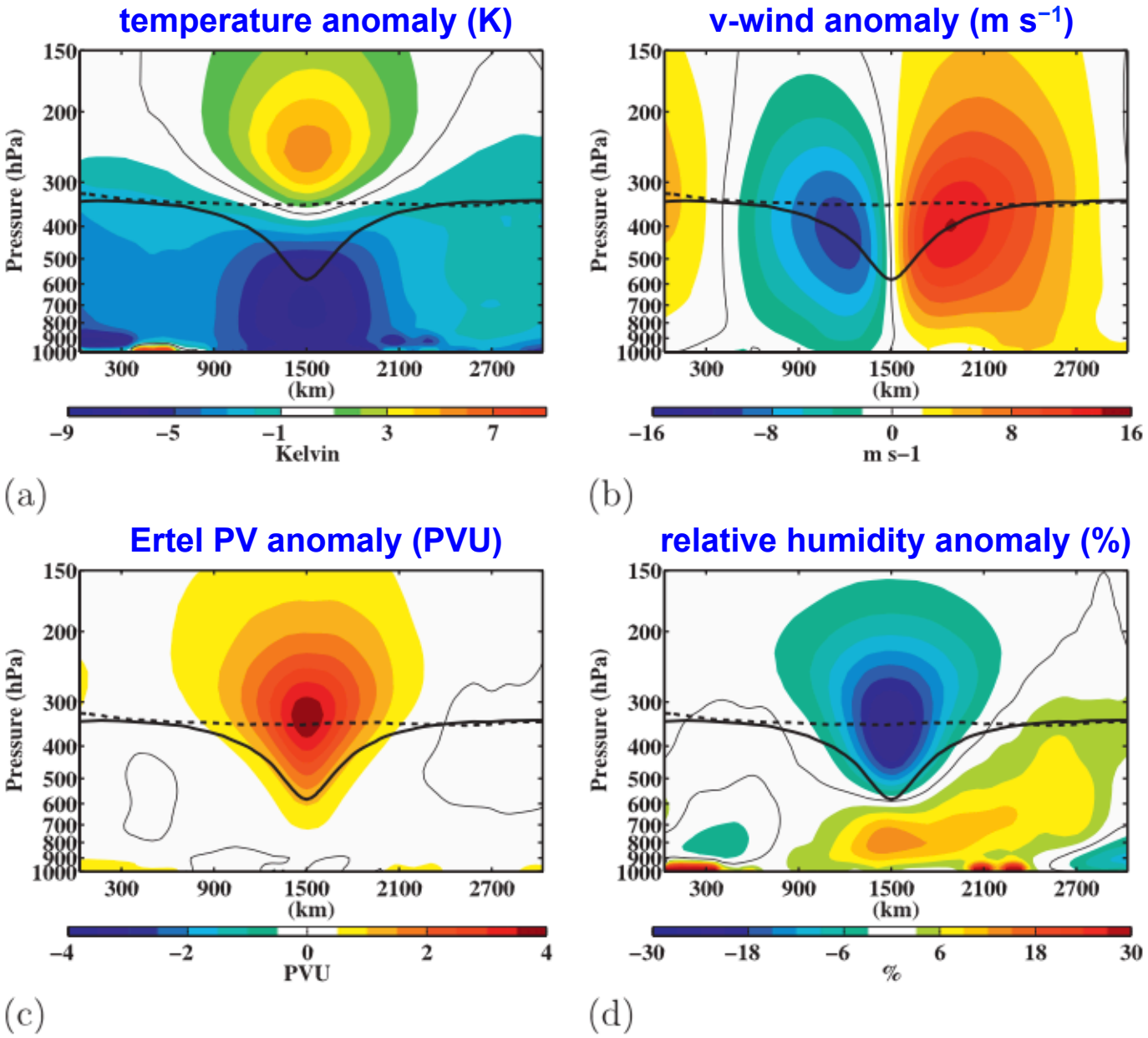

TPV Composite Structure

Cavallo and Hakim (2010)

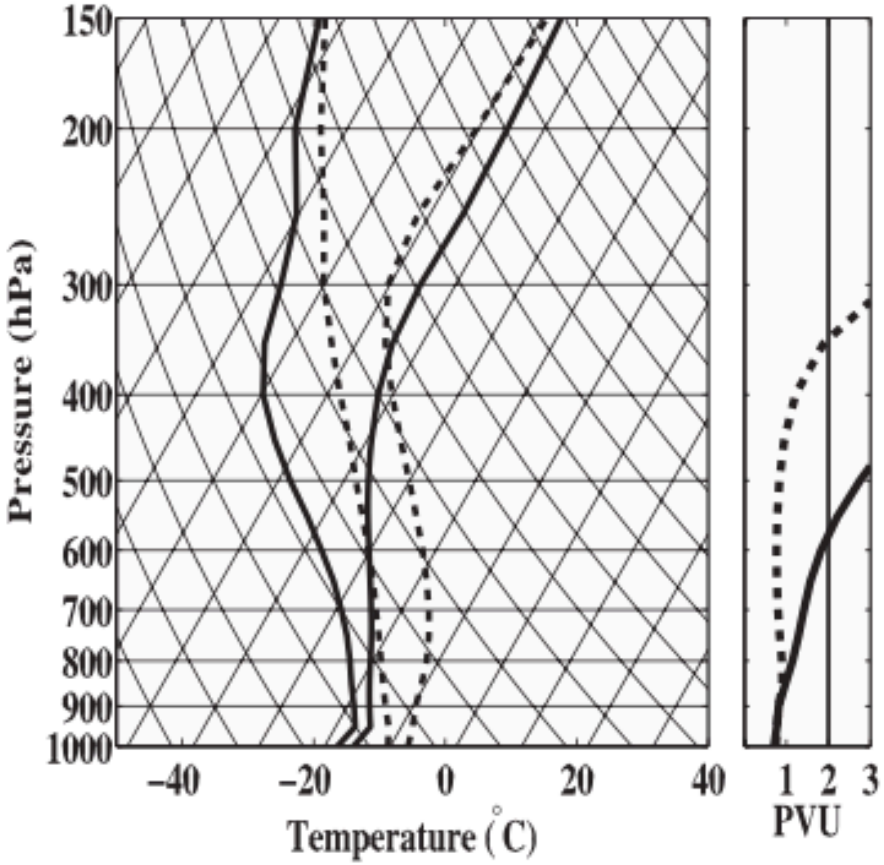

Composite temperature, dewpoint temperature, and PV at TPV core (solid) and background (dashed)

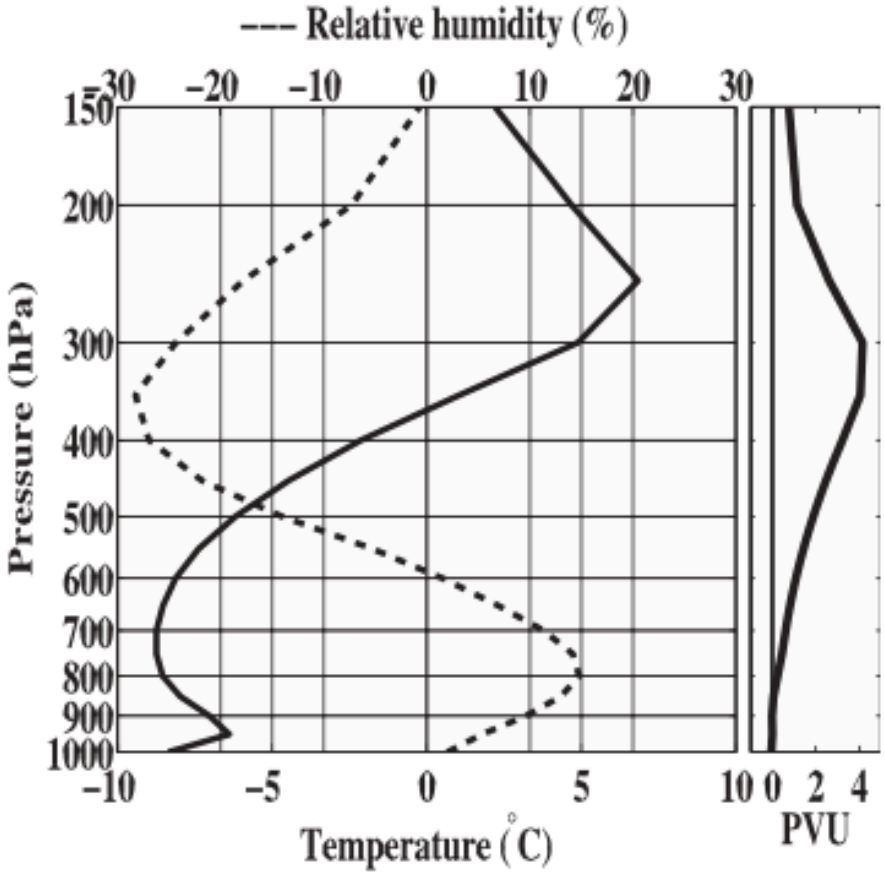

(left) TPV–background difference in temperature (solid) and relative humidity (dashed); (right) PV anomaly of TPV from background

Diabatic Impacts on Composite TPV

Cavallo and Hakim (2010)

Dθ/Dt

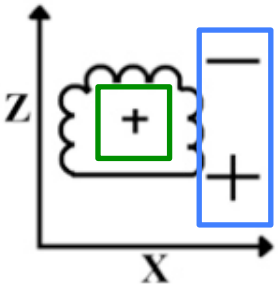

Latent Heating

Radiational heating

Dπ/Dt

$$\frac{D\Pi}{Dt} \simeq \frac{\zeta_a}{\rho}\frac{\partial}{\partial z}(\dot{\theta}_{\rm rad} + \dot{\theta}_{\rm lh}).$$

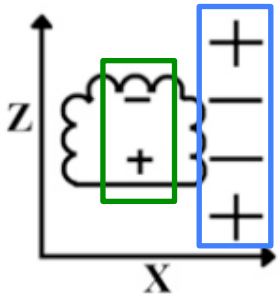

PV tendency from latent heating

PV tendency from radiational heating

Schematic above for case of small latent heating adapted from Fig. 3 in Cavallo and Hakim (2009).

radiative heating rate

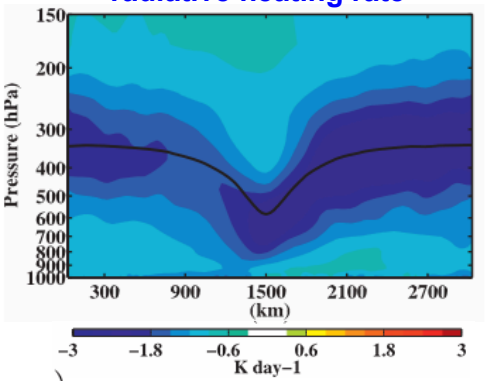

latent heating rate

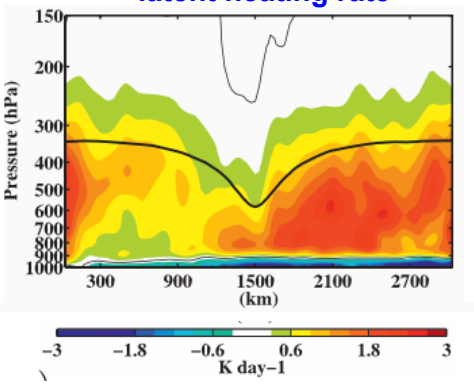

radiative heating rate anomaly

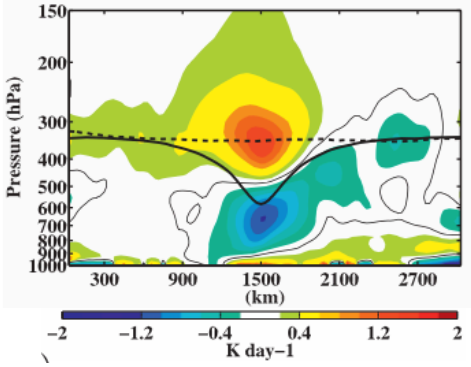

latent heating rate anomaly

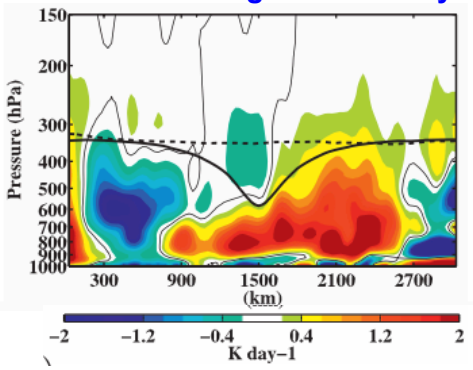

PV tendency due to radiation only

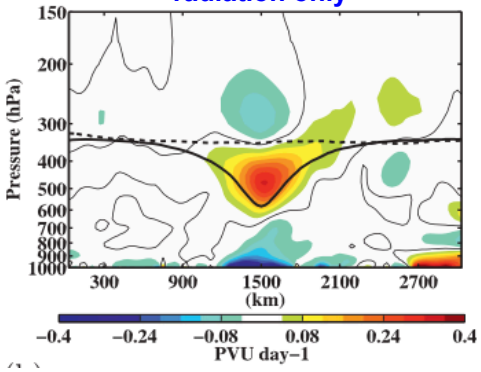

PV tendency due to latent heating only

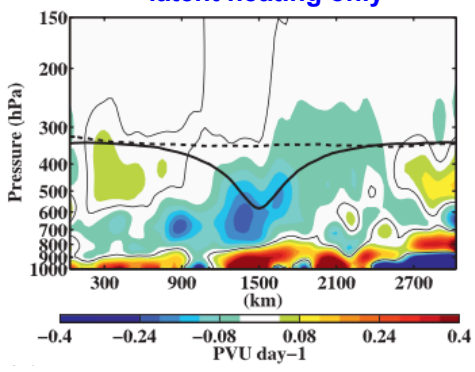

Diabatic Impacts on Composite TPV

Cavallo and Hakim (2010)

Dθ/Dt

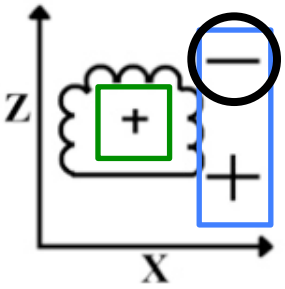

Latent Heating

Radiational heating

Dπ/Dt

$$\frac{D\Pi}{Dt} \simeq \frac{\zeta_a}{\rho}\frac{\partial}{\partial z}(\dot{\theta}_{\rm rad} + \dot{\theta}_{\rm lh}).$$

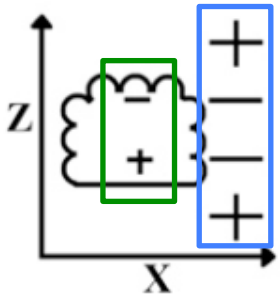

PV tendency from latent heating

PV tendency from radiational heating

Schematic above for case of small latent heating adapted from Fig. 3 in Cavallo and Hakim (2009).

radiative heating rate

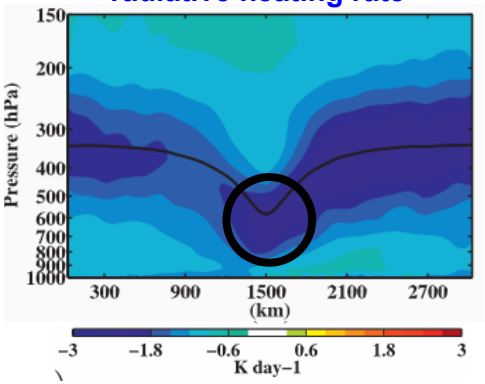

latent heating rate

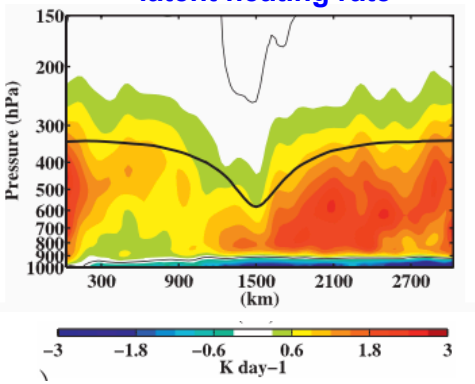

radiative heating rate anomaly

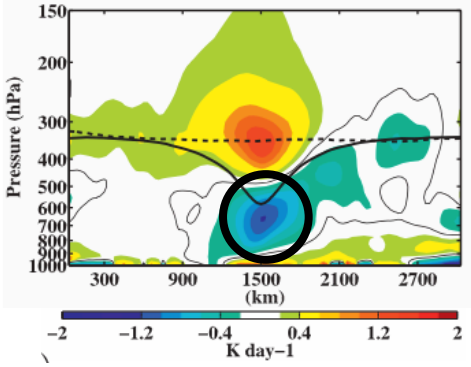

latent heating rate anomaly

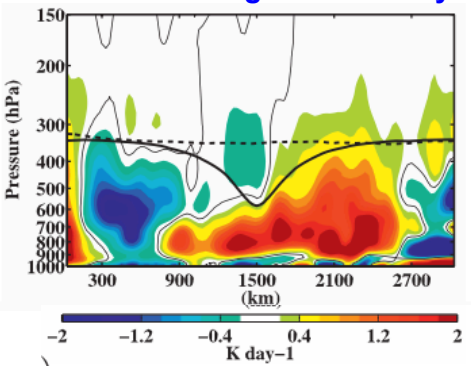

PV tendency due to radiation only

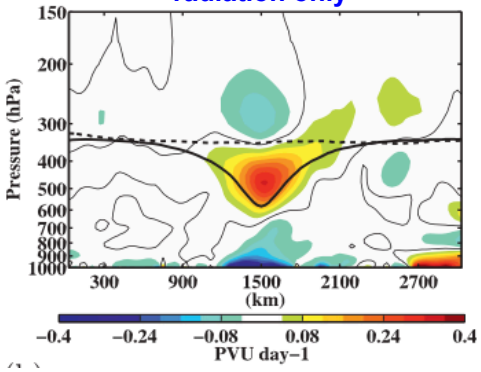

PV tendency due to latent heating only

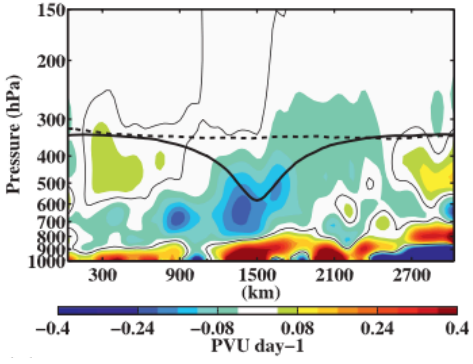

Diabatic Impacts on Composite TPV

Cavallo and Hakim (2010)

Dθ/Dt

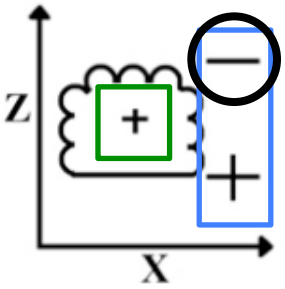

Latent Heating

Radiational heating

Dπ/Dt

$$\frac{D\Pi}{Dt} \simeq \frac{\zeta_a}{\rho}\frac{\partial}{\partial z}(\dot{\theta}_{\mathrm{rad}} + \dot{\theta}_{\mathrm{lh}})$$

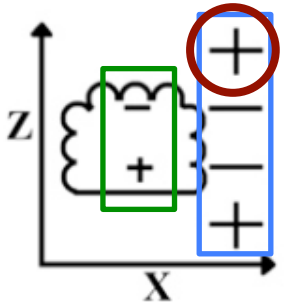

PV tendency from latent heating

PV tendency from radiational heating

Schematic above for case of small latent heating adapted from Fig. 3 in Cavallo and Hakim (2009).

radiative heating rate

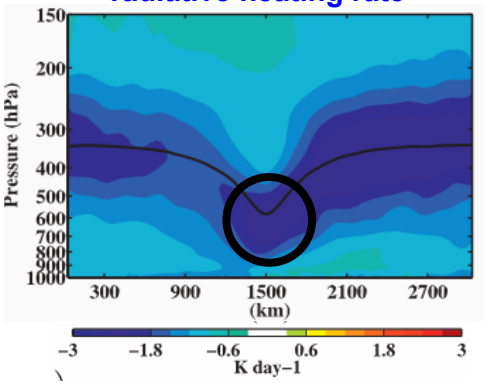

latent heating rate

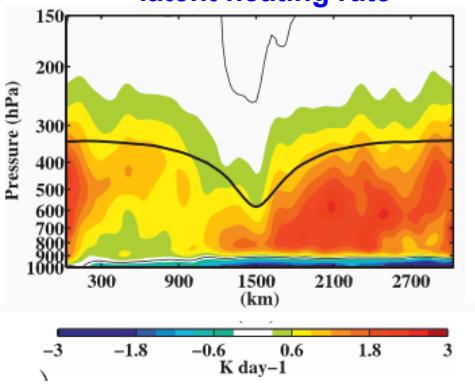

radiative heating rate anomaly

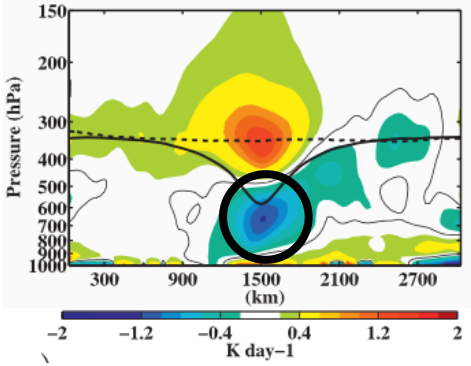

latent heating rate anomaly

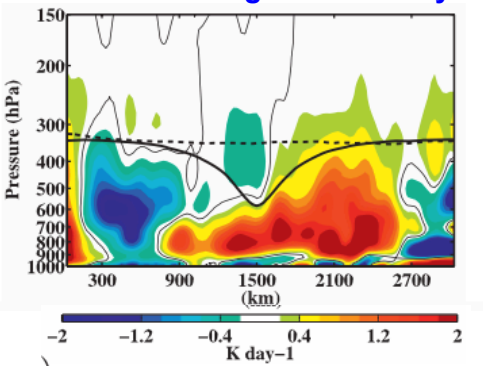

PV tendency due to radiation only

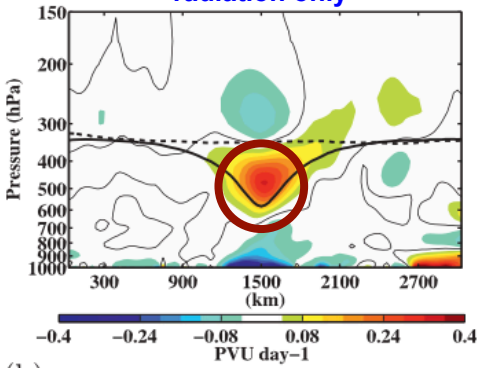

PV tendency due to latent heating only

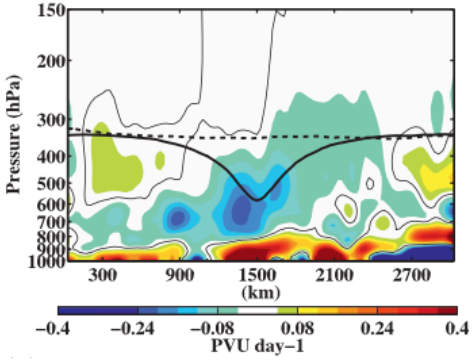

Diabatic Impacts on Composite TPV

Cavallo and Hakim (2010)

Dθ/Dt

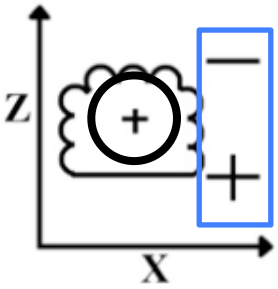

Latent Heating

Radiational heating

Dπ/Dt

$$\frac{D\Pi}{Dt} \simeq \frac{\zeta_a}{\rho}\frac{\partial}{\partial z}(\dot{\theta}_{\rm rad} + \dot{\theta}_{\rm lh}).$$

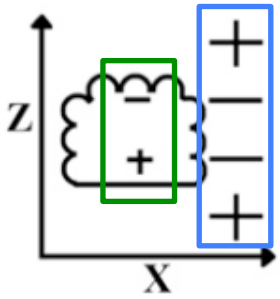

PV tendency from latent heating

PV tendency from radiational heating

Schematic above for case of small latent heating adapted from Fig. 3 in Cavallo and Hakim (2009).

radiative heating rate

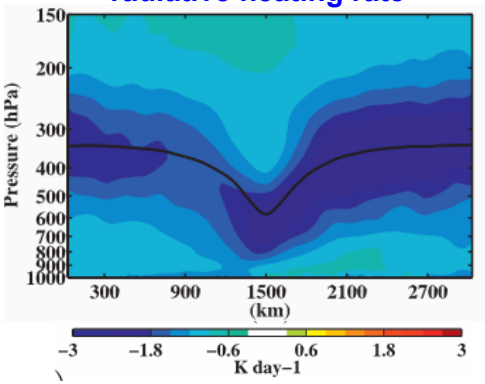

latent heating rate

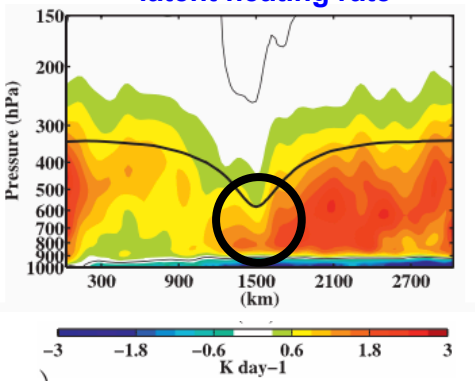

radiative heating rate anomaly

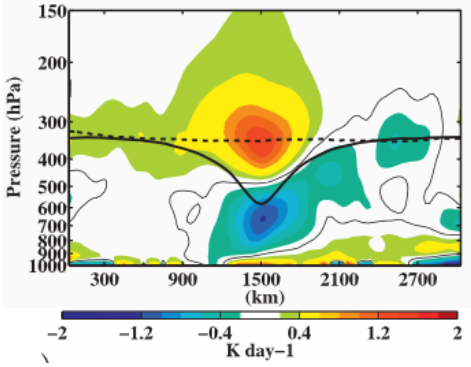

latent heating rate anomaly

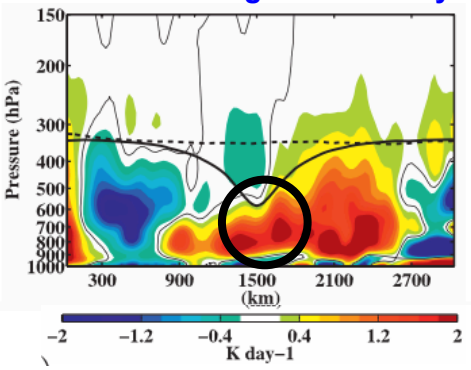

PV tendency due to radiation only

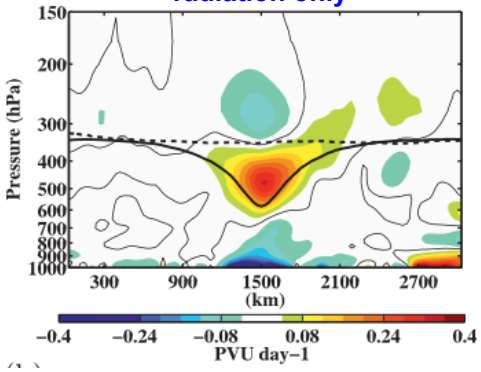

PV tendency due to latent heating only

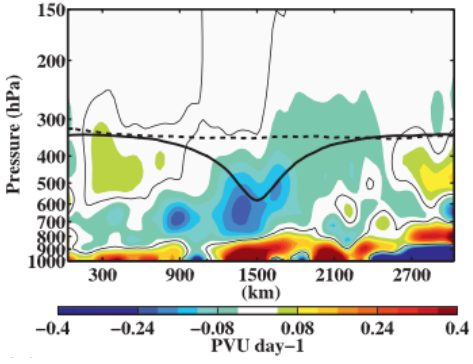

Diabatic Impacts on Composite TPV

Cavallo and Hakim (2010)

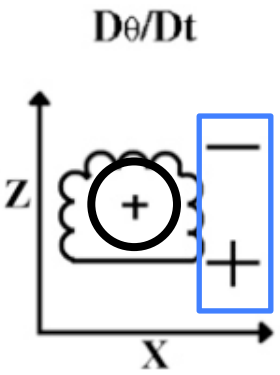

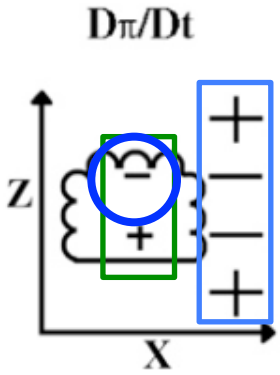

$$\frac{D\Pi}{Dt} \simeq \frac{\zeta_a}{\rho}\frac{\partial}{\partial z}(\dot{\theta}_{\mathrm{rad}} + \dot{\theta}_{\mathrm{lh}})$$

Schematic above for case of small latent heating adapted from Fig. 3 in Cavallo and Hakim (2009).

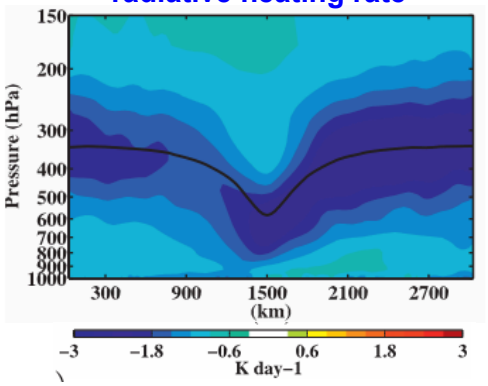

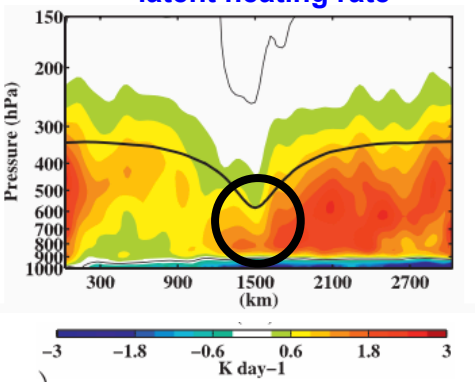

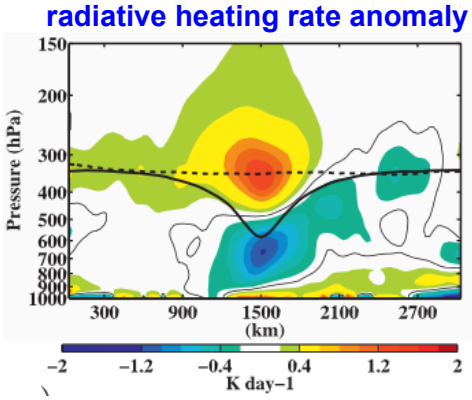

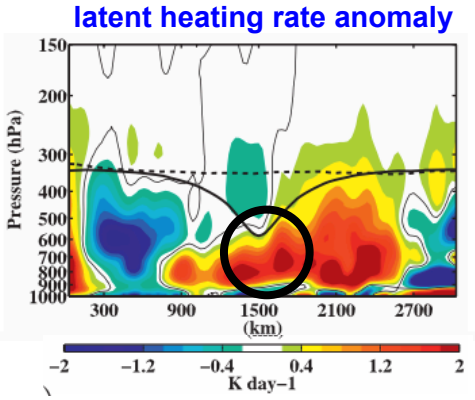

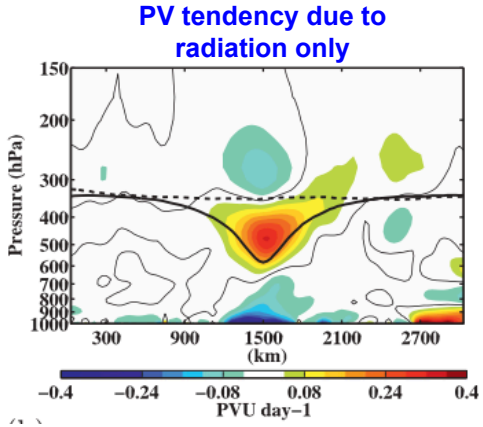

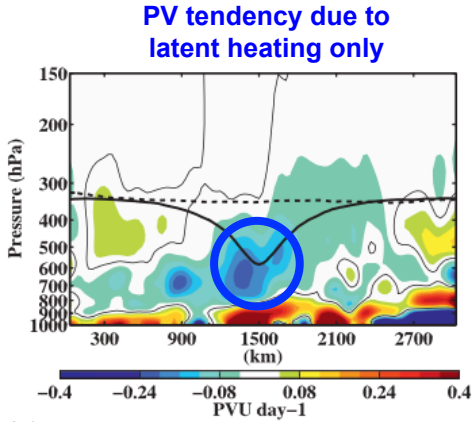

Diabatic Impacts on Composite TPV

Cavallo and Hakim (2010)

$D\theta/Dt$

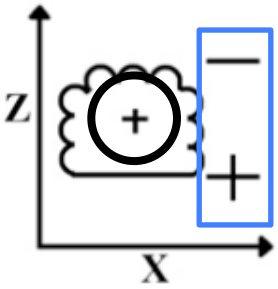

Latent Heating

Radiational heating

$D\pi/Dt$

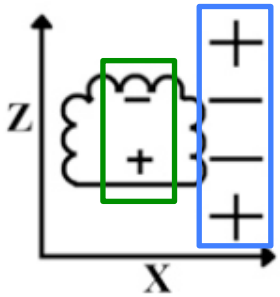

PV tendency from latent heating

PV tendency from radiational heating

$D\pi/Dt\,|_{sum}$

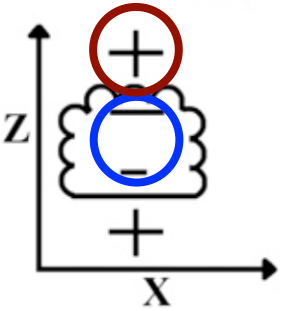

$$\frac{D\Pi}{Dt} \simeq \frac{\zeta_a}{\rho}\frac{\partial}{\partial z}(\dot{\theta}_{\rm rad} + \dot{\theta}_{\rm lh}).$$

Net PV tendency from latent heating and radiational heating

Schematic above for case of small latent heating adapted from Fig. 3 in Cavallo and Hakim (2009).

PV tendency due to all diabatic effects

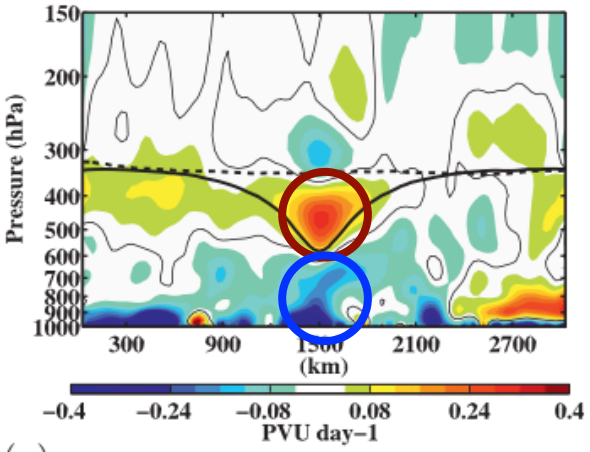

(a)

PV tendency due to radiation only

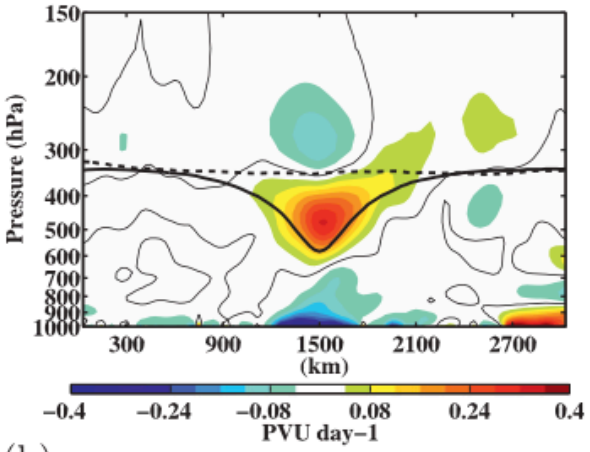

(b)

PV tendency due to latent heating only

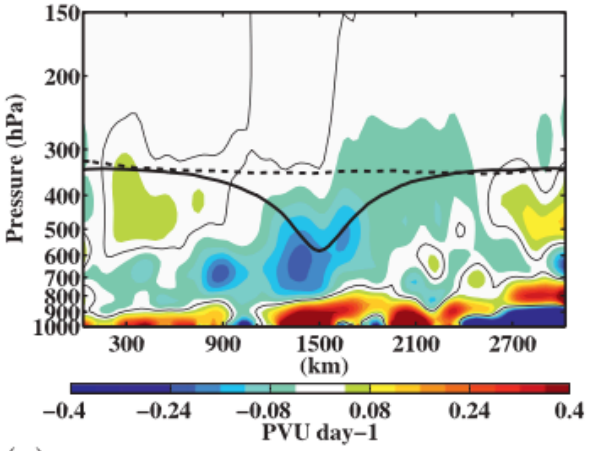

(c)

PV tendency due to all diabatic effects except radiation and latent heating

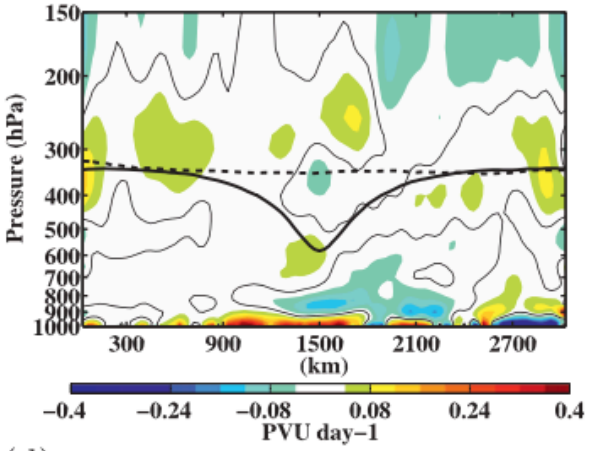

(d)

Cavallo and Hakim (2012)

- Created two 10-yr TPV climatologies (1990–99):
  - **NCEP NCAR Reanalysis Project (NNRP):** horizontal grid spacing: ~ 210 km (2.5°)
  - **WRF:** Forecasts initialized with NNRP data and boundary; boundary conditions updated with NNRP analyses every 6 h; horizontal grid spacing: 60 × 60 km

Expt	Vortex tracks	Genesis	Lysis
NNRP DJF	442	442	442
NNRP JJA	374	374	374
WRF DJF	7426	7277	7073
WRF JJA	6643	6502	6194
WRF DJF (no radiation)	7039	6829	6747
WRF JJA (no radiation)	5837	5670	5408

Adapted from Table 1 of Cavallo and Hakim (2012)

TPV Climatology

Cavallo and Hakim (2012)

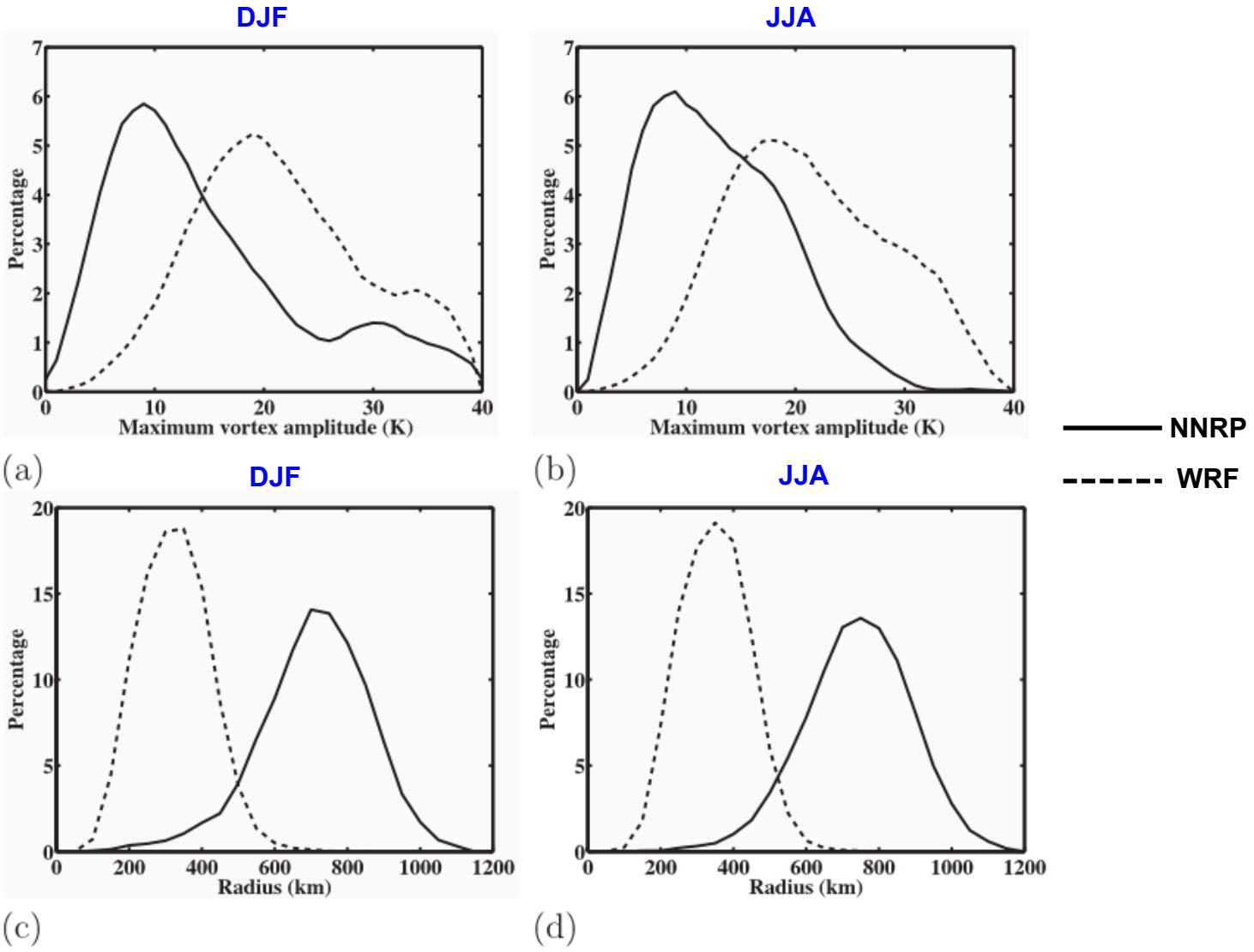

TPV properties of (top) maximum amplitude and (bottom) average radius for (left) winter and (right) summer for 1990–99. Adapted from Fig. 2 in Cavallo and Hakim (2012).

TPV Climatology

Cavallo and Hakim (2012)

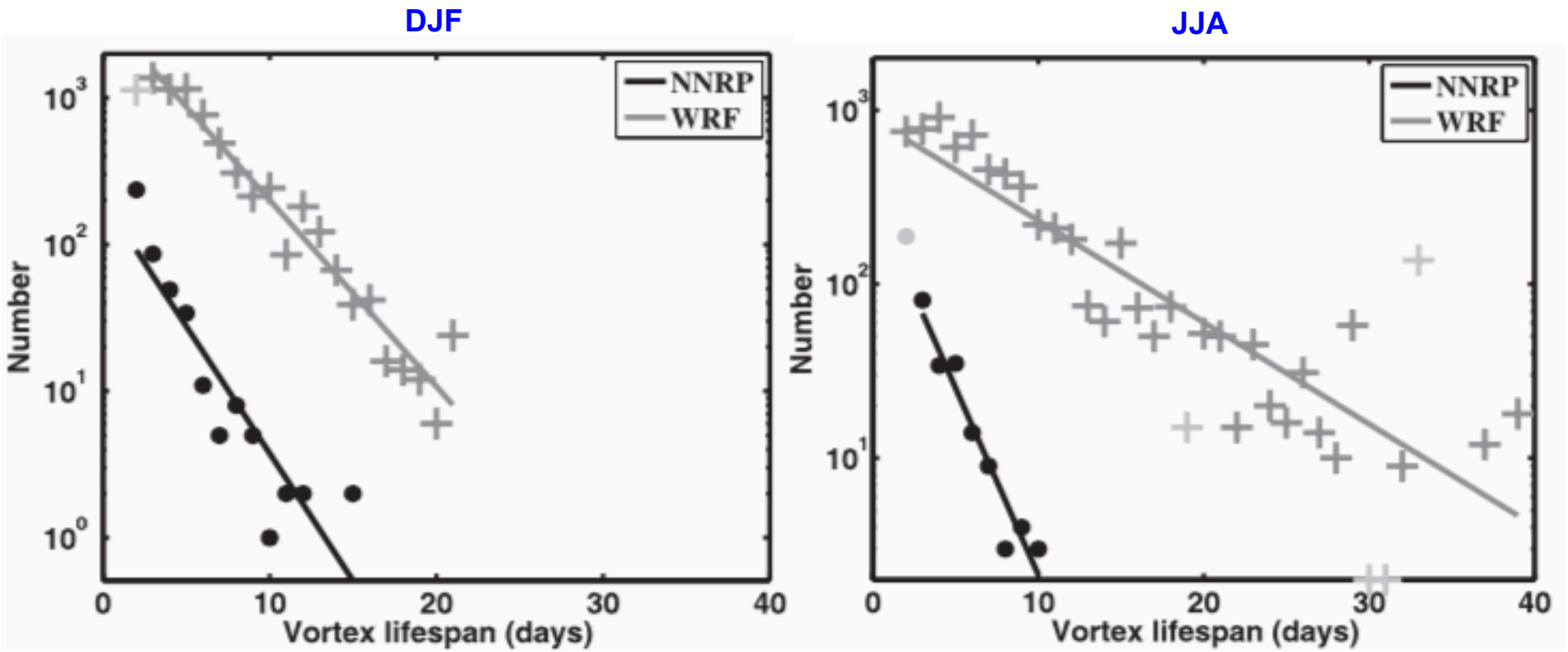

TPV lifetime distributions for (left) winter and (right) summer over 1990–99. Heavy line shows linear fit to exponential distributions from NNRP (black) and WRF (gray). Points not included in exponential fits are light gray. Adapted from Fig. 3 in Cavallo and Hakim (2012).

Impact of Radiation on TPVs

Cavallo and Hakim (2012)

- TPV amplitude increases (decreases) over time in full-physics (no radiation) climatologies
- On average, TPVs with long lifetimes tend to weaken in absence of radiative forcing

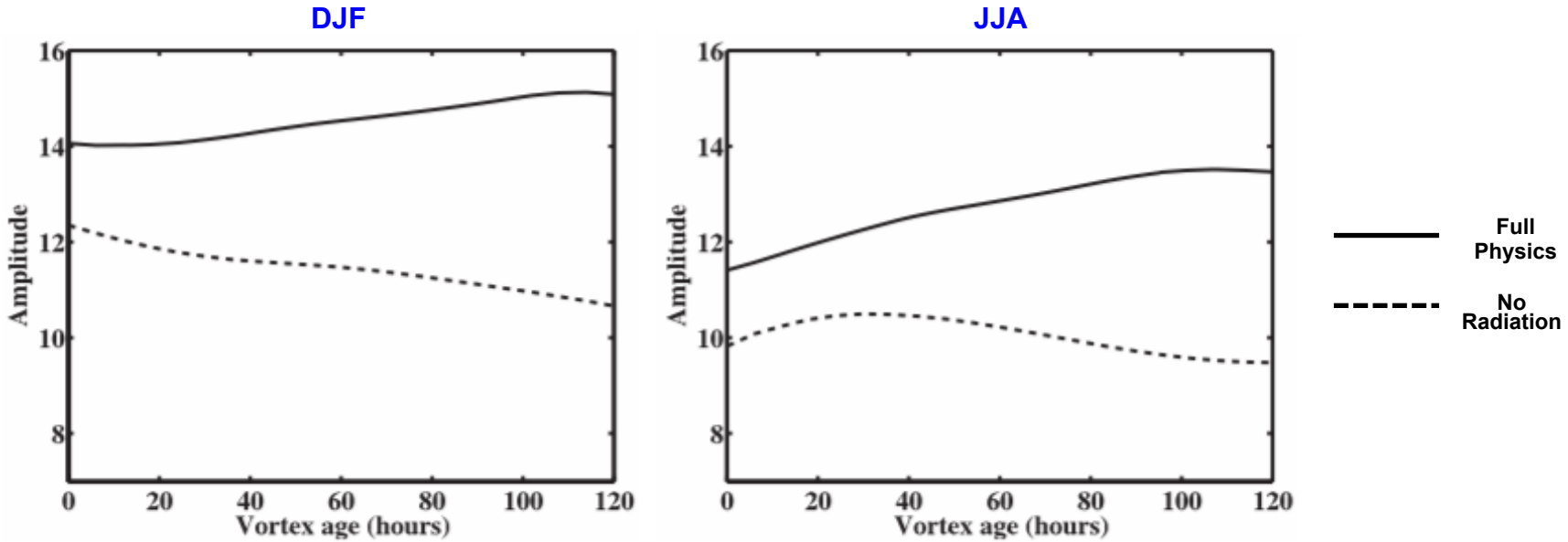

Average TPV tropopause potential temperature amplitude as a function of time for (left) winter and (right) summer over 1990–99 for TPVs surviving at least five days. Solid (dashed) lines correspond to WRF simulations with full physics (no radiation). Adapted from Fig. 7 in Cavallo and Hakim (2012).

Impact of Radiation on TPVs

Cavallo and Hakim (2012)

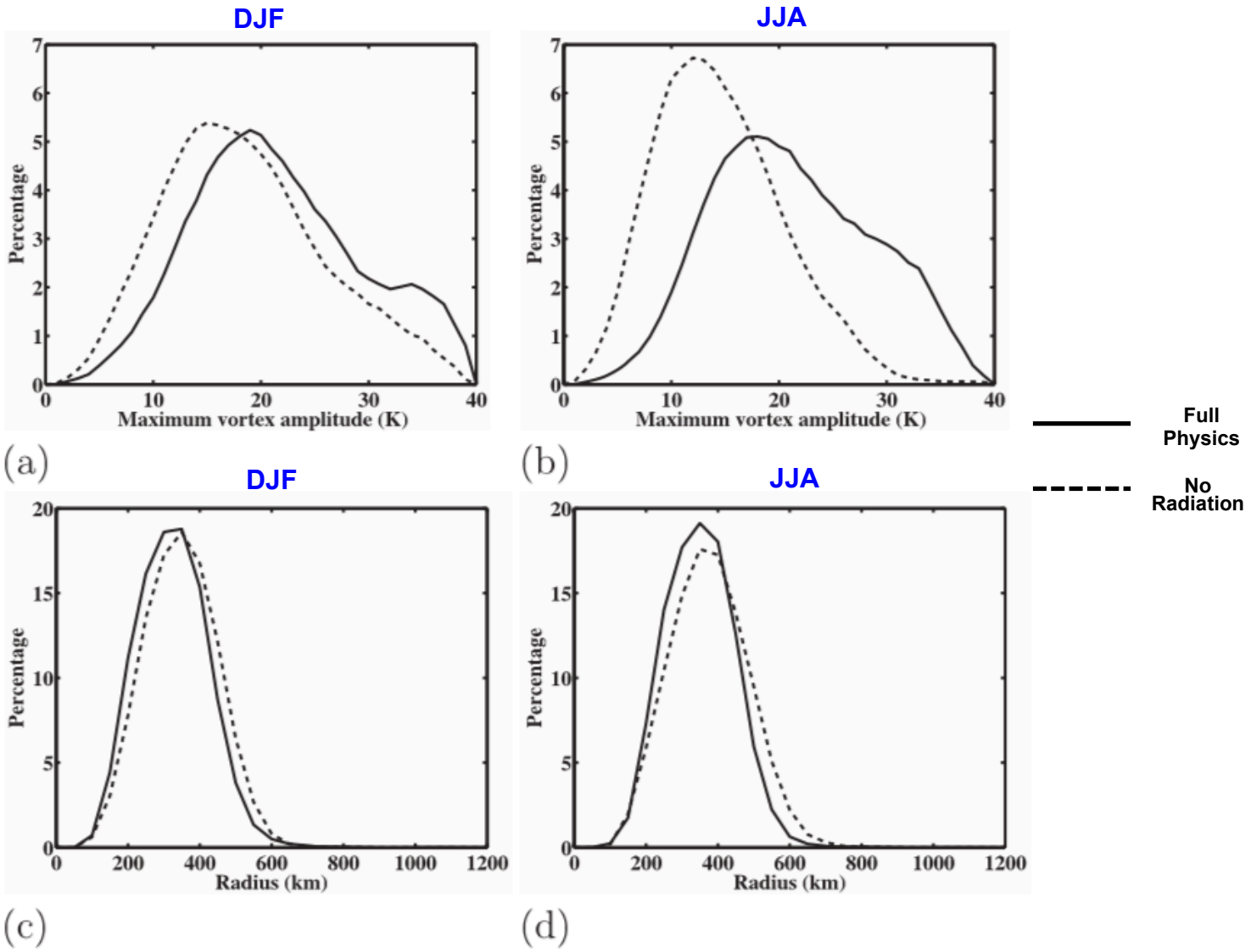

TPV properties of (top) maximum amplitude and (bottom) average radius for (left) winter and (right) summer for 1990–99. Solid (dashed) lines correspond to WRF simulations with full physics (no radiation). Adapted from Fig. 8 in Cavallo and Hakim (2012).

Impact of Radiation on TPVs

Cavallo and Hakim (2012)

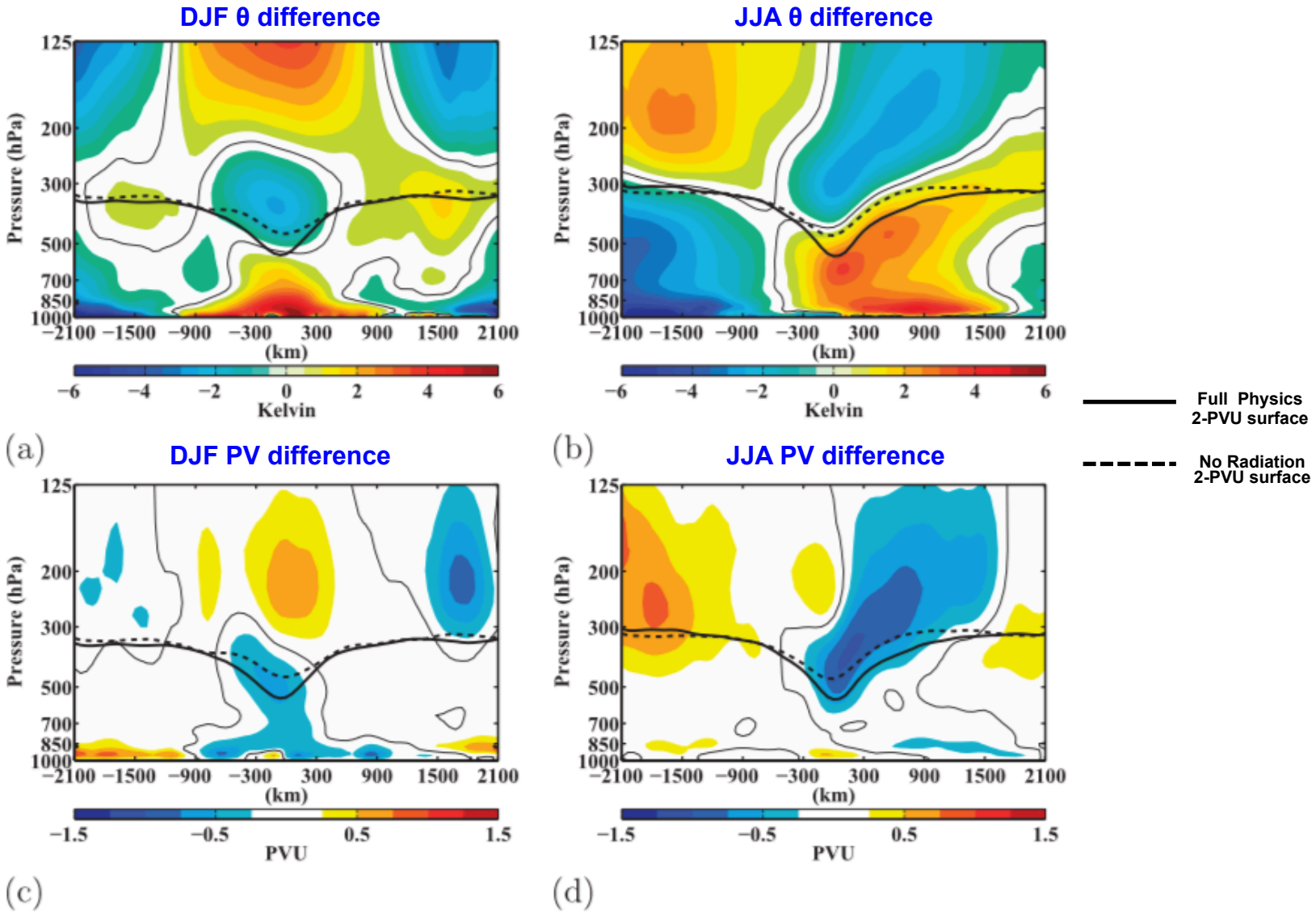

Composite cross-sectional difference (no radiation – full physics) anomalies in (top) potential temperature and (bottom) PV for (left) winter and (right) summer. Adapted from Fig. 12 in Cavallo and Hakim (2012).

Mechanisms for TPV Intensity Change

Cavallo and Hakim (2013)

- Performed idealized numerical modeling experiments using WRF to examine intensification mechanisms of TPVs
- Used a horizontal grid spacing of 24 km × 24 km, with 60 vertical levels, and a time step of 120 s

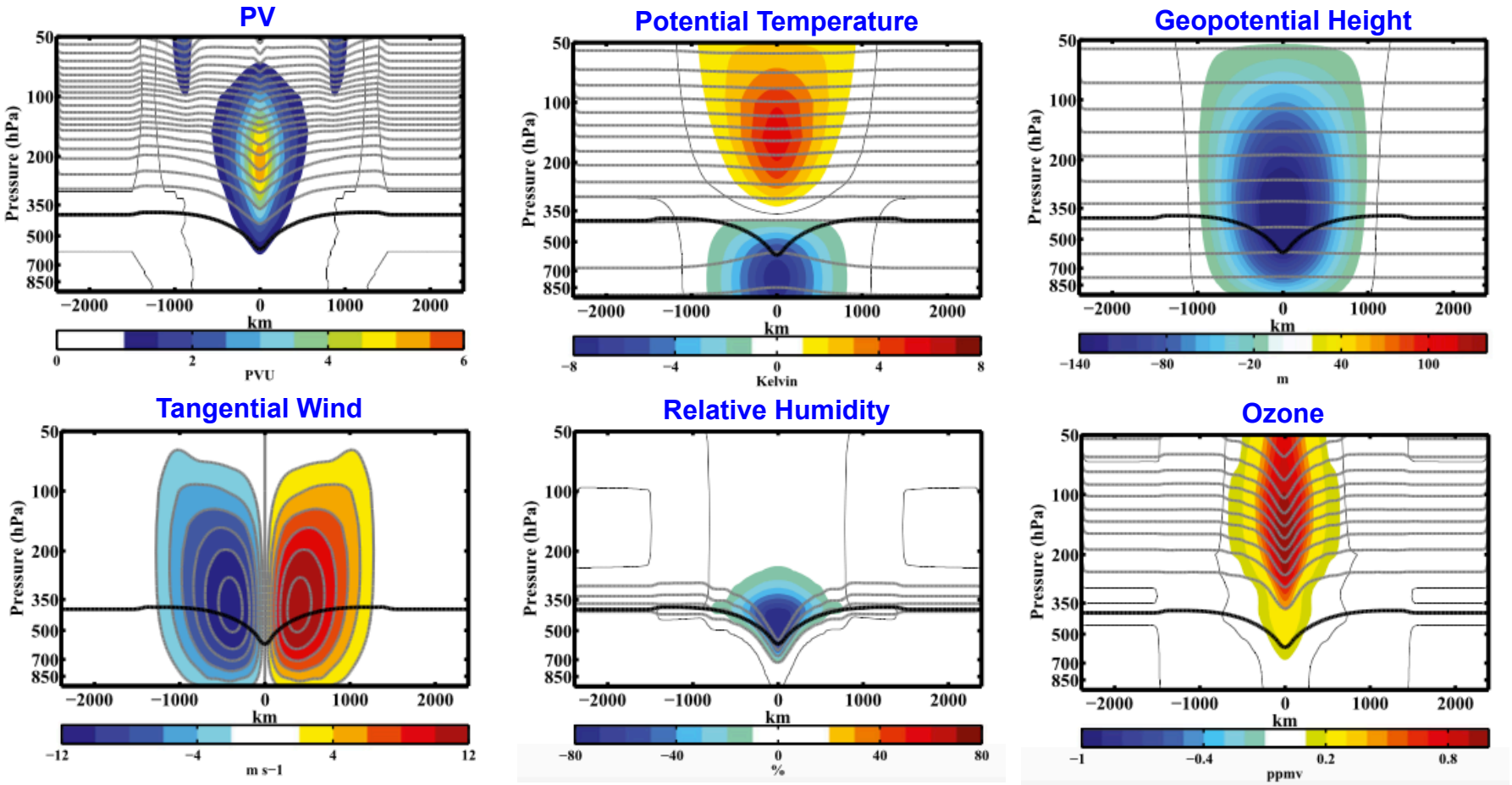

Initial condition cross-vortex sections. Anomalies are shown in color shading, while gray contours show field. Adapted from Fig. 2 in Cavallo and Hakim (2013).

Mechanisms for TPV Intensity Change

Cavallo and Hakim (2013)

TABLE 1. Summary of numerical simulation parameters longwave (LW) and shortwave (SW) radiation and microphysics (MP).

Expt	Description
E1	LW, without H_2O
E2	LW, with H_2O
E3	LW, SW
E4	LW, MP
E5	LW, SW, MP

$$\frac{D\Pi}{Dt} \simeq \frac{\boldsymbol{\omega}_a}{\rho} \cdot \nabla \left(\underbrace{\dot{\theta}_{\text{longwave}}}_{\text{A}} + \underbrace{\dot{\theta}_{\text{shortwave}}}_{\text{B}} + \underbrace{\dot{\theta}_{\text{latent heating}}}_{\text{C}} + \dot{\theta}_{\text{other}} \right)$$

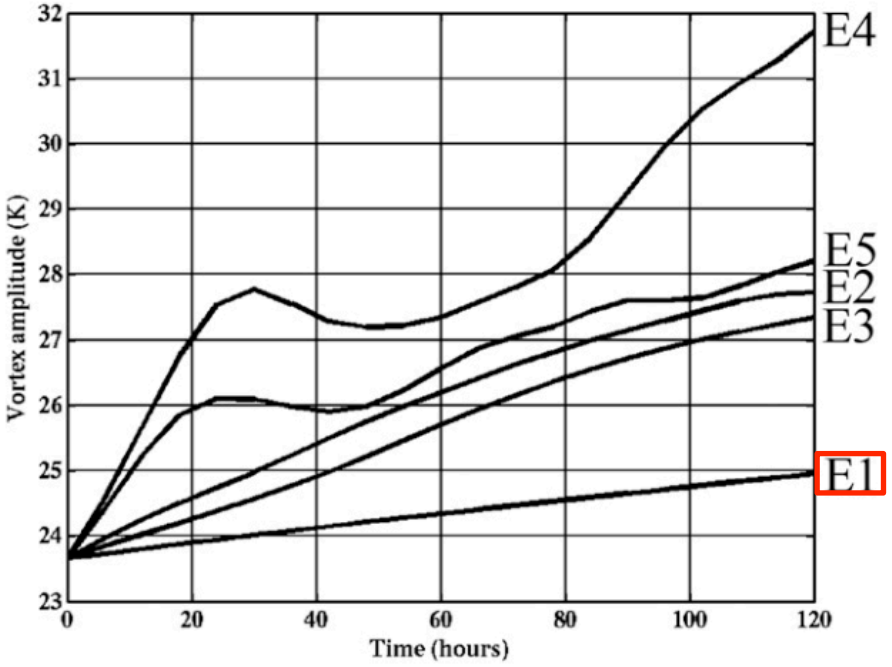

Time series of TPV amplitude for experiments 1–5 on 2 PVU surface. Adapted from Fig. 3 in Cavallo and Hakim (2013)

- E1: Longwave radiative forcing exclusive of water vapor
- Longwave radiative effects only due to temperature, carbon dioxide, and ozone
- Vortex intensifies at slow rate for ~150 days before weakening (not shown)

Mechanisms for TPV Intensity Change

Cavallo and Hakim (2013)

TABLE 1. Summary of numerical simulation parameters longwave (LW) and shortwave (SW) radiation and microphysics (MP).

Expt	Description
E1	LW, without H_2O
E2	LW, with H_2O
E3	LW, SW
E4	LW, MP
E5	LW, SW, MP

$$\frac{D\Pi}{Dt} \simeq \frac{\boldsymbol{\omega}_a}{\rho} \cdot \nabla \left(\underbrace{\dot{\theta}_{\text{longwave}}}_{\text{A}} + \underbrace{\dot{\theta}_{\text{shortwave}}}_{\text{B}} + \underbrace{\dot{\theta}_{\text{latent heating}}}_{\text{C}} + \dot{\theta}_{\text{other}} \right)$$

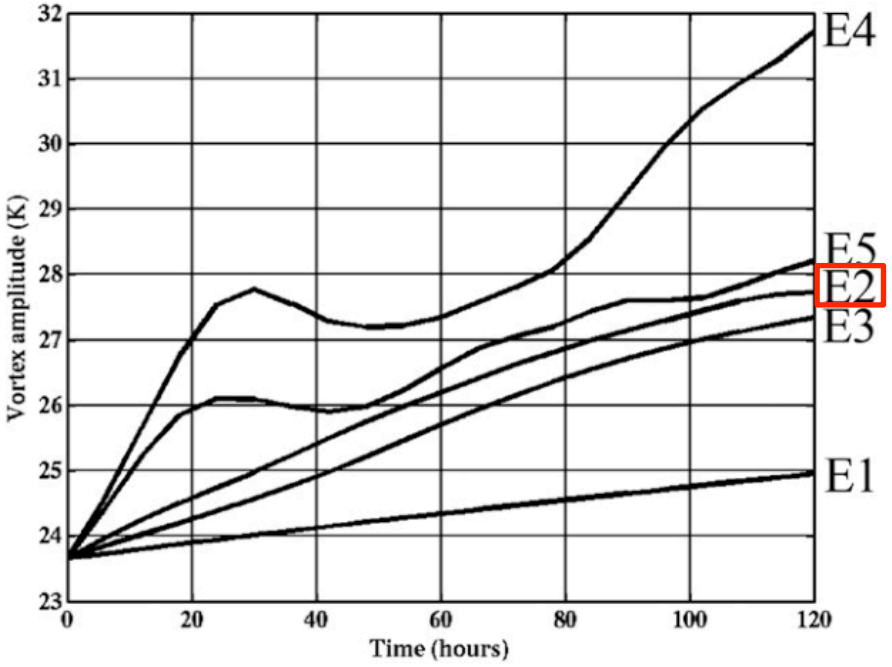

Time series of TPV amplitude for experiments 1–5 on 2 PVU surface. Adapted from Fig. 3 in Cavallo and Hakim (2013)

- E2: Longwave radiative forcing inclusive of water vapor
- Water vapor is strong absorber of longwave radiation
- Lowered tropopause in vortex core promotes vertically thin transition zone between relatively moist tropospheric air and dry stratospheric air
- Anomalously high vertical water vapor gradient leads to anomalous longwave cooling just below tropopause in vortex core
- With anomalous weak longwave cooling just above tropopause in vortex core, the positive vertical longwave heating gradient results in positive PV tendency near tropopause in vortex core

Mechanisms for TPV Intensity Change

Cavallo and Hakim (2013)

TABLE 1. Summary of numerical simulation parameters longwave (LW) and shortwave (SW) radiation and microphysics (MP).

Expt	Description
E1	LW, without H_2O
E2	LW, with H_2O
E3	LW, SW
E4	LW, MP
E5	LW, SW, MP

$$\frac{D\Pi}{Dt} \simeq \frac{\boldsymbol{\omega}_a}{\rho} \cdot \nabla \left(\underbrace{\dot{\theta}_{\text{longwave}}}_{\text{A}} + \underbrace{\dot{\theta}_{\text{shortwave}}}_{\text{B}} + \underbrace{\dot{\theta}_{\text{latent heating}}}_{\text{C}} + \dot{\theta}_{\text{other}} \right)$$

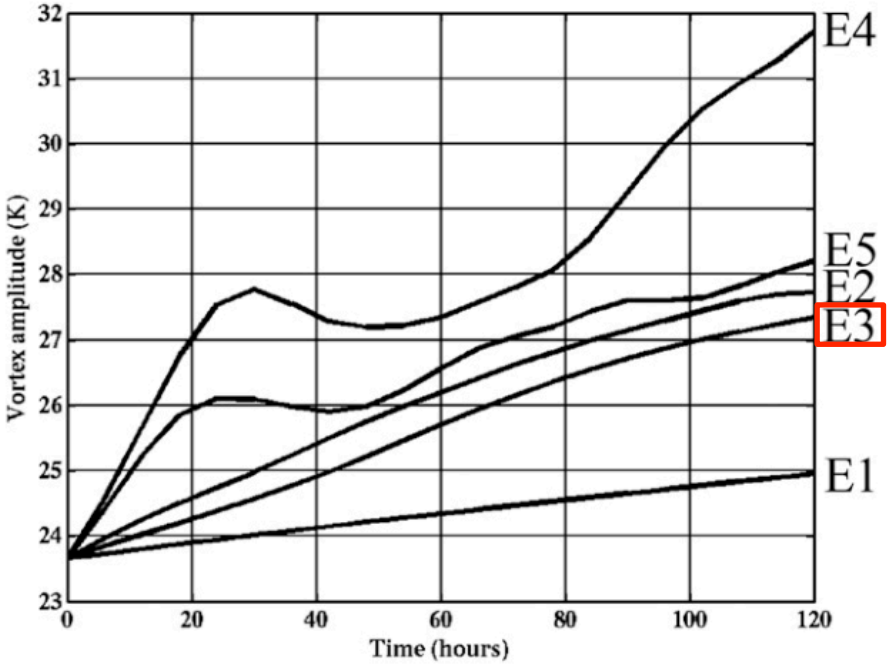

Time series of TPV amplitude for experiments 1–5 on 2 PVU surface. Adapted from Fig. 3 in Cavallo and Hakim (2013)

- E3: Longwave radiative forcing inclusive of water vapor and shortwave forcing
- Shortwave radiative heating rates are a maximum (minimum) ~100 hPa below (above) tropopause
- Shortwave heating results in negative PV tendency over tropopause in vortex core
- Shortwave radiation not strongly absorbed by water vapor, thus magnitudes of shortwave heating near tropopause is smaller than magnitudes of longwave cooling
- Longwave cooling rates offset partially by shortwave heating rates, so vortex strengthens still, but slightly less than w/o shortwave radiation

Mechanisms for TPV Intensity Change

Cavallo and Hakim (2013)

TABLE 1. Summary of numerical simulation parameters longwave (LW) and shortwave (SW) radiation and microphysics (MP).

Expt	Description
E1	LW, without H_2O
E2	LW, with H_2O
E3	LW, SW
E4	LW, MP
E5	LW, SW, MP

$$\frac{D\Pi}{Dt} \simeq \frac{\boldsymbol{\omega}_a}{\rho} \cdot \nabla \left(\underbrace{\dot{\theta}_{\text{longwave}}}_{\text{A}} + \underbrace{\dot{\theta}_{\text{shortwave}}}_{\text{B}} + \underbrace{\dot{\theta}_{\text{latent heating}}}_{\text{C}} + \dot{\theta}_{\text{other}} \right)$$

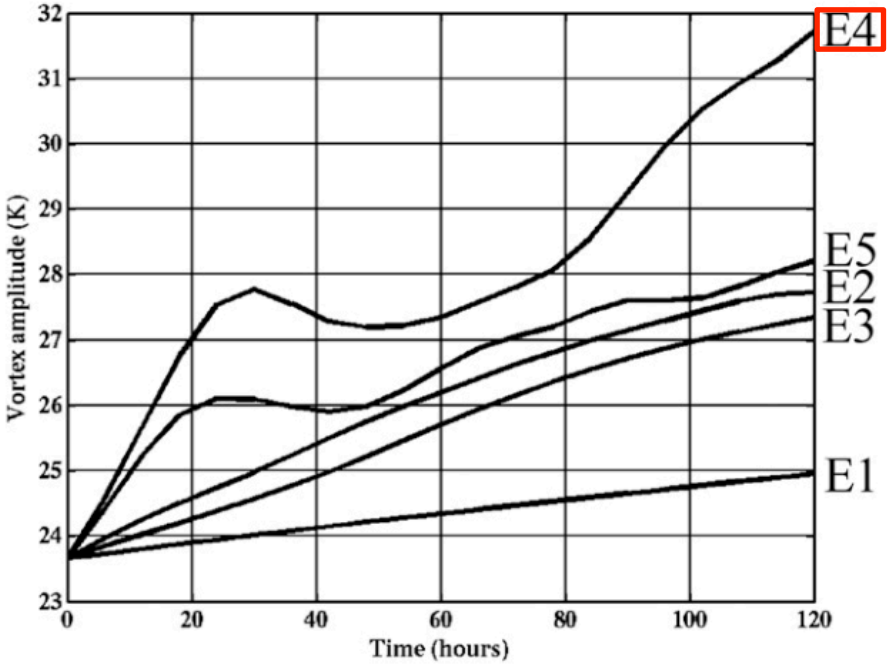

Time series of TPV amplitude for experiments 1–5 on 2 PVU surface. Adapted from Fig. 3 in Cavallo and Hakim (2013)

- E4: Longwave radiative forcing inclusive of water vapor and condensation of water vapor (representative of Arctic winter)
- Net longwave cooling is stronger, especially in lower and middle troposphere
- Thus, inclusion of cloud radiative forcing results in stronger longwave cooling gradient from below tropopause to above tropopause in vortex core, resulting in enhanced PV production in upper troposphere in vortex core
- Clouds more likely associated with TPVs due to reduced static stability and higher relative humidities in lower troposphere

Mechanisms for TPV Intensity Change

Cavallo and Hakim (2013)

TABLE 1. Summary of numerical simulation parameters longwave (LW) and shortwave (SW) radiation and microphysics (MP).

Expt	Description
E1	LW, without H_2O
E2	LW, with H_2O
E3	LW, SW
E4	LW, MP
E5	LW, SW, MP

$$\frac{D\Pi}{Dt} \simeq \frac{\boldsymbol{\omega}_a}{\rho} \cdot \nabla \left(\underbrace{\dot{\theta}_{\text{longwave}}}_{\text{A}} + \underbrace{\dot{\theta}_{\text{shortwave}}}_{\text{B}} + \underbrace{\dot{\theta}_{\text{latent heating}}}_{\text{C}} + \dot{\theta}_{\text{other}} \right)$$

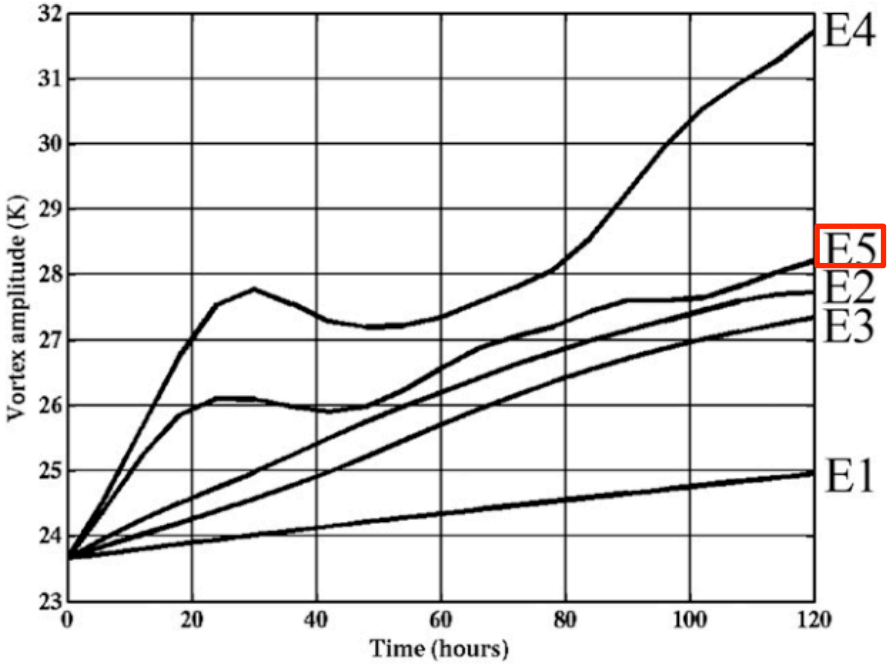

Time series of TPV amplitude for experiments 1–5 on 2 PVU surface. Adapted from Fig. 3 in Cavallo and Hakim (2013)

- E5: Longwave radiative forcing inclusive of water vapor, shortwave heating, and latent heating (representative of Arctic Summer)
- TPV intensification is slower with inclusion of shortwave radiation because there is a reduction of cloud in vortex core
- Longwave radiative cooling is thus smaller
- Longwave radiative cooling above cloud destabilizes air, promoting cloud maintenance, but shortwave radiative cooling partially offsets the cooling, resulting in reduction in cloud concentration
- Even if clouds diminish, vortex will still intensify due to presence of vertical water vapor gradient

References

- Cavallo, S. M., and G. J. Hakim, 2009: Potential Vorticity Diagnosis of a Tropopause Polar Cyclone. *Mon. Wea. Rev.*, **137**, 1358–1371.
- Cavallo, S. M., and G. J. Hakim, 2010: The composite structure of tropopause polar cyclones from a mesoscale model. *Mon. Wea. Rev.*, **138**, 3840–3857.
- Cavallo, S. M., and G. J. Hakim, 2012: Radiative Impact on Tropopause Polar Vortices over the Arctic. *Mon. Wea. Rev.*, **140**, 1683–1702.
- Cavallo, S. M., and G. J. Hakim, 2013: Physical Mechanisms of Tropopause Polar Vortex Intensity Change. *J. Atmos. Sci.*, **70**, 3359–3373.
- Hakim, G. J., L. F. Bosart, and D. Keyser, 1995: The Ohio Valley wave-merger cyclogenesis event of 25–26 January 1978. Part I: Multiscale case study. *Mon. Wea. Rev*., **123**, 2663–2692.
- Hakim, G. J., D. Keyser, and L. F. Bosart, 1996: The Ohio Valley wave-merger cyclogenesis event of 25–26 January 1978. Part II: Diagnosis using quasigeostrophic potential vorticity inversion. *Mon. Wea. Rev*., **124**, 2176–2205.
- Hakim, G. J., 2000: Climatology of coherent structures on the extratropical tropopause. *Mon. Wea. Rev*., **128**, 385–406.
- Hakim, G. J., and A. K. Canavan, 2005: Observed cyclone–anticyclone tropopause vortex asymmetries. *J. Atmos. Sci.*, **62**, 231–240.
- Hoskins, B. J., M. E. McIntyre, and A. W. Robertson, 1985: On the use and significance of isentropic potential vorticity maps. *Quart. J. Roy. Meteor. Soc*., **111**, 877–956.
- Pyle, M. E., et al., 2004: A diagnostic study of jet streaks: Kinematic signatures and relationship to coherent tropopause disturbances. *Mon. Wea. Rev.,* **132**, 297–319.
- Shapiro, M. A., T. Hampel and A. J. Krueger, 1987: The Arctic tropopause fold. *Mon. Wea. Rev*., **115**, 444–454.
- Takayabu, I., 1991: “Coupling development”: An efficient mechanism for the development of extratropical cyclones. *J. Meteor. Soc. Japan*, **69**, 609–628.
- Thorpe, A. J., 1985: Diagnosis of balanced vortex structure using potential vorticity. *J. Atmos. Sci*., **42**, 397–406.